DEFINING THE IMAGING BIOMARKERS AND TEMPORAL EFFECTS OF ISCHAEMIC AND NON-ISCHAEMIC INJURY ON THE MYOCARDIUM

Suchi K Grover, MBChB

School of Medicine

Flinders University

Submitted in fulfillment of the requirements of the degree of

Doctor of Philosophy

August, 2014

Abstract

Following a myocardial insult, there are cellular and pathophysiological changes that occur, resulting in adverse remodelling and eventually clinical sequelae. By this latter stage, most of the treatment options have limited value and often palliate the situation. Injury to the myocardium can follow an ischaemic or non-ischaemic insult, resulting in different adaptive responses. Furthermore, before irreversible damage occurs, defined by necrosis (acutely) and fibrosis (chronically), the initial changes are characterized by myocardial oedema and are considered to be reversible. Targeting the myocardium at this vulnerable but salvageable state may form a basis of future therapeutic options.

Despite emerging evidence regarding reversible injury following an acute ischaemic insult, there is lack of evidence as to the role of myocardial oedema following non-ischaemic injury, such as may be caused by chemotherapy. Even in ischaemic injury, the adaptive responses of the myocardium differ depending on whether the injury is acute or chronic. Myocardial stunning (usually following acute injury) and myocardial hibernation (often described as myocardial state in a chronically occluded vessel) have varying clinical time course. The aim of any therapy is to prevent irreversible damage, but often revascularisation itself can trigger further injury. Particularly in chronic ischaemic injury, there is limited understanding regarding the interplay

between cellular oxygenation, perfusion and contractile response of the myocardium.

The aim of this thesis are to 1) characterize the role of reversible and irreversible myocardial injury in acute and chronic ischaemic insult and 2) characterize the role of reversible and irreversible myocardial injury in non-ischaemic insult using non-invasive approaches.

The first study presented in this thesis in Chapter 3 explores the relationship between myocardial oedema defining area at risk and myocardial necrosis following an acute ischaemic insult such as anterior ST elevation myocardial infarction. We found that myocardial salvage index (calculated from area at risk) and degree of necrosis were predictive of adverse remodelling and left ventricular (LV) function at 90 days. In a multivariate model only infarct size assessed by late gadolinium enhancement remained the most robust marker for predicting late LV function.

Chapter 4 presents research investigating the relationship between LV dysfunction, myocardial oxygenation/perfusion and presence of scar in a chronically occluded vessel. The interplay between these factors is potentially important for predicting clinical outcome following revascularisation. The key

finding in this chapter is that the blood oxygen level dependent (BOLD) response (measuring myocardial oxygenation) is impaired in hibernating myocardium and that oxygenation improves post revascularisation.

Chapters 5, 6 and 7 detail response of the myocardium to non-ischaemic injury. We use the model of chemotherapy toxicity and study two agents (anthracyclines and trastuzumab), evaluating the different mechanisms by which they affect myocardial function. We then study the effect of these drugs on aortic compliance and distensibility which either directly or indirectly has a bearing on the remodelling observed in the myocardium. In chapter 5, we primarily discuss the effects of these drugs on the myocardium with acute reversible LV injury observed early following administration. We observed that the early functional LV decline, appeared to stabilize at 12 months. Chapter 6 evaluates persistent functional and more severe changes seen in the thinner walled right ventricle (RV) early after administration of these drugs and late (at 12-14 months). Chapter 7 examines changes in the aortic stiffness (using pulse wave velocity and distensibility) and show an acute rise in pulse wave velocity and decline in distensibility following administration of chemotherapy. These changes improve with cessation of potentially cardiotoxic drugs, although do not return to pre therapy levels. Furthermore, more severe changes were seen in the patients receiving anthracylines.

This thesis has led to an improved understanding of the mechanisms and adaptive responses of the myocardium following both acute and chronic ischaemic insult and non-ischaemic insult. Work of this nature may allow potential diagnostic and therapeutic targets as well as allow prediction of response to therapy in patients with these cardiomyopathies.

Declaration

This work contains no material which has been accepted for the award of any other degree or diploma in any university or other tertiary institution and, to the best of my knowledge and belief, contains no material previously published or written by another person, except where due reference has been made in the text.

I give consent to this copy of my thesis, when deposited in the University Library, being available for loan and photocopying, subject to the provisions of the Copyright Act 1968.

I also give permission for the digital version of my thesis to be made available on the web, via the University's digital research repository, the Library catalogue, the Australasian Digital Theses Program and also through web search engines.

Suchi Grover

1st August 2014

Acknowledgements

Over the course of my PhD, I have been fortunate to receive support from many people. I am profoundly grateful to each of these. I must make particular mention of some that have been an integral support over the last 4 years.

Firstly, to my principal supervisors I extend my sincerest gratitude for their guidance and example. Joseph Selvanayagam has been an inspiration, who leads by example and has provided leadership and support over the course of my PhD. Majo Joseph and Jonathan Gleadle, who were my co-supervisors, always provided motivation and encouragement. I have been privileged during my thesis to work with Carmine dePasquale, Bogda Koczwara, Kerry Cheong, Dusan Kotasek,Rohit Joshi and Richard Woodman and hope to continue to build relationships with them in the future. A special mention should be made for Darryl Leong, who has been a friend and mentor over the course of my PhD. I have appreciated his generosity with his time and his encouragement during the last four years.

To my colleagues during my PhD, I am thankful for the experiences I have shared with you, and without your support, this work would not have been possible. I have worked with many individuals across a number of sites in

Adelaide, but must single out Adhiraj Chakrabarty, Pey Wen Lou, Lucas Joerg, Per Lav Madsen, Govindarajan Srinivasan, Rachael Lloyd, Susie Parhnam for their friendship and counsel. I particularly want to thank Craig Bradbrook, Emma Smith, Angela Walls, Charlotte Stoddart, Cherie Ravenand Kylie Hood. Without their dedication, this work would have never reached its final end. Finally Amy Penhall, Rebecca Perry and Lynn Brown were my support in the echo department and I am very thankful to them for their help.

This research was supported by a direct project grant from the National Health and Medical Research Council of Australia and Kai Pharmaceuticals. I would like to thank the MF and MH Joyner scholarship from Flinders University, for my personal financial support without which this research would not have been possible.

Lastly, to my husband Nitish, who has provided a listening ear and laughs especially during the tough times in the course of my PhD. To my son Krish, who came along during this PhD and is too young to appreciate but reminds me about what is most important in life. My parents who have always supported and encouraged me in any endeavour, I have chosen in life. Lastly, my friends and my in laws who have been extremely helpful and have given me confidence, I thank you.

Peer Reviewed Journal Publications

Chapter 1

Grover S, Leong DP, Selvanayagam JB. Evaluation of left ventricular function using cardiac magnetic resonance imaging. J Nucl Card. 2011; 18: 351-365.

Grover S, Srinivasan G, Selvanayagam JB. Evaluation of myocardial viability with cardiac magnetic resonance. Progress in Cardiovascular diseases. 2011; 54(3): 204-14

Grover S, Srinivasan G, Selvanayagam JB. Myocardial Viability Imaging: Does It Still Have a Role in Patient Selection Prior to Coronary Revascularisation? Heart, Lung and Circulation. 2012; 21(8):468-79.

Chapter 3

This manuscript has been submitted to a cardiovascular journal for consideration of publication.

Grover S, Bell G, Lincoff M, Joerg L, Madsen P, Huang S, Low S, Figtree G, Chakrabarty A, Leong DP, Woodman RJ, Selvanayagam JB. Utility of CMR markers of myocardial injury in predicting LV functional recovery: results from PROTECTION AMI CMR sub study.

Chapter 4

This manuscript is in its final draft form, being reviewed by the co-authors and will be sent to a cardiovascular imaging journal for consideration of publication.

Chapter 5 and 6

A shortened version (Letter to the Editor) of this manuscript has been published in International Journal of Cardiology, 2013.

Grover S, Leong DP, Chakrabarty A, Joerg L, Kotasek D, Cheong K, Joshi R, Joseph MX, DePasquale C, Koczwara B, Selvanayagam JB. Left and right ventricular effects of anthracycline and trastuzumab chemotherapy: a prospective study using novel cardiac imaging and biochemical markers. Int J Cardiol. 2013 Oct 15;168(6):5465-7.

Chapter 7

Grover S, Lou PW, Bradbrook C, Cheong K, Kotasek D, Leong DP, Koczwara B, Selvanayagam JB. Early and late changes in markers of aortic stiffness with breast cancer therapy. Internal Medical Journal 2014 (*in* press).

Chapters 8 and 9

This chapter summarizes the main findings of the Thesis and discusses what relevance these findings have for clinical purpose. I will also aim to discuss future applications of this work and how it can be incorporated into our therapeutic strategies.

Abstracts

Grover S, DePasquale C, Cheong K, Penhall A, Joseph M, Koczwara B, Kotasek D, Leong DP, Selvanayagam JB. *The utility of novel cardiac imaging markers in predicting chemotherapy cardiotoxicity*. CSANZ Annual Scientific Meeting 2011.

Grover S, Bell G , Edwards C, Huang S, Leong DP, Joerg L, Lav Madsen P, Low S, Chakrabarty A, Selvanayagam JB. *Correlation of CMR and biochemical markers of myocardial injury in a multi-centre study: PROTECTION AMI CMR sub study.* Society of Cardiovascular Magnetic Resonance Imaging Annual Meeting 2012.

Grover S, DePasquale C, Leong DP, Chakrabarty A, Cheong K, Kotasek D, Joshi R, Penhall A, Joerg L , Joseph M , Koczwara B, Selvanayagam JB. *Early cardiac changes following anthracycline chemotherapy in breast cancer: a prospective study using advanced cardiac imaging and biochemical markers*. Society of Cardiovascular Magnetic Resonance Imaging Annual Meeting 2012.

Grover S, DePasquale C, Leong DP, Chakrabarty A, Cheong K, Kotasek D, Joshi R, Penhall A, Joerg L , Joseph M , Koczwara B, Selvanayagam JB. *Biventricular dysfunction following administration of anthracycline based chemotherapy in breast cancer: a prospective multi-centre study using advanced cardiac imaging and biochemical markers*. ESC Annual Scientific Meeting 2012 (poster).

Grover S, Bell G , Edwards C, Huang S, Leong DP, Joerg L, Lav Madsen P, Low S, Chakrabarty A, Figtree G, Selvanayagam JB. *Correlation of CMR and biochemical markers of myocardial injury in a multi-centre study: PROTECTION AMI CMR sub study*. CSANZ Annual Scientific Meeting 2012 (oral).

Grover S, DePasquale C, Leong DP, Chakrabarty A, Cheong K, Kotasek D, Joshi R, Penhall A, Joerg L , Joseph M , Koczwara B, Selvanayagam JB. *Biventricular dysfunction following administration of anthracycline (AC) chemotherapy in breast cancer: a prospective multi-centre study using advanced cardiac imaging and biochemical markers*. CSANZ Annual Scientific Meeting 2012 (oral).

Grover S, Leong DP, Joerg L, lav Madsen P, Chakrabarty A, Bell G, Selvanayagam JB. *Comparison of left ventricular ejection fraction with*

Multiple- gated acquisition scan and cardiac magnetic resonance in anterior myocardial infarcts. CSANZ Annual Scientific Meeting 2012 (poster).

Grover S, Srinivasan G, Bell G, Edwards C, Huang S, Leong DP, Bridgman C, Chakrabarty A, Figtree G, Selvanayagam JB. *Inter-observer variability for assessment of infarct size in a multi-centre study: PROTECTION AMI CMR sub study*. CSANZ Annual Scientific Meeting 2012 (poster).

Grover S, Srinivasan G, DePasquale C, Leong D, Chakrabarty A, Cheong K, Joshi R, Penhall A, Joseph M, Koczwara B, Selvanayagam JB. *Contemporary Breast Cancer chemotherapy leads to persistent late right ventricular myocardial dysfunction: a prospective multi-centre study*. SCMR 2013 (poster).

Grover S, Srinivasan G, DePasquale C, Leong D, Chakrabarty A, Cheong K, Joshi R, Penhall A, Joseph M, Koczwara B, Selvanayagam JB. *Early and late left ventricular effects of breast cancer chemotherapy: a prospective multi-centre study using advanced cardiac imaging.* SCMR 2013 (poster).

Grover S, Perry R, Leong DP, Joseph MX, Koczwara B, Selvanayagam JB. *Serial monitoring of LV function following chemotherapy: assessment using advanced echocardiography and cardiovascular magnetic resonance.* SCMR 2014 (poster).

Grover S, Leong DP, Bradbrook C, Walls A, Mazhar J, Selvanayagam JB. *Myocardial oxygenation in hibernating myocardium: insights from blood oxygen level dependent imaging pre and post revascularisation.* SCMR 2014 (poster).

Grover S, Leong DP, Bradbrook C, Walls A, Mazhar J, Selvanayagam JB. *Myocardial oxygenation in hibernating myocardium: insights from blood oxygen level dependent imaging pre and post revascularisation.* World Heart Federation's World Congress of Cardiology 2014 (oral).

Table of Contents

LIST OF ABBREVIATIONS

2D	-	two dimensional
3D	-	three dimensional
A	-	anthracycline
A wave	-	late diastolic filling velocity
AA	-	ascending aorta
AAR	-	area at risk
AMI	-	acute myocardial infarction
APEX-AMI	-	Assessment of Pexelizumab in Acute Myocardial Infarction
AHA	-	American Heart Association
AIF	-	arterial input function
ANR	-	artifact to noise ratio
AV	-	atrioventricular
BNP	-	brain natriuretic peptide
BOLD	-	blood oxygen level dependent
BP	-	blood pressure
BSA	-	body surface area
CABG	-	coronary artery bypass grafting
CAD	-	coronary artery disease
CHF	-	congestive heart failure
CK AUC	-	creatinine kinase area under the curve
CK-MB	-	peak CK-myocardial band
CMR	-	cardiovascular magnetic resonance
COPD	-	chronic obstructive pulmonary disease

CTX	-	cardiotoxicity
CV	-	cardiovascular
DBP	-	diastolic blood pressure
DCM	-	dilated cardiomyopathy
DDA	-	distal descending aorta
DICOM	-	digital imaging and communications in medicine
DNA	-	double stranded nucleic acid
DSE	-	dobutamine stress echocardiography
DSMR	-	dobutamine stress magnetic resonance
DT	-	deceleration time
E wave	-	peak early filling velocity
E’	-	pulse wave tissue velocity at the septal mitral annulus
ECG	-	electrocardiogram
EDP	-	end diastolic phase
EDV	-	end diastolic volume
EF	-	ejection fraction
ESP	-	end systolic phase
ESV	-	end systolic volume
FDA	-	food and drug administration
FDG	-	fluorodeoxyglucose
FOV	-	field of view
FWHM	-	full half width maximum
Gd-DTPA	-	gadolinium diethylenetriamine penta-acetic acid
GFR	-	glomerular filtration rate

GRE	-	gradient echo
GLS	-	global longitudinal strain
HEART	-	Heart Failure Revascularisation
HER	-	human epidermal growth factor
HF	-	heart failure
hs-CRP	-	high sensitive C reactive protein
hs-tnt	-	high sensitive troponin T
HR	-	heart rate
IHD	-	ischaemic heart disease
IR-FGE	-	segmented inversion recovery fast spin gradient echo
IV	-	intravenous
LA	-	left atrium
LAD	-	left anterior descending
LGE	-	late gadolinium enhancement
LIMA	-	left internal mammary artery
LLN	-	lower limits of normal
LV	-	left ventricle
LVOT	-	left ventricular outflow tract
MESA	-	Multi-Ethnic study of atherosclerosis
MM	-	myocardial mass
MPRI	-	myocardial perfusion reserve index
MRI	-	magnetic resonance imaging
MSI	-	myocardial salvage index
M:Sk	-	myocardial to skeletal muscle ratio

MV	-	mitral valve
MVO	-	microvascular obstruction
NMR	-	nuclear magnetic resonance
NT-pro-BNP	-	N-terminal B-type natriuretic peptide
PACS	-	Picture Archiving and Communication Systems
PC-CMR	-	phase contrast cardiovascular magnetic resonance
PCI	-	percutaneous coronary intervention
PDA	-	proximal descending aorta
PET	-	positron emission tomography
PPAR2	-	F-18-Fluorodeoxyglucose Positron Emission Tomography Imaging-Assisted Management of Patients With Severe Left Ventricular and Suspected Coronary Disease Dysfunction
PROTECTION-AMI		Selective Inhibition of Delta-protein Kinase C for the Reduction of Infarct Size in Acute Myocardial Infarction
QCA	-	quantitative coronary angiography
RA	-	right atrium
RF	-	radiofrequency
RNA	-	ribonucleic acid
ROI	-	region of interest
RPP	-	rate-pressure product
RV	-	right ventricle
RWM	-	regional wall motion
SA	-	short axis

SAR	-	specific absorption rate
SBP	-	systolic blood pressure
SD	-	standard deviation
SNR	-	signal to noise ratio
SPECT	-	single-photon emission computed tomography
SSFP	-	steady stage free precession
STEMI	-	ST-segment elevation myocardial infarction
STICH-VIABILITY	-	Surgical Treatment For Ischaemic Heart Failure
STIR	-	short-T1 triple inversion recovery
SV	-	stroke volume
T	-	Tesla
Tr	-	trastuzumab
T1	-	longitudinal relaxation
T2	-	transverse relaxation
T2W	-	T2 weighted
TDI	-	tissue Doppler imaging
TE	-	echo time
TI	-	inversion time
Tn I	-	troponin I
TIMI	-	thrombolysis in myocardial infarction
TR	-	repetition time
TTC	-	2,3,5-triphenyltetrazolium chloride
TTE	-	transthoracic echocardiography
VLA	-	vertical long axis

Chapter 1: Introduction

1.1 Myocardial Injury

The sequence of cellular events following an insult on the myocardium, involves a series of steps that finalize in pathophysiological changes seen in end-stage cardiac disease. Although the exact steps may vary depending on whether the insult is ischaemic or non-ischaemic in aetiology; the final pathway leads to alteration of size, shape and function of the ventricle in a process called ventricular remodelling [1]. At molecular and cellular level, changes occur in the myocyte including hypertrophy, alteration in the composition of the interstitial matrix and differential gene expression leading to death of the myocytes by apoptosis or necrosis.

1.1.1 Necrosis and apoptosis

Necrosis refers to destructive, uncontrolled manner of cell death whilst apoptosis is programmed cell death which is highly regulated. Often there is combination of the two pathologies, with ischaemic injury thought to be dominated by necrosis, whereas some non-ischaemic cardiomyopathies have a large degree of programmed cell death. Necrosis is rapid, irreversible process involving swelling of organelles and cells, disruption of mitochondria,

membrane rupture and cell lysis. It additionally damages neighbouring cells causing further destruction. Apoptosis on the other hand is structured energy dependent mechanism which leads to cell death without adjacent injury. It has been demonstrated in hearts of patients with dilated cardiomyopathy and arrhythmogenic right ventricular cardiomyopathy [2-4]. Our current techniques of injury detection can often detect necrotic damage greater than apoptotic harm to the myocardium.

1.2 Reversible Injury

1.2.1 Reversible injury in ischaemic cardiomyopathy

The pathophysiological changes leading to cell death are likely preceded by reversible cellular damage, particularly during ischaemic injury. Several animal studies have shown that myocytes have differential responses to ischaemic injury with subendocardial necrosis occurring after 20 to 40 minutes of temporary occlusion and the subepicardium escaping damage [5, 6]. It has been well documented that human myocardium can withstand brief periods of ischaemia without myocyte death. However with prolonged injury and development of a myocardial infarct, complex inflammatory and healing changes occur in the myocardium, in which dead myocardium is replaced with collagenous scar tissue. Fishbein et al. showed that histologically necrosis and

acute inflammation dominated in the first week, with chronic inflammation peaking in second week and thereon the process of replacement by connective tissue developed [7]. The effects of reperfusion itself can lead to further cascade of events causing more injury to the myocardium. Collectively known as 'reperfusion injury', these pathologies include myocardial stunning, micro vascular and endothelial dysfunction and irreversible cell damage or necrosis [8, 9]. Myocardial stunning (discussed in detail below) is defined as "*prolonged post-ischaemic dysfunction of viable tissue salvaged by reperfusion*" [10-12] and by far is the best established manifestation of reperfusion injury. Reperfusion can also lead to endothelial cell dysfunction causing vasoconstriction, platelet and leucocyte activation and formation of oxidative species that can cause further damage [13]. Rarely, severe micro vascular dysfunction can impair perfusion leading to "no reflow". Finally reperfusion may cause myocyte death, usually in severely ischaemic myocardium, and result in contraction band necrosis driven by influx of reperfusion derived calcium into myocytes. Limiting reperfusion injury has been the target of many recent studies [14-17].

1.2.2 Stunned and Hibernating myocardium

Injured myocardium as a consequence of prolonged ischaemia triggers a cascade of events that usually terminates in myocardial cell death (necrosis). However, the outcome of ischaemic injury in the typical clinical setting is

more complicated and sometimes may lead to reversible myocardial dysfunction. This dynamic state of the myocardium involves two separate, but possibly interrelated, entities – myocardial 'stunning' and 'hibernation'. Stunning, originally described by Heyndrickx et al., is reversible contractile dysfunction that occurs in the presence of restored coronary blood supply, following a brief period of coronary occlusion [12, 18]. In contrast, hibernating myocardium has been defined as a state of down-regulated contractile function in non-infarcted myocardium in the setting of severe coronary stenosis that improves after revascularisation [12, 18, 19]. Depending upon the clinical scenario, reversible myocardial dysfunction may arise from a combination of both these two factors. For example, in the immediate post acute myocardial infarction (AMI) phase and following successful reperfusion therapy, myocardial stunning may predominate [19-21]. Contractile recovery in this "stunned" state may occur spontaneously many weeks to months after restoration of a normal blood supply to the previously ischaemic myocardium [12, 22, 23]. Conversely, a substantial amount of hibernating myocardium may be found in up to 50% of patients with ischaemic cardiomyopathy [24, 25]. Importantly, hibernating myocardium requires the restoration of a normal blood supply for an improvement in contractile function; global increases in left ventricular (LV) ejection fraction following coronary artery bypass grafting may be seen in as many as 40% of patients with ischaemic cardiomyopathy [26].

The pathogenesis of hibernating myocardium is controversial. It is postulated that chronic ischaemia leads to down-regulation of contractile proteins [27-29], with abnormalities seen in metabolic and structural component of myocytes. Resting myocardial blood flow has been shown to be reduced in hibernating segments by 20-30% in earlier studies [30, 31] and up-to 40% using quantitative first pass cardiovascular magnetic resonance (CMR) perfusion imaging [29]. In contrast, studies involving positron emission tomography (PET) have suggested that regional perfusion and oxidative mechanisms may be *preserved* in hibernating segments [32-34]. Regardless of resting myocardial blood flow, it is generally agreed that coronary flow reserve is reduced in hibernating myocardium. Given the mismatch in myocardial contractility and flow, it is likely that repetitive stunning is a component of hibernation [12, 34]. Animal models have shown that chronic episodes of myocardial stunning may not permit full recovery and histological changes involving glycogen deposition and myolysis, traditionally seen with hibernating myocardium may occur [35]. It is likely, then, that myocardial stunning and hibernation represent a spectrum of a similar disease process.

1.2.3 Reversible injury in non-ischaemic cardiomyopathy

Non-ischaemic cardiomyopathy can be insidious in onset and hence acute reversible injury may be difficult to define. Recurrent or chronic myocarditis is considered a potential cause for development of dilated

cardiomyopathy (DCM). Hence inflammatory injury may be a possible mechanism for the observed ventricular changes in patients with DCM. Such inflammatory changes have been described following chemotherapy agents such as anthracylines as documented by CMR [36], however once the toxicity is established, changes are largely irreversible. Trastuzumab on the other hand, which is part of treatment of HER2 positive breast cancer, has a cardiomyopathy which may be largely reversible after cessation of the drug, particularly in the early stages. On biopsy, there have not been any ultra structural changes described [37] which is in contrast to anthracylines which have significant histological changes [38] (discussed in detail later).

1.3 Ischaemic Cardiomyopathy: Burden of disease

Cardiovascular disease dominates our national health profile, causing 3.2 million deaths (stroke and myocardial infarction) in 2004 [39]. Although mortality for the acute event has improved, significant burden on our community persists with chronic morbidity and loss of quality of life. The chain of events following an acute myocardial infarction, culminate in reversible or irreversible injury via the mechanisms described earlier.

The term ‘ischaemic cardiomyopathy’ refers to significant LV dysfunction (ejection fraction <40%) caused by coronary artery disease on coronary

angiography, as defined by a review of 1921 patients with symptomatic heart failure [40]. Therefore it encompasses patients with heart failure with a previous diagnosis of myocardial infarction or significant disease on angiography whether it is chronic (hibernating myocardium) or acute (stunned myocardium).

1.3.1 Clinical Relevance of Myocardial Viability

The presence of viable myocardium is one of the key determinants for revascularisation, based on a large collection of observational data that have evaluated viability testing in ischaemic cardiomyopathy and its role in clinical practice. In patients with LV ejection fraction (EF) below 35%, the peri-operative, in-hospital and one-year outcome is better when the need for revascularisation is guided by pre-operative assessment of viability and hibernation [41]. In patients being considered for cardiac transplantation, viability assessment can alter the ultimate choice of treatment (medical, revascularisation, or transplantation) in 57% of cases [42]. Allman et al. conducted a meta-analysis in 2002 that incorporated 24 studies using thallium-201 single-photon-emission computed tomography (SPECT) and dobutamine stress echocardiography (DSE) and showed the potential benefit of identifying viable myocardium in patients with LV dysfunction [43]. However this was conducted using observational and retrospective studies, as no randomized evidence was available at that time.

Three recent studies, PPAR-2 (F-18-Fluorodeoxyglucose Positron Emission Tomography Imaging-Assisted Management of Patients With Severe Left Ventricular Dysfunction and Suspected Coronary Disease) [44], HEART (Heart Failure Revascularisation) [45] and STICH-VIABILITY (Surgical Treatment For Ischaemic Heart Failure) [46] provided randomized evidence as to the role of revascularisation in patients with chronic ischaemic LV dysfunction and of viability testing in this population. The first to report, PPAR-2, evaluated a fluorodeoxyglucose PET based approach versus standard care, and although it failed to show significant difference between the two populations, a post-hoc sub-study suggested benefit in PET guided approach in centers with expertise in performing the tests [47]. The HEART study, evaluated patients with heart failure, coronary artery disease, and a LV ejection fraction < 35%, who had a substantial volume of viable myocardium with contractile dysfunction assessed by any standard imaging technique and randomly assigned them to a conservative versus an invasive strategy [45]. This study failed to show significant difference between the two groups but was subject to substantial limitations with patient recruitment.

In the STICH (main) study, 1212 patients with an ejection fraction of less than 35% and coronary disease amenable to coronary-artery bypass grafting (CABG) were randomly assigned to receive optimal medical therapy for heart failure and coronary disease (602 patients) or to receive optimal medical therapy plus CABG (610 patients). In the primary end point of death from any

cause, the study outcomes were negative: there was no significant difference in the rate of death from any cause between the two study groups. As expected, there was an early hazard to CABG that abated over 2 years. CABG was effective in significantly reducing the major secondary end points of the rate of death from cardiovascular causes and the rate of a composite of death or hospitalization. Published at the same time as the main study, the STICH-VIABILITY trial reported on 602 patients from within the main STICH trial whom underwent viability testing, using either SPECT, DSE, or both to assess myocardial viability on the basis of pre-specified thresholds. The study demonstrated that whilst presence of viable myocardium was associated with a greater likelihood of survival in patients with coronary artery disease and LV dysfunction, this relationship was not significant after adjustment for other baseline variables, such as LV end diastolic volume and ejection fraction.

Overall, the assessment of myocardial viability did not identify patients with a differential survival benefit from CABG, as compared with medical therapy alone. The results of this sub-study contradict the large body of observational evidence and, on first glance, seem counter-intuitive. However, several caveats need to be considered when evaluating the trial conclusions. Firstly, viability testing was not mandated or performed in a randomized manner but, rather, at the discretion of the investigators, depending on the availability of the test and other factors. This introduces substantial bias. The authors note that there were clinical differences between patients who were tested and those who

were not tested. Moreover, viability testing was performed utilizing SPECT and DSE which relay different information and other techniques such as PET and late gadolinium enhancements (LGE)-CMR were not used. Hence, although the STICH-VIABILITY study provides the largest patient cohort to-date in this area from a single study, the study conclusions need to be viewed with some caution.

1.4 Non-ischaemic cardiomyopathy: Burden of disease

Cardiomyopathies are diseases of the myocardium associated with cardiac dysfunction. Non-ischaemic cardiomyopathy encompasses a heterogeneous cohort excluding those with significant coronary artery disease. For the remainder of this chapter, we focus on non-ischaemic dilated cardiomyopathy which is the end result of many cardiac disease states including following toxic insult such as chemotherapy.

1.4.1 Dilated cardiomyopathy

DCM is a syndrome characterized by cardiac enlargement and systolic dysfunction. Histologically, there is interstitial and perivascular fibrosis noted, particularly involving the LV sub-endocardium. Myocytes vary in size, with some being hypertrophied, whilst others are atrophied. Although there are

multiple causative factors, nearly 50% are considered idiopathic [48], in which a significant proportion are likely familial. It is also considered to be the final common pathway that is the end-result of myocardial damage produced by a variety of agents including chemotherapy.

1.4.2 Chemotherapy Cardiotoxicity

Over the last 20 years, there has been a significant improvement in survival rate following chemotherapy which has come at a price, largely due to cardiotoxicity. Two types of cardiotoxicity occur, type I which is sinister and irreversible (anthracyline) and type 2 which is largely considered reversible (trastuzumab). Both agents are typically used in the treatment of breast cancer.

Breast cancer is the second most common form of cancer and the leading cause of death caused by malignancy in women. Breast cancer treatment is usually a multi-pronged approach. Breast cancer treatment plans involve surgery, chemotherapy, radiation, and hormonal therapy. In addition, approximately 20% of patients receive targeted therapy.

The treatment choice is dependent on hormone status (whether the tumour is stimulated to grow by oestrogen and progesterone) and whether the tumour over-expresses human epidermal growth factor receptor 2 (HER2) and can be treated with the HER2 receptor antagonist trastuzumab (Herceptin®).

1.4.2.1 Anthracylines

Anthracycline is an essential component of breast cancer treatment, and its use in combination regimens as adjuvant therapy is the standard of care for most women with early-stage disease [49]. In breast cancer two anthracyclines are generally used: doxorubicin and epirubicin, a semi synthetic derivative of doxorubicin. They contribute to the gold standard adjuvant therapy for breast cancer, and in metastatic disease they provide for improved response rate, time to disease progression, and overall survival [50]. The therapeutic activity of an anthracycline is mediated by its insertion into the double stranded nucleic acid (DNA) of replicating cells and its inhibition of topoisomerase II enzyme, thereby preventing DNA and ribonucleic acid (RNA) synthesis [51].

The cardiac toxicity of anthracyclines is well-known. Although clinical manifestations are rare, treatment with anthracyclines can lead to important cardiovascular complications.

The acute form occurs during the infusion or within the week and is often reversible with cessation of treatment, and has no predictive value for the future. Early-onset cardiotoxicity can occur within 1 year after anthracycline treatment, however the peak incidence is 3 months after the last anthracycline dose and mortality in these patients is high [52]. However, late cardiac anthracycline toxicity is the leading limiting factor in its use [53], especially in patients in whom this is used for curative or adjuvant purposes. Left ventricular dysfunction and congestive heart failure (CHF) may develop long after anthracycline therapy ends. Prolonged follow up, requiring serial cardiac imaging, is indicated even in asymptomatic patients.

1.4.2.2 Trastuzumab

Trastuzumab, a monoclonal antibody directed against the human epidermal growth factor 2 receptor, works on both the extracellular and the intracellular domains of the HER2 receptor [54-57] and continuously suppresses HER2 activity that otherwise may lead to tumor proliferation. Trastuzumab administration can result in sub-clinical and clinical CHF. The incidence and severity of LV cardiac dysfunction is highest in patients who receive trastuzumab concurrently with anthracycline-containing chemotherapy. Thus monitoring of LV function before, during and after treatment is mandatory.

1.4.2.3 Combined cardiotoxicity of anthracylines and trastuzumab

The combined toxic effect of trastuzumab and anthracyclines in long-term survivors of cancers can lead to increased rates of cardiac morbidity and mortality perhaps even with a supra-additive effect. Therefore it remains a persistent problem in cancer survivors leading to discontinuation of chemotherapy. Chemotherapy induced cardiomyopathy is treated according to the standard guidelines for CHF with LV dysfunction, by angiotensin converting enzyme inhibitors, beta blockers and diuretics.

Identification of patients at risk, prevention, early diagnosis, and effective treatment are all important goals. Most of these needs have been addressed by uncontrolled or small studies, and guidelines have relatively sparse information on which to base recommendations for care, other than careful monitoring of LV function and interrupting or discontinuing anthracyclines once significant decrease in LV ejection fraction is detected. At this point in time, however it is often too late [58].

1.4.2.4 Mechanisms of anthracycline and trastuzumab toxicity

The etiology of trastuzumab and anthracycline-induced cardiotoxicity is still not fully understood. Myocardial changes following anthracycline treatment include myocardial cell loss by necrosis or apoptosis, myofibrillar loss, distention of the sarcoplasmic reticulum, and mitochondrial swelling [59]. One hypothesis for doxorubicin-induced cardiotoxicity is that doxorubicin differentially increases reactive oxygen species within cardiac myocyte mitochondria, as compared to other tissues. Anthracyclines can induce the generation of oxygen-derived free radicals through two main pathways: a non-enzymatic pathway that utilizes iron, and an enzymatic mechanism using the mitochondrial respiratory chain. Free radicals are highly toxic, and can cause direct damage to proteins, lipids, and DNA. Adult myocytes are more susceptible, because myocytes are terminally differentiated and can not sufficiently replace cells damaged during treatment. Administering doxorubicin in humans results in an elevation of plasma and products of lipid peroxidation, and a decrease in plasma and tissue antioxidant levels. The level of doxorubicin-induced oxidative stress is up to 10 times greater in the heart than in other organs as liver, kidney, and spleen. The experience from concurrent anthracycline and trastuzumab therapy in metastatic breast cancer has triggered further research into the molecular mechanism of anthracycline induced cardiotoxicity. Gene targeting studies in mice show that HER2, a

proto-oncogene and a member of the erbB family of transmembrane tyrosine kinases, is essential for cardiac development, and conditional deletion of HER2 leads to the development of a dilated cardiomyopathy. In mice deficient in HER2 protein (or its associated ligand, neuregulin, a paracrine peptide messenger that activates HER2) the induction of cardiac stress pathways by an anthracycline promotes the onset of LV dysfunction. These results have provided an explanation for the increased cardiotoxicity observed with concurrent administration of anthracycline and trastuzumab [60, 61]. We are still unclear as to why the cardiotoxicity seen with trastuzumab alone is largely reversible, whilst it potentiates the more persistent cardiomyopathy seen with anthracyclines. Cardiac biopsies on patients with trastuzumab alone, show no evidence of irreversible ultra structural changes on pathology [37], while histological changes seen with anthracycline include myofibril loss, changes in contractile elements and mitochondrial and nuclear degeneration [38].

Further understanding into their mechanism was provided by a recent prospective study of 53 patients with early breast cancer, in which biomarkers were studied in conjunction with function analysis. Although the toxic effect of chemotherapy correlated with rise in troponin I (TnI) and brain naturietic peptide (BNP) at month 1; raised TnI levels at one month failed to demonstrate a relationship to cardiac outcome long term [62]. This could imply that TnI increase at the month 1 is related to the acute toxic injury, perhaps secondary to a ‘myocarditis’ caused by the chemotherapy agent, rather

than reflecting permanent damage as is seen in an infarct setting. They also showed that a raised BNP at baseline and month 1 was more likely to predict cardiac dysfunction [62]. BNP reflects myocyte tension and stretch, likely indicating that structural changes have occurred in the ventricle. It is also thought that perhaps persistent neurohormonal changes may occur with chemotherapy leading to adverse ventricular remodelling. The study failed to be conclusive due to limitations in numbers, but raises important concerns, as to what changes occur at the signaling/cellular level that lead some patients to develop cardiotoxicity and others to be spared. With no clear answer, the current practice with trastuzumab is, to serially monitor patients with LV EF assessments and delay their treatment until the function recovers/stabilizes.

1.4.2.5 Chemotherapy and Aortic Stiffness

One of the mechanisms proposed for the observed increase in CV events of cancer survivors is thought to be due to increased aortic stiffness. Adult vessels stiffen with age and diseased vessels are likely to have greater stiffness than healthy vessels. It has been demonstrated in human and animal studies that non-invasive measurement of aortic stiffness correlates with atherosclerosis found at necropsy [63]. Furthermore aortic atherosclerosis is thought to precede coronary atherosclerosis. Anthracyclines in particular may influence aortic stiffness, potentially due to increase in toxic oxygen free radicals and oxidative stress. This in turn may lead to abnormal endothelial

function, act as a stimulus for LV hypertrophy and reduced perfusion as a potential mechanism for the increase in CV events.

1.4.2.6 Risk factors for chemotherapy- induced cardiomyopathy

A number of risk factors for the development of chemotherapy-induced cardiotoxicity have been identified:

- dose
- age
- radiation therapy
- pre-existing cardiac risk factors
    - hypertension
    - hyperlipidemia
    - smoking (current or previous)
    - family history of ischaemic heart disease
    - diabetes mellitus

However, while some of these are known risk factors for the development of CHF in the general population, it is unclear from most studies whether they

potentiate the effects of anthracyclines or whether their effects are simply additive. A high cumulative anthracycline dose is the most recognized risk factor for cardiac damage and remains the best predictor of subsequent cardiac dysfunction. The estimated percentage of patients who developed CHF at a dose of 400 mg/m^2 was 3%, increasing to 7% at 550 mg/m^2, and to 18% at 700 mg/m^2. This led to a recommended limit on lifetime cumulative doxorubicin dose of 450 to 550 mg/m^2 [64]. Chemotherapy-induced cardiotoxicity may be more pronounced with advancing age [64]. In a retrospective analysis of three clinical trials involving 630 patients who were treated with doxorubicin, Swain and colleagues showed that patients more than 65 years old are more than twice likely to experience anthracycline-induced CHF compared with patients less than 65 years old. But the effect is only pronounced after a cumulative dose of 400 mg/m^2 [65, 66]. In the Danish study of metastatic breast cancer patients treated with epirubicin, Ryberg and colleagues showed that age at the start of epirubicin treatment had a significant association with risk of cardiotoxicity with the rate increasing by 29% for every 10 years of age [67]. People with preexisting cardiovascular risk factors are at increased risk for developing CHF in the absence of anthracycline therapy. Therefore, it is important to evaluate cardiotoxicity in the context of these cardiac risk factors and to understand how they interact with the treatment. In the study by Ryberg et al. cardiotoxicity was approximately three-fold higher in patients with a condition predisposing to heart disease (hypertension, diabetes, obesity, thyrotoxicosis, and chronic obstructive lung disease), independent of the

cumulative dose of epirubicin [67]. Other studies have suggested that patients with previous cardiac disease (coronary, valvular, or myocardial) and hypertension may have an increased risk of developing CHF when treated with an anthracycline [68, 69].

1.5 Assessment of myocardial function and injury

The ability to accurately assess myocardial function and injury pre and post revascularisation or following a toxic insult is of significant clinical importance. Non-invasive imaging of the left ventricle plays a vital role in the evaluation of most cardiac disease states. LV imaging may permit diagnosis of myocardial, coronary, and valvular pathology; provide prognostic information for patients with known cardiovascular disease; and allow monitoring response to therapy.

1.5.1 Assessment of myocardial function and injury with Cardiovascular Magnetic Resonance

CMR is considered the gold standard in the evaluation of volumes, mass and systolic function of both normal and abnormal left ventricles, owing to its high spatial resolution, excellent signal-to-noise ratio, and its ability to image the heart in a three-dimensional manner. CMR-based assessment of LV function

has both diagnostic and prognostic utility in patient evaluation [70]. During the same scan, information on myocardial fibrosis, viability, perfusion and valvular function can be ascertained, affording considerable versatility in patient assessment.

1.5.1.1 Background

First to independently describe the nuclear magnetic resonance (NMR) phenomenon in 1946, Bloch [71] and Purcell [72] shared the Nobel prize for its discovery. It took another 30 years before magnetic field gradients were used to encode the spatial distribution of nuclear spins and integrated to generate a 2D image from the NMR signal.

1.5.1.2 Generating the nuclear magnetic resonance signal

Magnetic resonance relies on a phenomenon called nuclear spin which is an intrinsic property of atoms with an odd number of protons or neutrons such as Hydrogen. Other atoms capable of this ability include Phosphorous, Sodium and Carbon. As hydrogen is the most prevalent atom (67%) in the human body, we use its intrinsic property for performing clinical magnetic resonance imaging (MRI). When placed in an external magnetic field, nuclear spins align themselves with the external field and rotate (precess) at a certain

frequency, known as the resonance frequency. The precession frequency (Larmor frequency) is determined by the type of atomic nucleus and strength of the magnetic field. The Larmor equation is

$$\omega_0 = \gamma B_0$$

ω = precession/resonance frequency

γ = gyromagnetic ratio

B_0 = external magnetic field

For hydrogen nuclei, the Larmor frequency is 42.56 MHz per tesla (T). Within a three dimensional (3D) space of the voxel in the body, the z axis is defined as being in the direction of the external magnetic field and xy-plane is 90 degrees to the z axis. Net magnetization is aligned with z axis and known as longitudinal magnetization. The protons spins precess out of phase with one another reducing the net magnetization in the xy-plane to 0, known as the transverse magnetization.

Nuclear magnetic resonance relies on the protons absorbing energy from radiofrequency (RF) radiation at a specific frequency when placed in a magnetic field. The absorption of RF radiation causes the protons to change

equilibrium, leading to detection of a 'faint' electrical signal by coils placed close to the patient. This signal is processed to form an image. For energy absorption to occur, the frequency of the delivered RF pulse must equal the resonance frequency. The more energy the RF pulse has and the longer its duration, the more the net magnetization will tilt or flip. The final angle made by the net magnetization with reference to the z axis is known as the flip angle (α).

1.5.1.3 Relaxation

Application of a 90 degree RF pulse causes the protons to lose their equilibrium. Their return to their original equilibrium is known as relaxation. There are two independent relaxation processes that occur simultaneously: recovery of longitudinal magnetization (known as spin-lattice, T1) and loss of transverse magnetization (known as spin-spin, T2). T1 relaxation times are dependent on the field strength of the external magnetic field, whilst T2 relaxation times are largely independent of the magnetic field. The differences in T1 and T2 relaxation times in different tissues are an important source of contrast (shades of grey) in MRI. Furthermore, images can be weighted to show differences predominantly due to T1 and T2 relaxation processes.

1.5.1.4 Creating magnetic resonance images

The final image created in MRI is a combination of a signal received from specific position in the body. This is largely dependent on proton density, T1 relaxation, T2 relaxation and any modification of the signal caused by motion. Every magnetic resonance image contains both T1 and T2 information, however by choosing the timing and length of the RF pulse, one particularly property can be highlighted. Additional magnetic fields can be used to generate detectable signals from particular locations in the body (known as spatial excitation) or cause them to precess at different frequencies. This data is deciphered using a two dimensional (2D) Fourier transformation and used to fill lines in a planar matrix known as *K* space. *K* space often referred to the 'temporary image space' in which complex values are encoded during MRI data acquisition based on pre-meditated pulse sequences. The image is then reconstructed using inverse Fourier transformation applications.

1.5.1.5 Image Contrast

One of the greatest advantages of MRI is its ability to differentiate between different soft tissues which can be widely manipulated. In a typical image acquisition the basic unit of each sequence (i.e. the 90°-180°-signal detection)

is repeated hundreds of times over. The weighting of the received image signal is dependent on the time intervened between RF excitation pulse and the acquisition, known as echo time (TE) and repetition time (TR) i.e. the time between successive 90° pulses. For example if a long TE is used, inherent differences in T2 times of tissues will become apparent. Tissues with a long T2 (e.g. water) will take longer to decay and their signal will be greater (or appear brighter in the image) than the signal from tissue with a short T2 (fat). In a similar manner TR governs T1 contrast. Tissues with a long TR (water) will take a long time to recover back to the equilibrium magnetization value, so therefore a short TR interval will make this tissue appear dark compared to tissue with a short T1 (fat). When TE and TR are chosen to minimize both these weightings, the signal contrast is only derived from the number or density of spins in a given tissue. This image is said to be 'proton-density weighted'.

1.6 Defining myocardial function with CMR

CMR, is highly superior to 2D echocardiography when examining global LV function [73] and allows for follow-up of patients in a temporal manner without cumulative radiation exposure. Its accuracy and reproducibility in the evaluation of volumes, function and mass, makes it the standard of reference for all imaging modalities [74-77]. As well as documenting LV function at a

single time point, it can be used to assess progressive cardiac remodelling, which is of clinical significance in patients with LV dysfunction.

Cine images acquired using steady state free precession (SSFP) sequences allow for superior blood-myocardium delineation, aiding in the accurate calculation of volumes and mass. Visual inspection of left and right ventricular (RV) architecture aids in assessing areas of regional hypokinesis, regional or global wall thinning and asymmetric or concentric hypertrophy. Furthermore measurement of end-diastolic wall thickness, using cine images has been shown to have utility in assessing viability [78, 79]. An end-diastolic LV wall thickness of <6mm by echocardiography [78] and more recently <5.5 mm by CMR [79, 80] predicts poor likelihood of myocardial viability.

1.7 Defining myocardial injury with CMR

In addition for its accuracy and reproducibility, one of the main advantages of CMR is its ability to characterise tissue. This was significantly revolutionized by the use of paramagnetic contrast agents such as gadolinium diethylenetriamine penta-acetic acid (Gd-DTPA). In use since 1984, Gd-DTPA is an extra-cellular contrast agent which is rapidly redistributed into extracellular space. Rehwald et al. noted significantly higher concentrations of Gd-DTPA in areas of expansion of extracellular space (up to 400%). This was examined in several disease states including infarction and oedema [81].

Administration of Gd-DTPA reduces the T1 relaxation times in acute and chronic myocardial infarcts and this property is exploited by MR-infarct imaging. Any T1-weighted MR sequence can highlight differences in normal and infarcted tissue and this is exaggerated by application of an inversion prepulse that nulls the signal from normal myocardium. The two most common sequences using this technique are segmented inversion recovery fast spin gradient echo (IR-FGE) and turboFLASH (segmented inversion recovery fast gradient echo sequence with Fast Low Angle Shot). In addition to nulling the myocardium, they produce visible T1 signal in areas of high Gd-DTPA concentration. Kim et al. showed direct correlation of areas of hyperenhancement on late gadolinium imaging and histopathology specimens [82]. Furthermore, this technique was comparable to PET [83] and superior to SPECT [84].

1.7.1 Assessment of myocardial viability with CMR

Two CMR techniques are currently used for the assessment of myocardial viability. Late gadolinium cardiovascular magnetic resonance (LGE-CMR), a technique unique to CMR, that defines the transmural extent of scar, and dobutamine stress CMR (DSMR), a method analogous to dobutamine echocardiography that measures the contractile reserve of dysfunctional myocardium and is interpreted by visual analysis. Tables 2.1 and 2.2 summarize the performance of these various CMR techniques to predict recovery of function post-revascularisation.

1.7.1.1 Late gadolinium enhancement CMR

This is defined as regions of increased image intensity on T1 weighted images using a segmented inversion recovery fast gradient echo sequence, acquired more than five minutes after the intravenous administration of a gadolinium based contrast agent. Using this new sequence, signal intensity differences of nearly 500% have been identified between irreversibly injured (scar, myo-necrosis) and normal myocardium [82, 85, 86]. Examples of LGE-CMR are shown in figures 1.1-1.5.

Animal studies support the notion that the hyper-enhanced regions (in the setting of coronary disease/occlusion) correspond to areas that have sustained irreversible ischaemic injury. Kim et al. reported the seminal study describing LGE-CMR in a canine heart model, where the left anterior descending artery was instrumented and occluded. LGE-CMR of the explanted hearts was compared with 2,3,5-triphenyltetrazolium chloride (TTC) stained pathology (the histological 'gold standard' of myocardial necrosis) at 1 day, 3 days, or 8 weeks after instrumentation, with near perfect correlation demonstrated between hyperenhancement on LGE-CMR and histopathology [82].

These findings then laid the foundation for subsequent clinical studies that demonstrated that the extent of LGE on a segmental basis is a crucial determinant of recovery of myocardial wall thickening, both in the setting of

acute (but probably not in the very early post MI period-see below) and chronic myocardial injury. Choi et al. studied 24 patients (presenting with their first myocardial infarction) with LGE-CMR performed within a week of the acute event. They found that the best predictor of global improvement at 2 to 3 months was the extent of dysfunctional myocardium without any or with <25% hyperenhancement [87]. These findings were replicated by Gerber et al. in 20 patients, when they found that the absence of hyperenhancement in dysfunctional segments had a sensitivity of 82% for predicting contractile recovery [88]. Beek et al. further highlighted the relationship between LGE, segmental wall thickening and segmental extent of hyper-enhancement in 30 patients following an acute reperfused MI [89]. The study showed that extent of hyper-enhancement at *7 days* following infarct predicted likelihood of functional improvement in stunned myocardium at 13 +/-3 weeks. However, they also demonstrated that 25% of segments with transmural hyper-enhancement had the tendency for functional improvement at 13 weeks. Dall'armellina et al. have recently defined dynamic changes in the extent of T2 oedema imaging and LGE by performing serial CMR scans in 30 patients with acutely reperfused STEMI [90]. They established that myocardial oedema is maximal and constant over the first week after myocardial infarction, providing a stable window for the retrospective evaluation of area at risk. Importantly, the extent of LGE *seen at 12-48 hours* was a weak predictor of functional recovery at 6 months. Unfortunately, although oedema imaging was performed at 5-7 days, LGE was not done at this time point in

this study, and hence one cannot directly compare the LGE findings of this study with the earlier studies. Nevertheless, the results underscore the need for caution when using LGE very early (<48 hours) after myocardial injury as a marker of myocardial salvage.

In the setting of chronic ischaemic cardiomyopathy, to date there have been two clinical studies examining the utility of the transmural extent of LGE in predicting recovery of contractile function. The first was performed by the Kim group [91] in a cohort of 41 patients undergoing revascularisation by either percutaneous transluminal coronary angioplasty or CABG. They found that the likelihood of improvement in regional function after revascularisation decreased progressively as the transmural extent of LGE before revascularisation increased. These same authors reported regional functional improvement rates at 3 months of 78% in segments without LGE, 59% in segments with 1-25% LGE, and 2% in segments with > 75% LGE. This was subsequently confirmed in a study from Selvanayagam et al., which exclusively examined patients after surgical revascularisation [92]. This study found regional function improved in 82% of segments with no pre-existing LGE, 64% of segments with 1-25% LGE, and 37% of segments with 26-50% LGE. The percentage of segments (with no, or <25% LGE) demonstrating improved regional function in this study was slightly higher than that observed by Kim et al., and may be closer to the true rate of functional recovery, since the follow up scan was at 6 rather than at 3 months after revascularisation as in

Kim et al. study. When only segments with severe pre-operative dysfunction (i.e. severe hypokinesia, dyskinesia, or akinesia) were considered in this study, the positive and negative predictive values were higher, at 81% and 72%, respectively. The ability of LGE-CMR to evaluate those segments that have severe dysfunction prior to surgery (and often the most difficult to evaluate with other imaging techniques) with high diagnostic accuracy is a major strength of this technique.

One of the key determinants of prognosis in ischaemic heart disease is LV end-diastolic volume and ejection fraction [93]. Kim et al. utilizing LGE-CMR [91], and Rizello et al. employing DSE [94], have shown a linear relationship between number of viable segments pre-revascularisation and change in LV ejection fraction post-revascularisation. Pegg et al. have recently elegantly demonstrated that the sum of normal plus viable segments of greater than 10 on a 16 segment American Heart Association model will accurately predict increase in LV ejection fraction. Fifty patients underwent CMR to assess LV function and viability before and 6 months after CABG. Viability was defined as transmural hyperenhancement of <50% (i.e. a binary variable) and the presence of 10 or more viable or normal segments predicted a gain of 3% in LV ejection fraction with a sensitivity and specificity of 95% and 75% respectively [95]. The authors also demonstrated that transmural viability cut-offs of <25% or >75% and a cut-off of >4 viable segments were less useful predictors of global LV recovery.

1.7.1.2 Dobutamine Stress CMR (DSMR)

Given its ability to visualize myocardial segments accurately, CMR can be used to define ventricular function during pharmacological stress, principally with dobutamine (DSMR). Although DSMR imaging has been performed since 1992 [96], early studies to document inducible myocardial ischaemia were limited by an inability to image the entire cardiac cycle during peak stress and concerns about patient safety. Recent software and hardware advances have enabled investigators to overcome some of these limitations. Shorter repetition times, phase encoding grouping and phased array surface coils allow for acquisition of images with high temporal resolution and with spatial resolution sufficient to delineate the endocardial border during peak stress [97]. Earlier concerns of patient safety have been alleviated by the introduction of haemodynamic monitoring and wall motion display software that allows the physician to safely monitor patients during stress testing.

Similar to DSE, a lack of increase in either wall motion or systolic wall thickening, a reduction of both, or significant changes in the rotational pattern of LV myocardium ("tethering") with increasing dobutamine dose are indicative of pathological findings. Nine studies with 250 patients using DSMR to predict recovery of function have been published with a mean sensitivity of 74% (range 50–89%) and a mean specificity of 84% (range 70–

95%). Hence, DSMR has a high specificity with a marginally lower sensitivity, compared to nuclear techniques.

More recently, the efficacy of DSMR has been enhanced by employing myocardial tagging. Geskin et al., explored the addition of myocardial tagging, signifying that improvement in the midwall and subepicardium circumferential shortening predicted future functional recovery of the left ventricle after revascularisation [98]. Similar results have been demonstrated in single vessel disease, one week after successful reperfusion of anterior infarcts [99]. Traditionally DSE has been the established tool for evaluation of contractile reserve and several studies have compared these two modalities with and without tagging. Results indicate increased sensitivity and slightly lower specificity for DSMR with tagging as compared to DSE, signifying accuracy of 78% for DSMR and 72% for DSE [100].

1.7.1.3 Combined LGE-CMR and DSMR

The ability of CMR to assess both scar and contractile reserve can potentially be utilized in a combined LGE-CMR and low dose DSMR protocol. Kaandorp et al. tested this hypothesis in 48 patients with ischaemic cardiomyopathy and found that 61% of segments with an intermediate extent (51 -75%) of scar tissue on CMR had contractile reserve and 39% lack

contractile reserve [101]. They concluded that in these segments, low-dose DSMR might be required to optimally define the likelihood of functional recovery following revascularisation. However, this study did not provide follow-up functional imaging after revascularisation and hence, cannot directly assess the usefulness of the combined approach for viability determination.

More recently, a number of studies have confirmed the utility of accompanying contractile reserve appraisal in addition to LGE, particularly in patients with intermediate transmural hyperenhancement [102-105]. Bove et al. highlighted that a normal dobutamine response to a 1% to 50% transmural hyperenhancement aided in establishing viability in these segments [104]. In a prospectively designed study pre and post CABG, subjects underwent LGE and the group with intermediate transmurality (i.e. 1 to 50%) was subject to a low dose dobutamine CMR examination. In this particular cohort, the predictive capacity of LGE lies between 40 and 60% [91]. It is in this intermediate range (25-75%), that the addition of low dose dobutamine has shown utility, albeit at the cost of performing a slightly more complex examination.

1.7.1.4 Stress Imaging

The development of rapid gradient systems and hence short measurement times, allows high resolution cine imaging during rest and stress. This technique is particularly utilized in dobutamine stress CMR, in which imaging at heart rates of 200 can be performed. For the remainder of this chapter, we will focus on first pass perfusion imaging with gadolinium as was utilized in our subsequent clinical work.

1.7.1.5 First pass perfusion

This technique relies on imaging in multiple planes at every R-R interval to track an intravenous bolus of contrast dynamically as it courses through cardiac chambers and into the myocardium. It utilizes a T1-weighted protocol, in which the myocardium appears dark until the contrast arrives via blood flow or perfusion. Analysis is performed using qualitative, semi-quantitative or fully quantitative methods. Clinically, qualitative analysis is considered adequate. Quantitative analysis can be obtained via deconvolution methods [106] and compartmental analysis [107]. The former technique has been shown to correlate inversely with Framingham risk scores in a large population study [108]. There was also good correlation with microspheres over a wide range of myocardial blood flows [109]. Compartmental analysis

on the other hand has also shown to correlate inversely with the degree of stenosis [110], however when compared to PET, underestimated myocardial perfusion reserve.

Perfusion imaging at 3T, employed in our study allows increase signal to noise ratio (SNR) at the cost of increased artifact to noise ratio (ANR) including Gibbs, motion and chemical shift artifacts. Furthermore increased field inhomogenities (B_0 and B_1) and increases in specific absorption rate (SAR), can make perfusion imaging at 3T challenging. In addition the T1 is increased at 3T and T2* reduced and these combined can lead to a reduced signal and perfusion contrast. Gd-DTPA relaxivity also changes at the higher field strength magnet and this leads to reduced T1 shortening effect of the contrast. Yet the overall contrast to noise ratio for myocardial enhancement is improved at 3T due to higher pre-contrast T1 in the tissues.

A recent meta-analysis has shown that this technique has sensitivity and specificity of 91% and 81% respectively for detection of CAD in patients presenting with subacute/ acute chest pain [111]. Similar to other stress modalities, a negative study has good prognostic outlook [112, 113]. Jahnke et al. evaluated 513 patients with a combined myocardial perfusion and dobutamine CMR examination and report event free survival rates of 99.3% at 3 years in patients with a negative result as compared to 83.5% with a positive

scan [114]. Ischaemia and viability information can be derived concurrently as part of the same CMR examination without significant prolongation of imaging time. Dobutamine CMR [115], the recently validated Blood Oxygenation level dependent (BOLD) CMR [116] (discussed in detail later) and Exercise CMR [117], all offer **non contrast** methods of ischaemia and/or viability assessment in CAD patients, and can be particularly attractive in renal patients where gadolinium chelate are contraindicated.

1.7.1.6 Combined ischaemia and viability assessment

Detection of ischaemia in the vulnerable myocardium is of clinical importance. Several techniques allow us to concurrently examine myocardial ischaemia and viability in patients with ischaemic cardiomyopathy. The conventional biphasic response seen in DSE, of improved contractility at low dose and subsequent deterioration at high dose, can be adapted to the DSMR environment, although literature is sparse with regards to validity. Two studies have evaluated simultaneous ischaemia and viability using stress first pass perfusion imaging and LGE-CMR [118, 119]. Both these studies suggested that this approach leads to improved specificity of coronary artery stenosis detection. Therefore in a viability scan, addition of stress imaging may highlight a large area of jeopardized myocardium and this would prove particularly useful in patients with intermediate LGE. No study has evaluated this hypothesis; nonetheless, it would suffice that if the area of ischaemia is

considerably greater than the region of transmural thickness, that revascularisation may lead to improvement in contractility, and potentially prognosis.

1.7.1.7 Myocardial Oedema Imaging

CMR uses a technique based on T2 weighted (T2W) imaging to assess myocardial oedema and reliably identify acute, potentially reversible myocardial injury. Water-bound protons have long T2 relaxation times, resulting in increased signal intensity on T2W imaging sequences. In acute ischaemic injury for example, it has been noted that water content in the myocardium increases by 3 to 5% and up to 28% following reperfusion [120]. This leads to prolonged T2 relaxation time and subsequently a transmural increase in signal intensity. This zone of signal intensity has been recently shown to correlate with area at risk consisting of reversible and irreversible myocardial injury [121, 122].

1.7.1.8 Myocardial Salvage

LGE CMR can be considered the current gold standard for in vivo infarct visualization at every stage of myocardial infarction. Serial LGE imaging has shown that infarct size decreases by 20-30% in the first months after the acute

event [123, 124]. Infarct regression is likely the result of the healing process and the replacement of inflammation, haemorrhage, oedema and necrotic myocytes by collagenous scar. Notwithstanding the utility of LGE-CMR, it would be logical to add assessment of myocardial oedema to viability scans in patients with acute ischaemic injury. Several studies have shown that T2-weighted imaging sensitively detects acute infarct-associated oedema [125-127]. Abdel-Aty et al. successfully demonstrated this ability in differentiating acute and chronic infarcts by combining delayed enhanced and T2-weighted CMR [128]. Expanding on its use in identifying acute injury, Aletras et al. explored the ability of T2-weighted CMR to define area at risk [121] and Friedrich et al. furthered the delineation of reversible and irreversible injury within this area [122]. Novel targeted therapy can be tailored to target this vulnerable myocardium that is potentially salvageable.

1.7.1.9 Myocardial Oedema in myocarditis

Recently an international consensus described the combination of CMR findings required for diagnosis of myocarditis. Known as the Lake Louis criteria; they include presence of oedema, hyperemia and fibrosis/necrosis. Presence of two out of three yields a sensitivity of 67% and a specificity of 91% [129]. Sequences assessing myocardial oedema may show increased signal intensity in a global or regional pattern with the former using skeletal muscle as a reference standard.

1.7.1.10 Blood oxygen level dependent (BOLD) Imaging

Blood oxygen level dependent imaging relies on intrinsic contrast created by deoxyhaemoglobin to provide a non-contrast means of assessing myocardial oxygenation. Magnetic properties of oxygenation were first described by Pauling, in which he demonstrated that deoxygenated haemoglobin acted as a paramagnetic agent by increasing spin-spin interaction [130]. This in turn accelerates transverse magnetization decay shortening spin-spin relaxation time. Hence, the BOLD effect describes the signal loss on T2 or T2* sequences (sensitive to loss of transverse magnetization) due to increase in deoxyhaemoglobin [131-133].

1.7.1.11 Utility of BOLD in detection of coronary artery disease

BOLD imaging in the heart allows a direct method for evaluating functional status of the myocardium. The potential for BOLD MRI to detect regional and global oxygenation changes due to coronary artery disease (CAD) were first described nearly 20 years ago [134, 135]. Pharmacological agents such as dipyramidole and adenosine are utilized to cause coronary artery vasodilation. These agents can increase baseline coronary venous oxygenation from 20 to 30% to 70 to 80% in healthy vessels. In contrast, stenotic vessels show minimal increase from basal state to vasodilation [136]. This leads to identification of myocardial segments with reduced perfusion reserve.

Using animal models, BOLD imaging has been validated against invasive measurement of perfusion and microcirculatory oxygenation [137-141]. The potential benefits of BOLD imaging were also confirmed in recent human studies [116, 132, 133]. However, many early studies were hampered by limitations inherent in the BOLD sequence such as low signal-to-noise ratios, long acquisition times and occurrence of imaging artifacts mimicking regional deoxygenation [142, 143]. The recent use of steady-state free precession sequence [131] and its utility on higher field magnet has circumvented many of these difficulties [116, 144].

As highlighted in work by Karamitsos and colleagues [116], the relationship between regional blood flow, epicardial coronary stenosis and oxygenation is multi-faceted. Because ischaemia is the initiator of the ischaemic cascade, abnormalities in perfusion and oxygenation occur early; however, they may not occur simultaneously in CAD. Thus oxygenation assessment may provide mechanistic information on the changes occurring with significant coronary stenosis. As discussed earlier, controversy remains regarding resting myocardial blood flow in hibernating myocardium. Additionally, it is uncertain as to why up to 40% of dysfunctional segments with no or minimal scar fail to improve after revascularisation [95]. The precise mechanism remains unclear, and may potentially be due to chronic irreversible adaption to ischemia. Evaluation of oxygenation in this cohort particularly may yield

insight into myocyte injury and be used as a tool to predict functional recovery.

1.8 Measurement of Aorta Stiffness and Distensibility

Two important CMR techniques are utilized to assess aortic stiffness. The first is pulse wave velocity which evaluates propagation of pulse or flow through the aorta. Secondly, aortic distensiblity which estimates the change in luminal cross sectional area over unit change in blood pressure. Both of these are discussed in detail in the methodology section.

There is a growing awareness that abnormalities in function of large arteries may play a role in the pathogenesis of cardiovascular disease. Markers of arterial stiffness are associated with adverse clinical outcome [145-147]. Arterial stiffening is associated with number of cardiovascular risk factors raising the possibility that it may represent a surrogate for atherosclerotic vascular disease; however its effect is considered to be beyond that of just propagating risk of atherosclerosis.

1.9 Utility of echocardiography in myocardial assessment

Echocardiography has become a routine part of assessment in patients with suspected or known heart disease. It has been well established for diagnosis, prognosis and monitoring of patients with cardiac conditions. In our studies, we utilized echocardiographic tools for assessment of diastolic function, global longitudinal strain and tricuspid annular systolic plane excursion. For the remainder of this chapter, I will focus on the value of these echocardiographic parameters in assessing cardiomyopathy.

1.10 Diastolic function

Normal diastole is an active process with emptying of blood from left atrium (LA) into the LV. Seventy to eighty percent of LV filling occurs in this manner, with the remainder 20-30% being attributed to atrial contraction. Diastolic dysfunction leads to reduction is this early diastolic filling process. It is common in our general population [148] and confers important prognostic value in patients with organic heart disease[149].

1.10.1 Echocardiographic assessment of diastolic function

Echocardiography is the technique of choice in evaluation of diastolic function. Amongst the parameters available for assessment of diastolic function, trans-mitral flow velocities and tissue Doppler imaging are the quickest to acquire and have the least interobserver variability [150]. Other parameters include left atrial volume and function, pulmonary flow velocities and deformation measurements such as strain and torsion. For the purpose of this chapter, I will focus on simple measurements of diastolic function such as trans-mitral flow velocities and tissue Doppler imaging.

1.10.1.1 Mitral Inflow

Primary measurements of mitral inflow include the peak early filling (E-wave) and late diastolic filling (A-wave) velocities, the E/A ratio, deceleration time (DT) of early filling velocity, and the isovolumetric relaxation time. The measurements are significant influenced by age; with E and E/A ratio decreasing with increasing age, whilst DT and A velocity rise. Furthermore mitral inflow velocities are subject to influence by heart rate and rhythm, mitral annular size, cardiac output and LA function. Mitral inflow patterns are defined by E/A ratio and DT, and divided into normal, impaired relaxation

(Grade 1), pseudonormal (Grade 2), reversible restrictive (Grade 3) and fixed restrictive (Grade 4). In healthy, young individuals, most of the LV filling occurs in early diastole, giving rise to a prominent E wave. With ageing or diastolic dysfunction, there is increase in LV stiffness and reduced early LV filling. This leads to a decrease in the amplitude of the E-wave and a prominent A-wave. The challenge in diastolic assessment is the distinction between pseudonormal and normal pattern. It is assisted by employing the Valsalva maneuver, which results in reversal of E/A ratio in pseudo-normality but not in normal diastolic function. In grade 3 diastolic dysfunction, the E:A ratio is >2:1 and DT is <140ms, however this distinct pattern is only seen in approximately 10% of patients with heart failure and preserved ejection fraction. The Valsalva maneuver is also employed in differentiating Grade 3 and 4 diastolic function. Grade 3 is characterized by abrupt flow of blood from left atrium into the left ventricle. This reverses with the Valsalva maneuver, however is irreversible in Grade 4 diastolic dysfunction.

The utility of diastolic assessment largely depends on the clinical scenario it is incorporated in. For example, in patients with dilated cardiomyopathy mitral inflow velocities are considered to correlate better with cardiac filling pressures, functional class and prognosis than LVEF [151-153]. In contrast, patients with ischaemic heart disease and normal LV function, there is poor correlation between mitral velocities and haemodynamics [154]. In a study examining the temporal effects of anthracyline therapy, transient changes were

found in LVEF, whereas persistent diastolic function abnormalities were noted when serially examined with echocardiography [155].

1.9.1.2 Tissue Doppler annular early and late velocities

Mitral annular velocities are used to estimate LV relaxation and combines with peak E velocity to generate an E/E' ratio; the latter is used to predict LV filling pressures [156-158]. Using septal E/E' ratio, a ratio <8 is considered normal, whilst >15 is associated with increased filling pressures [158]. Recent guidelines advocate average of septal and lateral E' velocities particularly in regional dysfunction.

1.10.2 Deformation assessment

Strain measures deformation and can be assessed in a variety of manners. Systolic strain refers to percentage shortening when measured in the long axis (longitudinal strain) and percentage thickening when measured in the short axis (radial strain). Systolic strain rate represents the rate or speed of myocardial shortening or thickening, respectively. Myocardial strain and strain rate are excellent parameters for the quantification of regional contractility and may also provide important information in the evaluation of diastolic function. Until recently, the only clinical method for measuring myocardial strain was

tissue tagging by CMR, however this complex method with significant post processing analysis has not become widespread in its use.

Strain can be measured by tissue Doppler method and 2D speckle tracking. The former method has been comprehensively evaluated in assessment of regional systolic dysfunction [159, 160]. 2D strain, a more recent development measures strain by tracking speckles in grayscale echocardiographic images [161, 162]. These function as natural acoustic markers that can be tracked frame to frame, allowing automated measurement of distance between the speckles. This is then utilized to generate velocities and strain measurements. Although angle-independent and considered superior to tissue Doppler, 2D strain is subject to limitation due to image quality and low frame rates.

Current software allows regional strain scores to be averaged to yield a global strain score. This score has been established as an accurate index of LV systolic function, in patients with ischaemic heart disease (IHD) [163, 164]. Furthermore, global strain has been demonstrated to confer addition prognostic information to conventional echocardiographic indices in prediction of cardiovascular events [165]. Therefore, strain by speckle tracking allows assessment of regional and global systolic function. Becker et al. have demonstrated close agreement between speckle-tracking strain imaging and

CMR evaluation of regional wall function. However, it is the ability of strain, particularly global longitudinal strain in predicting early, subclinical LV dysfunction that has made it routine in many clinical practices. It has shown significant efficacy in evaluating patients for chemotherapy cardiotoxicity [166, 167].

1.10.3 Tricuspid annular systolic plane excursion

The importance of RV function in predicting outcome of heart failure patients is well established [168, 169], yet it is a ventricle that is limited in its echocardiographic evaluation due to its unique geometry. Several surrogate echocardiographic indices have been established including fractional area change, tricuspid annular systolic plane excursion, strain and strain rate, myocardial performance index and isovolumic relaxation [170-174]. For the purpose of our research we employed TAPSE, as it is the most well established and now routinely employed tool in echocardiographic assessment of RV.

Ghio et al found that TAPSE <15mm added incremental prognostic information to New York Heart Association (NYHA) clinical class, LVEF and mitral deceleration time in patients with heart failure [169]. In addition, recent

work by Tanidi et al. found surrogate markers of RV function, including TAPSE were altered by administration of anthracyline chemotherapy [175].

1.10.4 Summary

After an insult (ischaemic or non-ischaemic), changes occur in the myocardium at the cellular and biochemical level that trigger a cascade of events leading to myocardial injury. To better define this process, we first need to accurately assess myocardial injury and then understand the temporal relationship between the insult and the end-result.

This thesis focuses upon three pathological states of cardiac insult and injury: acute myocardial injury following ischaemic insult, chronic myocardial injury following ischaemic insult and non-ischaemic cardiomyopathy following chemotherapy. Acute myocardial injury is associated with myocardial stunning. Revascularisation itself can lead to alterations in myocardial cellular metabolism and following restoration of blood supply; reperfusion injury follows. With our first study, we measured CMR parameters of acute myocardial injury and identify predictors of recovery at follow up (90 days). Our second study focused on those patients with chronic myocardial dysfunction secondary to ischaemic cardiomyopathy. Here, we wanted to focus on hibernating myocardium and study the interplay between

oxygenation and perfusion before and after revascularisation. Finally, we examined the non-ischaemic insult, establishing markers of myocardial injury following chemotherapy. In this cohort, we were aiming to study the changes in myocardial function with chemotherapy. We further wanted to evaluate a potential mechanism for the changes observed, whether it be inflammation or fibrosis.

Figures

Figure 1.1

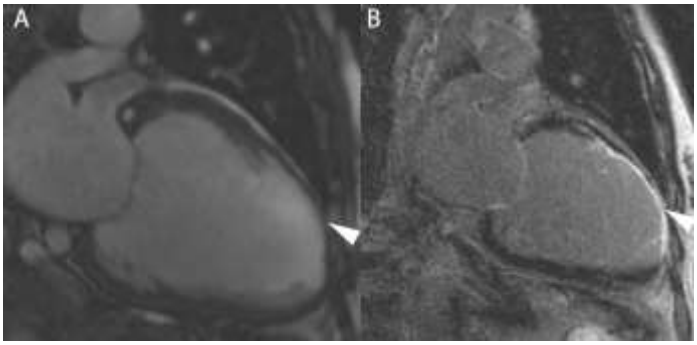

Figure shows the end-diastolic frame of steady state free precession (SSFP) cine (A), and corresponding LGE image (B), in the 2 chamber view in a patient with large anterior infarct. White arrowhead in figure A corresponds to thinning of the ventricle with subsequent arrowhead in figure B relating to transmural LGE.

Figure 1.2

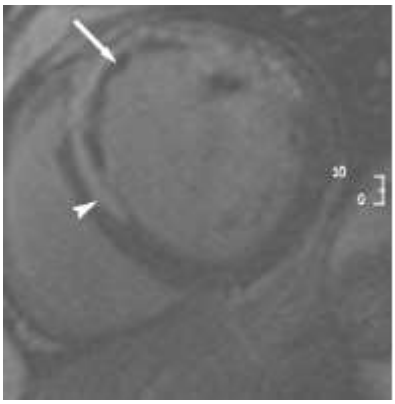

Microvascular obstruction (MVO) characterized by hypoenhanced region (white arrow), surrounded by hyperenhancement (white arrowhead) on late gadolinium imaging within the myocardium.

Figure 1.3

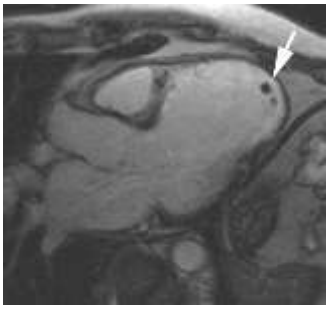

Left ventricular outflow tract (LVOT) view, showing avascular filling defect (white arrow) surrounded by transmural hyperenhancement with LGE imaging, consistent with left ventricular thrombus.

Figure 1.4

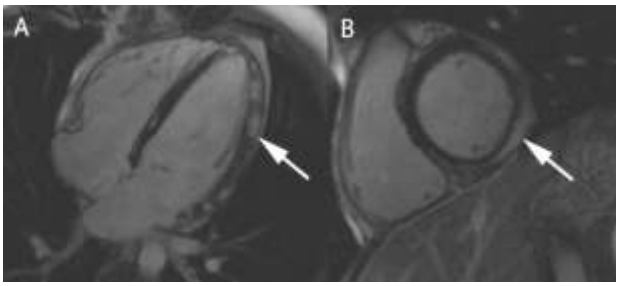

Features of acute myocarditis with sub-epicardial hyperenhancement seen in lateral wall in the HLA view (A) and inferolateral wall in corresponding short axis view (B).

Figure 1.5

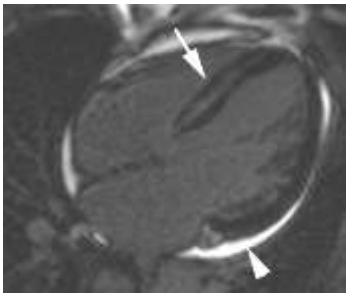

Horizontal long axis (HLA) view demonstrating mid wall hyperenhancement (white arrow) which is characteristic of non-ischaemic pattern and global circumferential pericardial effusion (white arrowhead).

Chapter 2: Methods

This chapter describes in detail the protocol for cardiovascular magnetic resonance image acquisition and each sequence utilized. Furthermore it also elaborates on the echocardiographic protocol utilized in the chemotherapy cardiotoxicity study. Chapters 3-7 will feature the evaluation of LV/RV function, myocardial oedema, perfusion and BOLD imaging and late gadolinium enhancement as pertinent to each study in different patient groups.

2.1 Patient selection and participation

A typical cardiac magnetic resonance scan requires adequate preparation. The patient needs a thorough explanation of the procedure, a good electrocardiogram (ECG) and correct positioning. During the scan, the patient is required to lie in supine position and follow breath holding instructions for 30 to 60 minutes. All scans described in this approach were performed on Siemens 1.5 T (Area) or 3.0 T (Trio) scanners, using a phased array coil placed on the anterior chest wall. Typical exclusion criteria include implantable devices such as pacemakers or defibrillators, epicardial pacing wires, orbital metallic fragments, hydrocephalus shunts or cerebral aneurysm clips. Importantly, a metallic object that displayed "weakly" ferromagnetic qualities in association with a 1.5 Tesla MRI system may exhibit substantial

magnetic field interactions during exposure to a 3 Tesla MRI system. Other metallic implants which were particularly important in our cohort on 3T, were aortic and cardiac stents. Patients were specifically asked regarding claustrophobia and only approached if they felt they could undergo the examination. In accordance with US Food and Drug Administration (FDA) guidelines in 2007, all CMR performed for research purposes required a glomerular filtration rate (GFR) of >60mL/min unless specifically approved by the local ethics committee for a lower cut-off. Patients were allowed to take all medications prior to imaging. A subset of the study cohort refused intravenous (IV) cannulation and therefore could not have contrast administered. A baseline ECG, heart rate (HR) and blood pressure (BP) measurements (pre and post adenosine administration) were performed for all stress scans. Scans were terminated at patients' request, generally because of breathlessness, chest pain during adenosine or anxiety. Patients were counseled and reassured throughout the scan to ensure patient compliance.

2.2 Acquisition of cardiac images

2.2.1 Cine CMR imaging protocol

The following method is employed at our institution, and is a widely accepted approach to quantify LV volumes, mass and function [176]. After careful

preparation of the patient and explanation of the importance of consistent breath-hold technique, multi-slice, multi-planar localizer images are performed in a single breath-hold. Prescribing a plane from the transverse plane using the mitral valve and the apex of the left ventricle as anatomical markers, localizer ('pilot') images are obtained in the vertical long axis (VLA) (Figure2.1). The resultant VLA pilot is then used to prescribe the horizontal long axis (HLA) pilot using the same anatomical landmarks (Figure 2.1).

It is important to accurately define the base of the heart when using this or a similar piloting method. As illustrated in figure 2.1, using the HLA and VLA pilots, three short axis (SA) slices are acquired with the basal slice parallel to the atrio-ventricular (AV) groove (Figure 2.1). The distance between the slices is chosen such that they encompass the basal, mid and apical regions of the ventricle. These 'scout' images can then be used to plan cine images in two long-axis (HLA, VLA), and left ventricular outflow tract (LVOT) views (Figure 2.2).

When acquiring the short axis volume stack from the 2 long axis cines, the position of the basal slice is critical. Most errors in volume calculation are introduced here if this stage is not carefully planned. Using the end-diastolic frames from the VLA and HLA cines, the first slice is placed in the AV groove. Subsequent slices are placed parallel to this covering the entire

ventricle (Figure 2.3). Typically slice thickness is 7-8 mm with a 3 or 2mm inter-slice gap. Imaging is usually performed in expiration as this generally produces a more consistent, reproducible breath-hold position.

2.2.2 T2W-STIR imaging

T2 W imaging can reliably be used to identify acute, potentially reversible myocardial injury. This process does not require contrast agents as the myocardial free water affects the magnetic properties of the tissue, thus providing inherent image contrast. The following protocol is an accepted methodology to identify myocardial oedema in ischaemic injury and myocarditis and is utilized at our institution currently. It utilizes a T2 weighted using a short-T1 triple inversion recovery (STIR) prepared fast echo sequence. This relies on dual suppression of fat and flowing blood to highlight differences in regional oedema and normal myocardium. Although prolonged T2 relaxation times of water bound protons generate their own specific brightness, the differences in myocardial oedema rely on subtle differences in T2 values of normal (45-50ms) and injured myocardium (60-65ms). These images are susceptible to low contrast to noise ratio, although are considered to have acceptable reproducibility [177].

T2W-STIR images were acquired in 3 long axis planes and 3 short axis slices representing basal, mid and distal for non-ischaemic cardiomyopathy patients (i.e. in chemotherapy cardiotoxicity) and all short axis slices for ischaemic cardiomyopathy (i.e. Selective Inhibition of Delta-protein Kinase C for the Reduction of Infarct Size in Acute Myocardial Infarction (PROTECTION-AMI) study)). The images were acquired on every second R-R interval for adequate inversion recovery. All images were performed on breath-hold with the following parameters; dark blood T2-weighted turbo spin echo short-axis images were obtained (TR 1,800 to 2,100 ms, TE 74 ms, 8 mm slice thickness, 4 mm interslice gap, matrix 256x175).

2.2.3 Late gadolinium enhancement

Late gadolinium enhancement utilizes the off-label use of extracellular gadolinium-based contrast agents Gd-DPTA. We utilized commercially available Gd-DTPA agent known as gadobutrol; trade name Gadovist, Bayer Healthcare pharmaceuticals. Gd-DTPA was administered intravenously by hand as a single bolus injection at a dose of 0.1mmol/kg of body weight for all cardiomyopathy examinations, 0.2mmol/kg for all infarct examinations or by power injector and dual bolus injections of 0.045mmol/kg for semi quantitative perfusion. Late gadolinium imaging was performed after a 6 minute delay with a T1- weighted inversion recovery-prepared multislice true fast imaging with steady-state precession sequence with magnitude and phase-

sensitive reconstruction. Images were acquired sequentially in the short axis, followed by horizontal and vertical long-axis images and LVOT views (TR 700 ms, TE 1.0 ms, fractional anisotropy 40°, 8 mm slice thickness, 1.6 mm interslice gap, matrix 192x144). The inversion time (TI) was meticulously adjusted to null the remote normal myocardium by an experienced operator (Figure 2.4). TI refers to period of time between the 180° pulse and centre of acquisition of K space lines. The TI is chosen when there is no net magnetization vector in the normal myocardium and it appears to be adequately nulled (usually at 300ms for 1.5T and 350ms for 3T). If this proved difficult, a TI scout was performed. This acquires several images through a range of inversion times (TI 270-450ms), from which the image displaying adequate nulling and hence the TI can be selected. As imaging proceeds, the TI is adjusted according to wash-out of Gd-DTPA and usually involves increments of TI of 10ms per 2 to 3 images on the 1.5T, usually more rapid on the 3T magnet.

2.2.4 Perfusion Imaging

The basic requirement for a first pass perfusion sequence is to provide adequate T1 contrast, cover relevant myocardial segments and achieve adequate spatial resolution. T1 contrast is generated using a non-selective, 90° RF saturation pulse, followed by fast imaging of each slice with gradient echo (GRE), gradient echo-planar or steady state free precession imaging (Figure

2.5). Coverage of relevant myocardial segments is achieved by interleaved acquisition of arbitrarily oriented slices. Typical parameters employed during perfusion imaging are slice thickness of 5 to 10mm and inplane resolution of 1.5 to 3mm. Based on the resolution, field of view (FOV) and use of acceleration imaging; each image acquisition can take between 50 to 200ms. Parallel imaging is often required to accelerate image acquisition. Although SSFP imaging has improved signal to noise ratio, it is subject to off-resonance artifacts that limit the repetition time. GRE is employed as the method of choice at 1.5 or 3T at most institutions.

A typical perfusion scan involves imaging during stress and rest. Adenosine (0.14mg/kg/min) and Dipyramidole (0.56mg/kg in 4 minutes) are the two most common vasodilators used. Adenosine is short acting (half life 10 seconds) as compared to Dipyramidole (half life 30 minutes) and hence preferred in most MR perfusion studies. Stress imaging is often performed first in 3 short axis slices, to avoid the gadolinium entering areas of infarction and masking potential ischaemia. A gap of ten minutes between stress and rest images were used for the purpose of our study. Typical perfusion and viability (often done concurrently) study protocol is presented in Figure 2.6. These drugs are contraindicated in severe conduction disease, chronic obstructive pulmonary disease (COPD) or asthma, and severe carotid stenosis. Typical side-effects include headache, mild flushing and chest discomfort. Patients with significant CAD may experience angina pectoris. Xanthanine inhibitors can

abolish the affects of these drugs and hence all caffeinated drinks and theophylline are avoided 24 hours prior to the study.

Perfusion imaging in BOLD hibernating study

This study was performed on 3T Trio Siemens scanner. All patients continued all cardiac medications including beta blockers. Patients were asked to report any chest pain during the adenosine infusion and questioned specifically in relation to angina symptoms. The following parameters were used; ECG gated T1 – weighted turbo flash gradient echo sequence (Echo time 1.01, TR – 204 repetition time – 1.94, voxel size 2.3 x 1.8 x 6mm), 6 mm slice thickness, TI – 140, Flip Angle 10º.

2.2.5 Blood oxygen level dependent imaging

Blood oxygen level dependent imaging is a non-contrast technique to measure myocardial oxygenation. It capitalizes on the fact that deoxyhaemoglobin behaves like an intrinsic contrast agent, due to altered proton signal and hence has paramagnetic properties. Examples of this property are seen in accumulation of haemoglobin degradation products in myocardial haemorrhage, iron deposition in haemochromatosis and accumulation of

deoxyhaemoglobin in myocardial ischaemia. Largely utilized in neuro MRI, the BOLD phenomenon is utilized to perform functional brain imaging and has important role in acute ischaemic injury. In the myocardium, increases in deoxyhaemoglobin in capillary blood lead to T2* shortening which can be visualized on T2* maps or regional decrease on T2* weighted images. It is important to remember that the observed changes represent the venous component of the capillary bed and therefore do not represent the actual cardiac myocyte oxygenation. However, the capillary bed symbolizes the balance between myocardial oxygenation supply and demand and therefore can be considered to be an actual marker of tissue oxygenation.

Initially utilizing echo-planar and T2 weighted spiral images, the early human BOLD studies were limited due to motion and susceptibility artifacts. More recent SSFP images have shown great improvement with regards to artifacts, although at the cost of lowered sensitivity for detecting myocardial oxygenation. This sequence particularly depends on adequate repetition time.

This study has utilized an SSFP based sequence and performed it on 3T scanner, with increased signal to noise ratio and hence improved sensitivity. Although with the higher field strength, artifacts are more likely, the overall image quality and sensitivity is improved at the higher magnetic strength. BOLD and perfusion imaging were performed as part of the same protocol.

Hence patients were required to be caffeine free for 24 hours prior to the scan. For BOLD imaging, patients were monitored with ECG, sphygmomanometry and pulse oximetry. Following cine imaging, rest BOLD imaging was performed in a mid ventricular slice. Multiple images were acquired in corresponding to matching cine image until 6 slices were available with adequate image quality. A T2-prepared ECG-gated SSFP sequence (echo time, 1.43 ms; repetition time, 2.86 ms; T2 preparation time, 40 ms; matrix, 168x192; slice thickness, 8 mm; flip angle, 44°). If required, frequency scouting and shim adjustments were performed to minimize off resonance artifacts. For stress imaging, after 1 min of intravenous adenosine (0.14 mg/kg/min), 4 to 6 stress BOLD images were consecutively acquired in the same short-axis plane. Adenosine was infused for up to 5 minutes or until tolerated. Stress perfusion imaging was performed just prior to the adenosine being ceased.

2.2.6 Aorta Distensiblity Imaging

Using the sagittal and transverse HASTE images, cine imaging was performed in the oblique sagittal plane to generate a view encompassing the entire aorta – traditionally called ‘hockey stick’ view. Ascending aorta (AA) and the proximal descending aorta (PDA) were planned perpendicular to the hockey stick at the level of the middle pulmonary artery using steady-state free precession cine sequences with an in plane resolution and slice thickness of

1.97 mm and 7mm. The distal descending aorta (DDA) was planned perpendicular to the hockey stick at the level of the diaphragm (Figure 2.7). Images were transferred offline to planimeter the maximum and minimum endoluminal area. Blood pressure was measured from the left arm with a brachial arm sphygmomanometer during distensibility measurements of the aorta.

2.2.7 Velocity Encoded Imaging

The intrinsic motion sensitivity of MRI that leads to artifact in many sequences, can be utilized in phase contrast angiography to image vessels. This property uses the local spin magnetization as a vector quantity to extract phase encoded images from the measured MR signal. By using appropriate velocity encoded gradients, we can measure two datasets with different velocity dependent signal phase at identical acquisition parameters. The underlying flow or motion can be measured using quantitative assessment of velocities by subtracting the two resulting phase images.

2.2.7.1 Pulse wave velocity imaging of the aorta

Pulse wave velocity imaging was performed in the AA and PDA using a high-resolution gradient-echo pulse sequence with a velocity-encoding gradient for

phase contrast MRI. A temporal resolution of 11 mm was applied to assess peak velocities (AA, PDA, and DDA); forward, reverse, and net aortic flow (AA); and to determine proximal (comprising the AA and the aortic arch) and distal pulse wave velocities in the descending aorta [178].

2.3 Analysis

2.3.1 CMR function Analysis

Currently quantification of LV functional data is performed off-line using either the MRI vendor provided software platform, or a variety of third party software packages; the latter employed at our institution (Q MASS, MEDIS Medical Imaging; CAAS MRV, PIE medical imaging; and CMR 42, Circle Cardiovascular Imaging) that can be installed on all major computer operating systems. These vendors usually provide full digital imaging and communications in medicine (DICOM) connectivity and therefore can be used as a stand-alone solution, integrated into existing network environments including major PACS systems (Picture Archiving and Communication Systems).

The LV and RV analysis begins by defining the end-diastolic phase (EDP). Using a mid-ventricular slice, the phases are advanced until the smallest cavity size is reached by visual estimate. This phase is marked as the end-systolic phase (ESP). Most software programs require identification of the EDP, ESP, base and apex so that the endocardial border can be automatically tracked and volumes calculated (Figure 2.8). Myocardial mass was calculated as the product of end-diastolic LV myocardial volume and 1.05g/cm^3 (specific density of myocardium).

The greatest sources of variability in the measurement of LV volumes should be acknowledged. The selection of the most basal slice represents the most common error when LV volumes are assessed [179]. By convention the most basal slice is defined as the one where 50% of the slice circumference comprises myocardium. Other sources of error include contour definition and inexperienced operators although the variability induced by the latter can be reduced by a short period of intensive training involving standardized data acquisition, simulated off-line analysis and mentoring [180]. The RV end-diastolic phase begins just beneath the pulmonary valve. Features differentiating the right atrium (RA) from the RV (common source of error), include absence of trabeculae, thin smooth wall and the cavity enlarges in systole. RV mass is traditionally not calculated unless there is RV hypertrophy present.

Regional wall motion (RWM) was analyzed in accordance with previously published criteria [92] and was graded as 0, normal; 1, mild or moderate hypokinesia; 2, severe hypokinesia; 3, akinesia; and 4, dyskinesia.

2.3.2 Myocardial Oedema (T2W-STIR) imaging Analysis

Offline image analysis was performed using dedicated soft ware, (CMR 42, Circle Cardiovascular Imaging, Calgary) similar to function analysis. Three short axis slices were acquired for assessment of myocardial oedema, representing basal, mid and distal myocardium for non-ischaemic cardiomyopathy. All short axis slices were acquired for area at risk following ischaemic injury assessment and divided into 16 segments (6 for basal and mid, and 4 for distal) based on the American Heart association (AHA) model. Subendocardial and subepicardial contours of the LV were manually traced. In case of ambiguity regarding these contours, cine images of corresponding slice positions were assessed to differentiate LV myocardium from the intense signal caused by slow flowing blood. To perform semi-quantitative assessment for myocardial area at risk, intensity thresholds were set at 2 SD for STIR images with the reference being placed in remote myocardium [181]. For chemotherapy cardiotoxicity, the reference was placed in the skeletal muscle. A ratio of >2.0 was considered significant for myocardial oedema as has been

published previously [129]. Although no specific effects of chemotherapy have been described on the skeletal muscle, it is theoretically possible that there is some degree of inflammation present on the skeletal muscle. The sensitivity of detecting myocardial inflammation will be reduced if there is skeletal inflammation present.

2.3.3 Late gadolinium enhancement Analysis

The simplest method of quantification is visual assessment scored on a 17 segment model; (0 = no hyperenhancement, 1 = 1-25%, 2 = 26 to 50%, 3 = 51 to 75% and 4 = 76 to 100%). Infarct size is calculated by summing of each score, defined by the mid-point of the range and dividing by 17, allowing for accurate assessment within 1.2% of LV mass [182, 183]. Alternatively infarct size can by quantified by manual planimetry in a semi-automated technique. Amado et al. conducted the seminal study in quantifying LGE using the 2 validated methods: full width half maximum (FWHM) and standard deviation method. They validated these methods against triphenyltetrazolium chloride staining, considered the histological gold standard of myocardial necrosis (irreversible injury). The FWHM, as implied in the name, assessed the all areas that are 50% of the maximal signal intensity in the hyperenhanced region whilst the SD method relies on adequate suppression of the remote myocardium signal [184]. FWHM was found to be superior to 6 standard deviation method in this study. These findings have recently been contradicted

by Bleek et al., with a study evaluating these techniques against functional recovery after revascularisation, considered the clinical gold standard of viability. Quantification methods were found to have a strong influence on the extent of segmental enhancement and infarct size, with 6SD being the most accurate at predicting segmental functional recovery [185]. FWHM and 6SD are both well validated methods and we advocate familiarity with one method and employment of the same method for serial imaging. For the purpose of our study, we used the SD method. Hyperenhanced pixels were defined as those with image intensities >5SD (considered similar in accuracy to 6SD) above the mean of image intensities in a remote myocardial region in the same image. We chose 5SD to improve sensitivity, yet not compromising the overall accuracy of measuring infarct size. A further region of infarct was quantified with image intensity as >2SD greater than remote myocardium. This was defined as the infarct at periphery, with 5SD infarct size used to quantify the core infarct region. Infarct heterogeneity was defined as the region of difference between the periphery infarct (2SD infarct size) and the core infarct (5SD infarct size) [186]. Microvascular obstruction was visualized using LGE images and quantified by manual planimetry of hypoenhanced region surrounded by LGE in each short axis slice [187, 188]. We wanted to evaluate persistent microvascular obstruction on LGE images as this has been previously described to predict late myocardial recovery. Myocardial Salvage was calculated as the difference between reversible myocardial injury (using T2W images to identify oedematous myocardium)

and irreversible myocardial injury (as defined by 5SD infarct size on LGE images) [122].

2.3.4 Perfusion Analysis

Qualitative assessment is adequate for clinical reporting. However, for research purposes, semi-quantitative and quantitative methods are employed. The myocardium is segmented into 16 segments using the AHA model. Endocardium and epicardium contours are defined and extrapolated through the remaining cardiac phases. Careful consideration is required to avoid contaminating the myocardial signal from adjacent blood pool. To perform quantitative perfusion, a region of interest (ROI) is place within the wall in order to track the dynamic changes in the observed signal intensity. Although this sounds simplistic, it is made challenging by displacement of segments due to respiratory motion and arrhythmias. Secondly, potential problems arise due to the non-linear relationship between contrast and signal intensity, particularly at higher contrast doses. This is especially during the peak enhancement phase, where the response of the signal intensity may be diminished due to saturation and lead to the concentration being underestimated. Whilst performing quantitative analysis of dynamic first-pass perfusion images, we need to account for the effect of potential variations in the rate, amount, and timing of the delivery of the contrast agent in the blood (the arterial input function, AIF) on the resulting enhancement of the heart

wall. This can be achieved by placing a ROI in the LV cavity and following the sequential changes in the blood. A number of approaches are available to diminish the affects of AIF on the observed tissue enhancement. These include calculating the time of arrival of the contrast agent, time of peak enhancement and the slope of the peak enhancement curve and correcting them for the same AIF parameters. However, these are only approximate methods and do not allow the full calculation of transit through the tissues or account for extravasation of the contrast. This can be achieved by 'deconvolution' which is a mathematical approach to 'undo' the effects of AIF from the observed tissue response and calculate the mean transit time and blood flow [106]. This requires a reduced dose of Gadolinium chelate at 0.045mmol/kg to be used. Due to the cumbersome nature of this technique, a relative index of myocardial perfusion reserve can be calculated by generating stress and rest myocardial perfusion slopes and performing Fermi-fitting of signal intensity with time, correcting for blood pool and heart rate. A myocardial perfusion reserve index is derived by ratio of stress versus rest signal intensity slopes.

For the purpose of our study, we performed semi-quantitative analysis. This was done in the perfusion module of the software. Endocardium and epicardium were manually traced in all 50 phases and adjusted for respiratory motion. Blood pool contour was also manually drawn. Automated algorithm was applied to compare the signal intensities in 6 segments with blood pool

and relative perfusion index (PI) in stress and rest were measured. Myocardial perfusion reserve index was calculated using (PI stress – PI rest/PI rest). The mid ventricular slice was selected using the mid slice of the short axis cine stack where papillary muscle was clearly visualized. This allowed all 6 segments of function, perfusion and BOLD to be matched.

2.3.5 BOLD imaging analysis

All analysis was performed using dedicated soft ware, (CMR 42, Circle Cardiovascular Imaging, Calgary). For BOLD assessment endocardial and epicardial contours were traced. The myocardium was divided into 6 equiangular segments based on the mid ventricular slice of the AHA model. The segments were mid anterior, anterolateral, inferolateral, inferior, inferoseptum and anteroseptum. Mean signal intensity was measured in each segment and corrected for heart rate due its affect on T1 relaxation. The following equation was used for correction:

$$S = S_0/(1-\beta e^{-TR/T1})$$

T1 – 1220ms, β= 0.59 (determined empirically for this sequence). The S0 is the measured SI, S = calculated SI and TR is the image-dependent time between acquisitions of sections of K-space[116]. This is governed by the

heart rate and indeed replaced by the R-R interval. The relative SI is calculated using the following equation:

$$\Delta SI\ (\%) = \frac{\text{Mean SI (stress)} - \text{mean SI (rest)}}{\text{Mean SI (rest)}} \times 100$$

2.3.6 Aortic distensibility and pulse wave velocity imaging analysis

Image analysis was performed off-line using CMR 42. Initially the cine images were magnified 400 to 800x and inner vessel area was contoured in systole and diastole to generate the maximum and minimum cross-sectional area. These measurements were used to calculate relative area change and aortic distensibility (relative change in cross-sectional area for a given pressure change) and aortic stiffness index (ratio of logarithm systolic/diastolic pressure to relative change in cross sectional area) [189-191]. Flow images were analyzed using the flow module of CMR 42. Pulse wave velocities were calculated by dividing the distance between the two measurements and time of arrival of the pulse wave at each time points. The latter was defined as the time point where the velocity reached half its maximum value [189, 192].

2.4 Transthoracic Echocardiographic Image Acquisition

Patients were placed in the left lateral decubitus position using a commercially available system (Vivid I, General Electric Healthcare, Horten, Norway). Images were obtained using a 3.5Mhz transducer, at a depth of 16cm in the apical views. Grey-scale images of the left ventricle were acquired in 3 apical views (4chamber, 2 chamber and apical long axis). Depth and sector width were adjust to achieve frame rates between 60 to 80 per/second. Transmitral blood flow velocities (E and A wave) were measured by pulse wave Doppler at mitral valve leaflet tips. Two flow velocity envelopes are seen during diastole in persons with sinus rhythm: the E-wave, representing the early, passive filling of the left ventricle, and the A-wave, that happens late in diastole, representing the active filling, the atrial contraction. Tissue velocity imaging is used to measure velocity of myocardial motion using Doppler principles. To measure longitudinal myocardial velocities, the sample volume is placed in the ventricular myocardium immediately adjacent to the mitral annulus. TAPSE was measured by M-mode echocardiography at the lateral tricuspid annulus. A minimum of 3 consecutive cardiac cycles were recorded for each image. Images were recorded digitally in cine-loop format and analysed with commercial software (EchoPac version 7.0.0 General Electric-Vingmed).

2.4.1Transthoracic Echocardiographic Analysis

LV strain profiles were derived by speckle-tracking (2D strain): following manual tracing of the endocardial border and adjustment of region of interest width to encompass LV myocardium. Strain versus time curves were obtained for 18 segments from 3 apical views. The peak systolic strain was measured and averaged to provide the global LV longitudinal strain score. Mitral inflow velocities were measured to provide peak E, A velocities. Diastolic E' velocity was measured offline by placing the sample volume at the septal mitral annulus and measuring the peak tissue velocity. An E: E' ratio of >15 represents elevated filling pressures and E: E' of <8 correlates with normal filling pressures.

2.5 Clinical Trials

The aims and specifications of each trial are described in the respective chapters. In brief, we performed 3 different studies. Written, informed consent was obtained from patients for all 3 studies. The first study involved acute MI patients, for which our centre participated and was the core-laboratory for CMR sub-study. My role specifically in this was to analyze all late gadolinium and T2W images to assess, infarct size, microvascular obstruction, infarct heterogeneity, area at risk and myocardial salvage. This was under

Professor Selvanayagam who was the principal investigator of the CMR sub-study. Functional data analysis was performed by Drs Lucas Joerg and Per Lav Madsen. Inter-observer variability was provided by Dr Adhiraj Chakrabarty and Dr Govindarajan Srinivasan. The second study involved chronic myocardial infarcts. This is also an investigator led study under the guidance of Professor Joseph Selvanayagam. I am responsible for recruiting patients and data collection. I have performed the BOLD and perfusion analysis. At separate time point, I have in a blinded manner performed the functional and late gadolinium analysis. Inter-observer reproducibility was provided by Dr Pey Wen Lou and Dr Susie Parnham. The third study involved non-ischaemic cardiomyopathy, specifically patients receiving chemotherapy cardiotoxicity. This was an investigator led study under the guidance of Professor Joseph Selvanayagam. I managed the entire study, recruiting patients, aiding in CMR image acquisition and performing their echocardiograms as well as collecting blood for biochemistry analysis. I performed all myocardial oedema and late gadolinium anlaysis with interobserver variability and functional analysis being provided by Dr Adhiraj Chakrabarty. As part of this study, I also studied aortic stiffness in a subset of patients (approximately 50%). Here I was involved in image acquisition and analysis. Interobserver reproducibility was provided by Dr Pey Wen Lou. All 3 studies had statistical analysis performed by Dr. Darryl Leong and Professor Richard Woodman who have significant expertise in biostatistics.

2.5.1 Ethics

All trials underwent independent review by local research ethics committee prior to commencement. The local research ethics committee (Flinders Medical Centre) unique identifier numbers are:

PROTECTION AMI - ETHICS NO 254/08

CHEMOTHERAPY CARDIOTOXICITY - ETHICS NO : 24/10

BOLD HIBERNATING MYOCARDIUM - ETHICS NO: 31/09

Figures

Figure 2.1

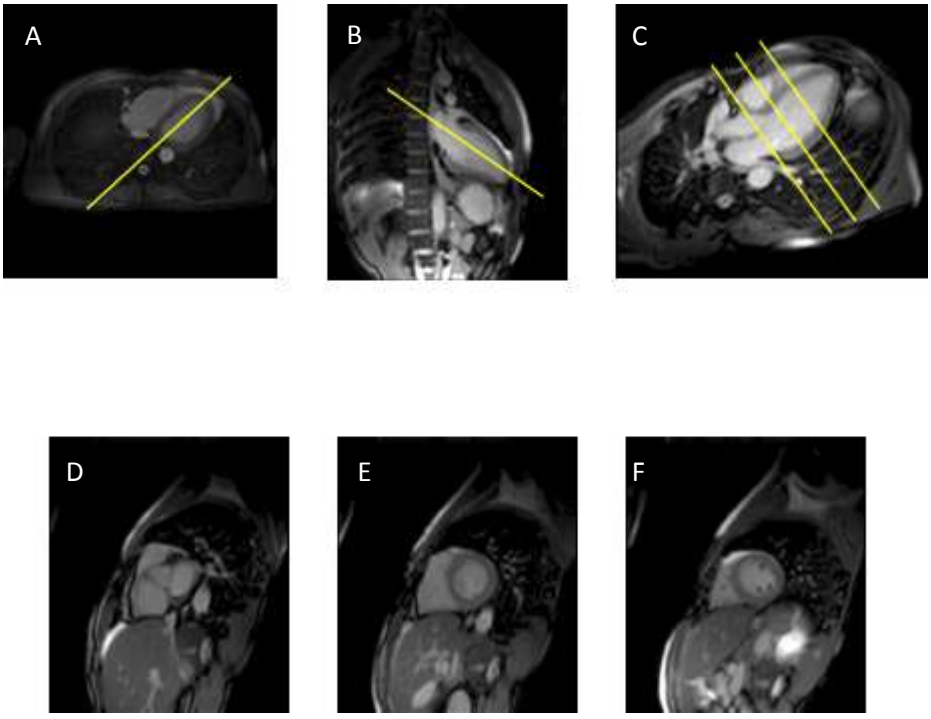

Sequence of images (A-K) demonstrating the correct acquisition of the long axis and short axis planes for cine imaging. Initially, multi-planar localizer images are performed in a single breath-hold (A). Using the transverse localizer (A), in the plane indicated by the solid line in (A), pilot images are then performed in the vertical long axis (VLA) plane (B). The resultant VLA pilot is used to prescribe (as indicated by the solid line in (B)) the horizontal long axis (HLA) pilot (C) Using the HLA and VLA pilots, three short axis (SA) slices (D-F) are next acquired with the basal slice parallel to the atrio-ventricular (AV) groove (indicated by 3 solid lines in (C)).

Figure 2.2

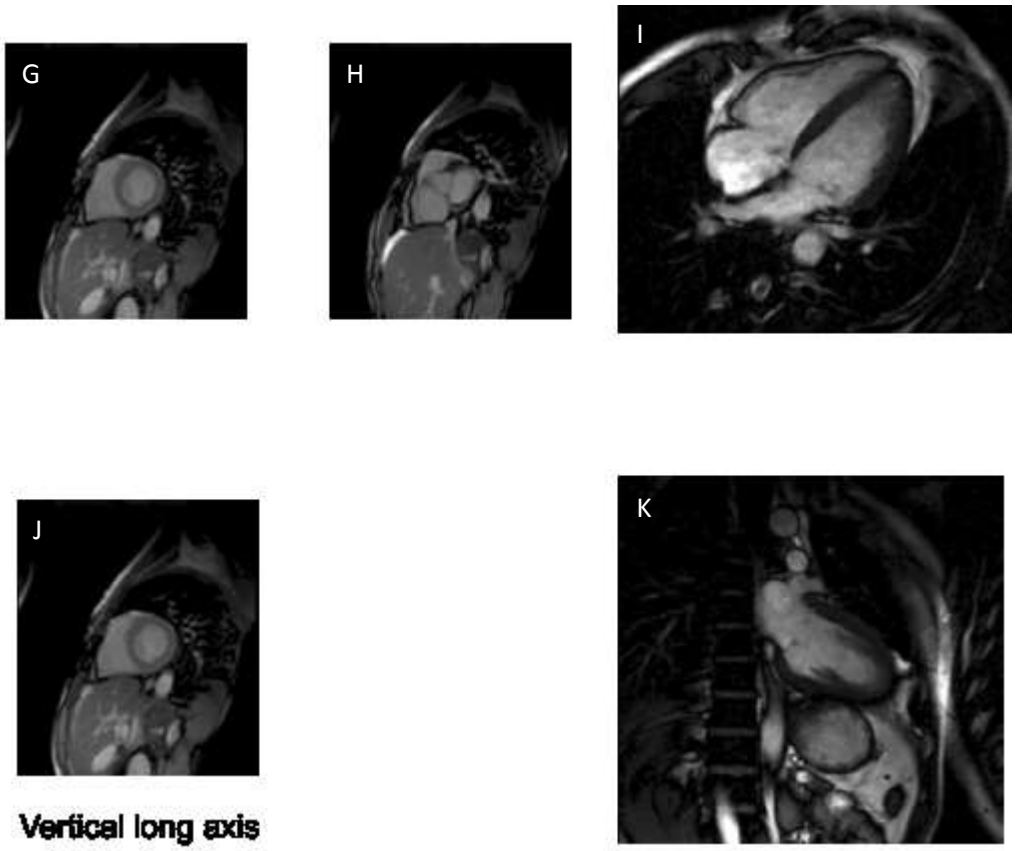

To acquire the HLA cine (I) the mid ventricular SA pilot (G, E) is used to position the slice through the maximum lateral dimensions of both ventricles and avoid the LVOT as illustrated by panels G & H. To acquire the VLA cine (K), the mid ventricular SA pilot is again used and placed in the plane as indicated in panel J.

Figure 2.3

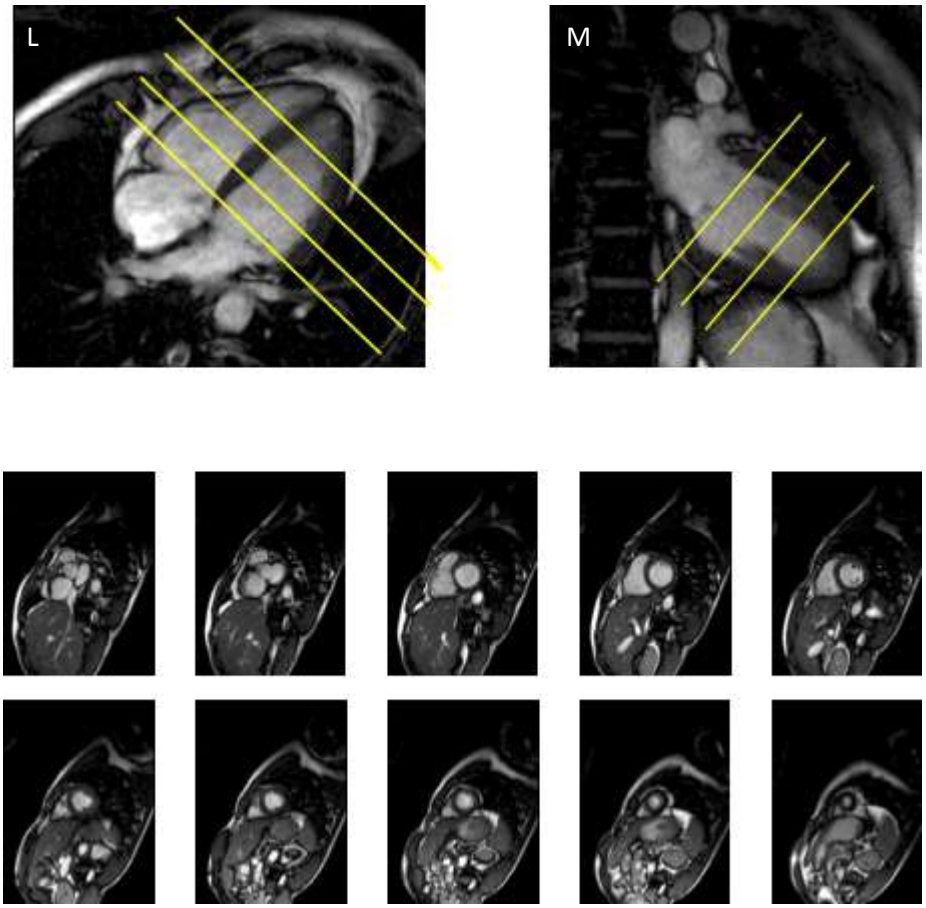

This demonstrates the resultant HLA (L), VLA (M) and short axis cine stack from base to apex (bottom panel).

Figures 2.1-2.3 are cited in Evaluation of left ventricular function using cardiac magnetic resonance imaging. J Nucl Card. 2011; 18: 351-365.

Figure 2.4

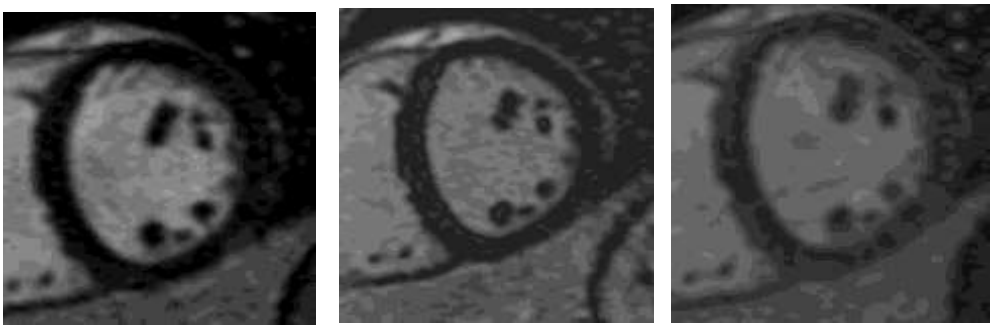

Appropriately nulled	**Inversion recovery**	**Inversion recovery**
Myocardium	**too low**	**too high**
TI 300ms	**TI 260ms**	**TI 350ms**

Examples of nulling of myocardium based on different TI times performed on 1.5T, 6 minutes after administering 0.1mmol/kg of Gadolinium chelate.

Figure 2.5

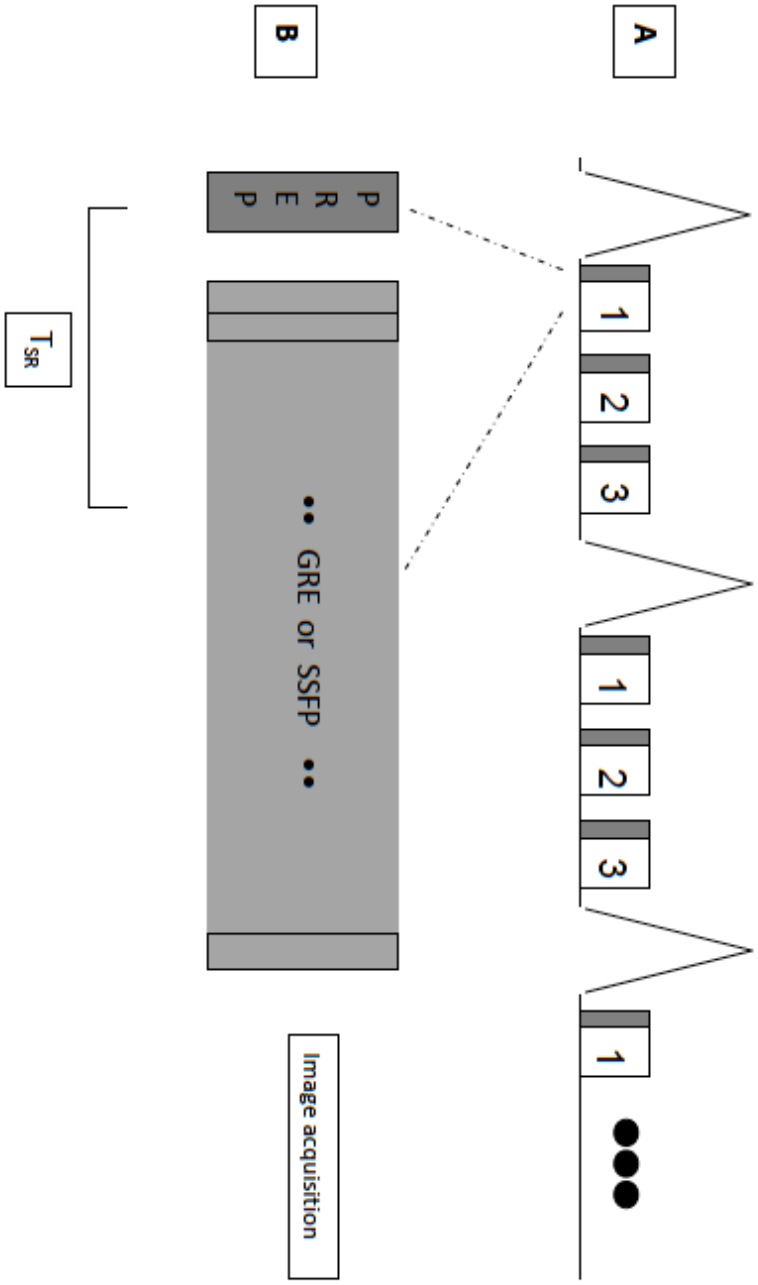

*Adapted from G*erber *et al. Journal of Cardiovascular Magnetic Resonance* 2008 **10**:18

Example of a typical perfusion sequence. Part A demonstrates acquisitions being ECG gated with multiple slices acquired every 2 R-R intervals. Part B shows T1 contrast being generated by using a saturation pulse (dark grey) followed by fast imaging of each slice (light grey). T_R refers to saturation recovery time which is responsible for the image contrast.

Figure 2.6

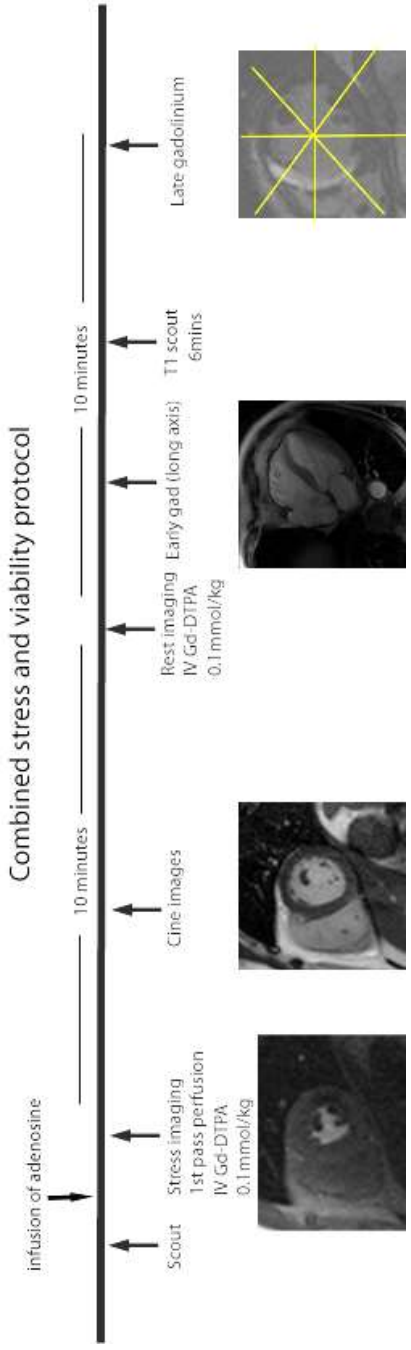

Example of combined stress and viability protocol (as employed at our institution). *Cited in Evaluation of myocardial viability, Progress in Cardiovascular Diseases, 2011; 54(3): 204-214*

Figure 2.7: Imaging of the aorta

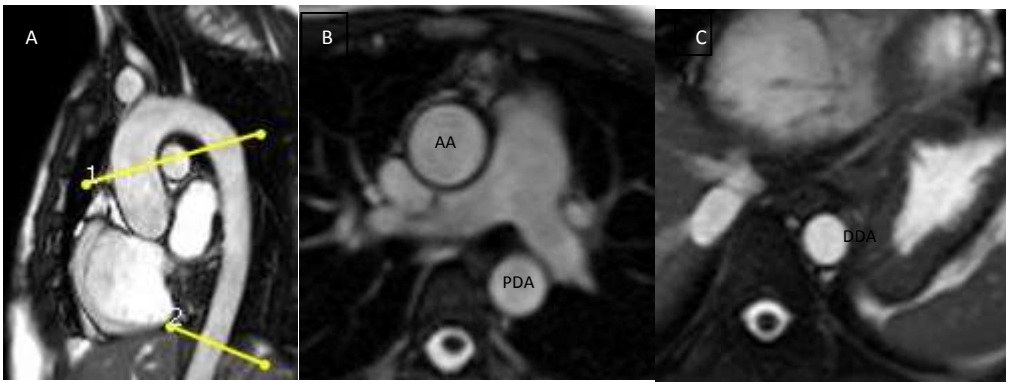

SSFP image in the traditional sagittal plane of aorta (hockey stick) in A, demonstrating planning of the ascending aorta (AA) and proximal descending aorta (PDA) shown by 1 and distal descending aorta (DDA) shown by 2. Part B and C demonstrate the resultant cross cut SSFP images of AA, PDA and DDA.

Figure 2.8

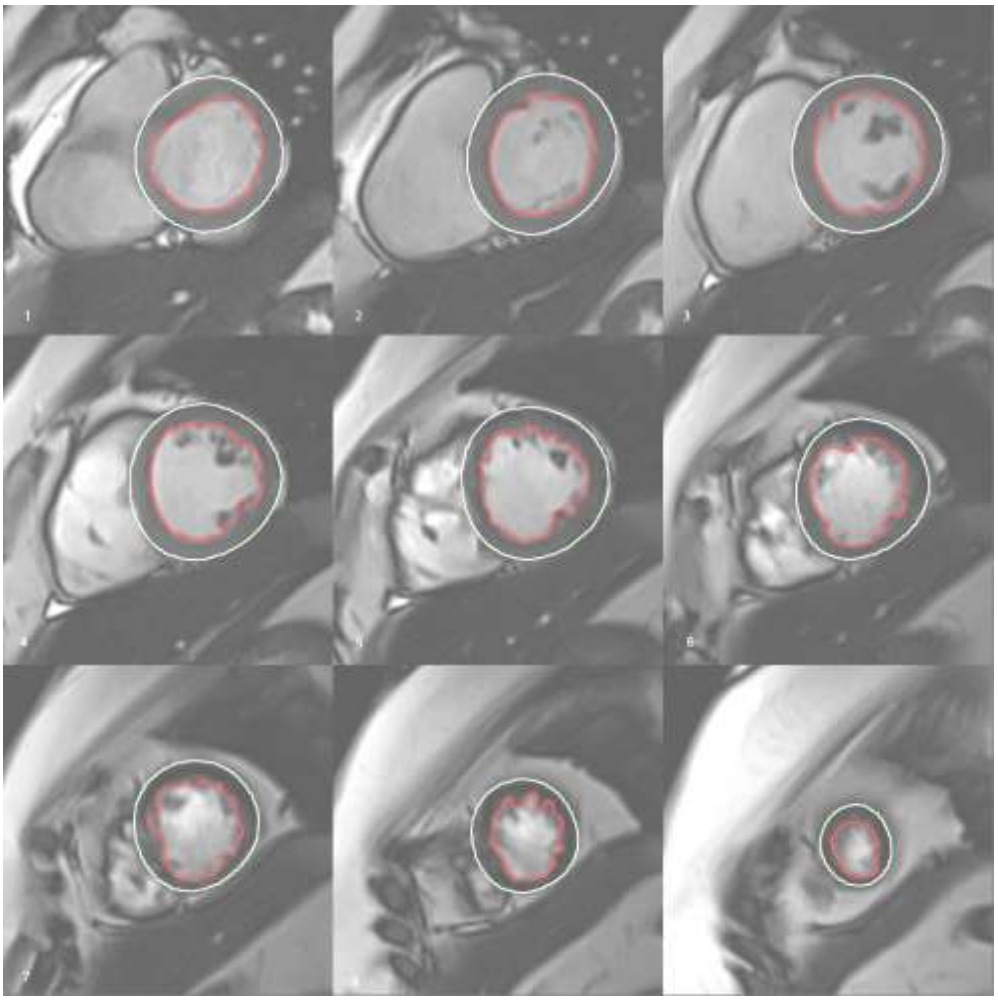

Short axis left ventricular (LV) stack, showing semi-automated contour detection in the end-diastolic phase. Endocardial (red) and Epicardial (green) borders are tracked throughout the series allowing quantification of end-diastolic mass and volume.

Table 2.1 Dobutamine stress CMR (DSMR) for the assessment of myocardial viability

Studies of DSMR	No of patients	Mean Age (year)	LVEF (%)	Segments with recovery (%)	Sensitivity (%) No of segments	Specificity (%) No of segments
Baer et al.[193]	52	58	41	50	86 (24/28)	92 (22/24)
Baer et al.[194]	35	59	42	52	81 (NA)	95 (NA)
Gunning et al.[195]	23	61	24	57	50 (NA)	81 (NA)
Sayad et al.[196]	10	NA	NA	60	89 (25/28)	93 (14/15)
Baer et al.[79]	43	58	41	46	89 (24/27)	94 (15/16)
Sandstede et al.[197]	25	58	NA	51	61 (65/106)	90 (91/101)
Trent et al.[198]	25	64	53	40	71 (81/114)	70 (163/232)
Dendale et al.[199]	24	NA	NA	46	91 (NA)	69 (NA)
Saito et al.[100]	22	69	NA	NA	76 (NA)	86(NA)

LVEF, left ventricular ejection fraction; NA, not available

Table 2.2 Late gadolinium enhancement (LGE) CMR for the assessment of myocardial viability

Studies of LGE	No of patients	Mean Age (year)	LVEF (%)	Segments with recovery (%)	Sensitivity (%) No of segments	Specificity (%) No of segments
Kim et al.[91]	41	63	43	53	97 (411/425)	44 (211/379)
Lauerma et al.[102]	10	69	44	66	62 (NA)	98 (NA)
Selvanayagam et al.[92]	52	61	62	59	95 (326/343)	27 (71/269)
Wellnhofer et al.[103]	29	68	32	NA	90 (111/124)	52 (85/164)
Gutberlet et al.[200]	20	64	29	87	93 (NA)	39 (NA)
Pegg et al.[95]	33	62	38	63	95 (NA)	75 (NA)

LVEF, left ventricular ejection fraction; NA, not available

Chapter 3: Utility of CMR markers of myocardial injury in predicting LV functional recovery: results from PROTECTION AMI CMR sub-study

3.1 Introduction

Identifying patients with significant myocardial area at risk (AAR) in the setting of acute ST elevation myocardial infarction is important. The patients with the largest AAR potentially achieve the greatest benefits from myocardial salvage therapy, whether it be pharmacological [201], or interventional [202].

Cardiovascular Magnetic Resonance has emerged as a powerful tool for assessing the impact of myocardial salvage strategies in the setting of STEMI, due to its accuracy, reproducibility and ability to concurrently assess left ventricular function, infarct size [91], myocardial salvage [122], microvascular obstruction [188] and infarct heterogeneity [203]. All of these parameters have shown promise in clinical trials to predict adverse clinical sequelae post STEMI and/or the likelihood of LV functional recovery; however the trials are limited to single-centre studies. The PROTECTION-AMI study evaluated three doses of delcasertib (KAI-9803), a protein kinase C inhibitor and placebo in reperfusion injury associated with percutaneous coronary intervention (PCI). This was a multi-center, double-blind trial performed in patients presenting within 6 hours of the onset of symptoms and

undergoing primary PCI for anterior (the primary analysis cohort, n = 1010 patients) or inferior (an exploratory cohort, n=166 patients) STEMI.

In summary, the PROTECTION-AMI showed no difference between delcasertib and placebo for the primary endpoint of enzymatic infarct size or for continuous electrocardiographic measurements of reperfusion or left ventricle ejection fraction at 90 days.

Patients recruited in the anterior STEMI cohort in the main study were eligible for the CMR substudy. They were selected by investigators at each CMR substudy participating site. Utilizing this cohort of patients with anterior STEMI, the aim of the present study, was to identify the best CMR parameter assessment for adverse LV remodelling in a multi-centre, multi-vendor setting. Furthermore, we sought to correlate these CMR parameters against routinely performed biochemical markers of myocardial injury (creatinine kinase, creatinine kinase isoenzyme myocardial band and troponin I (TnI)). Our hypothesis was that CMR late gadolinium enhancement would be superior to biochemical markers of injury and other CMR parameters of myocardial injury for predicting 90 day LV function.

3.2 Methods

The study design of Inhibition of Delta-protein Kinase C for the Reduction of Infarct Size in Acute Myocardial Infarction (PROTECTION-AMI) study has been published previously [204]. Briefly 1176 patients were enrolled (1010 in the anterior STEMI cohort, 166 in the inferior STEMI cohort) at 114 sites in 18 countries. Participants were randomized to placebo (249 patients) or one of three delcasertib groups with doses of 50 mg/hr (254 patients), 150 mg/hr (248 patients) or 450 mg/hr (246 patients). The drug was administered intravenously immediately after randomization and before cardiac catheterization and percutaneous coronary intervention, and was continued for up to 2.5 hours. Delcasertib was compared with placebo with respect to infarct size following anterior STEMI as assessed by CK-MB area under curve (AUC) during the index hospitalization in subjects undergoing PCI.

PROTECTION AMI Cardiovascular Magnetic Resonance sub-study design

Patients, undergoing primary PCI for anterior myocardial infarction as part of PROTECTION-AMI trial were enrolled into the CMR sub-study at participating centres. From 1010 patients in 114 sites in the main study, 96 patients in 24 sites consented to participate in the CMR sub-study. Patients underwent two dedicated CMR imaging studies, between days 3 to 5 and on day 90 (±1week) following index primary PCI. The institutional review board

at each participating hospital approved the protocol, and patients were required to provide written informed consent.

3.2.1 CMR Protocol

All scans were performed on a 1.5 or 3T scanners from a variety of vendors (Phillips, Siemens and General Electric). The methodology for this study has been presented in detail in chapter 2. Briefly, short axis cine CMR was performed using slice thickness of 8 mm with 2mm slice gap that encompassed the entire LV from base to apex. To evaluate myocardial oedema, a breath-hold, black blood, short-T1 triple inversion recovery pulse sequence was applied with the following parameters; repetition time 2 x R-to-R intervals, echo time of 65ms (Philips scanners: 100 ms) and inversion time 140ms, field of view 34 to 38 cm, matrix 256x256 (or 256 x 192). T2 images were acquired using the same slice thickness/gap as the cines and late enhancement images. Whenever possible the matrix was kept identical to that of late enhancement images. Late gadolinium enhancement (LGE) images were obtained 10 minutes after 0.2 mmol/kg of intravenous gadolinium (Gd-DTPA, Gadovist, Bayer, Germany) using a T1 weighted inversion-recovery gradient-echo based sequence (using either a spoiled GE technique or a balanced technique). Sequences were either multi breath-hold two-dimensional, or single breath-hold three-dimensional. For the 2D multi breath-hold approach a slice thickness of 8 mm and inter slice gap of 2 mm was used.

For the 3D single breath-hold approach a slice thickness of 6 mm with 15 slices within a single breath-hold was performed.

3.2.2 CMR Image Analysis

Analysis of CMR images has been presented in detail in chapter 2. In short, endocardial and epicardial tracings were drawn in the end-diastolic and end-systolic frame using CAAS-MRV analysis software version 2.0 (Pie Medical Imaging, Maastricht, the Netherlands). The end-diastolic frame was defined as the frame showing the largest cavity area, and the end-systolic frame was defined as the frame showing the smallest cavity area in a mid ventricular slice [205]. Left ventricular volumes, mass and left ventricular ejection fraction were calculated and indexed to body surface area (BSA). The LV cavity was divided into 17 segments according to a standardized model [206]. Regional wall motion was analyzed by a separate, experienced observer blinded to the LGE finding, in accordance with previously published criteria [92]. RWM was graded as 0, normal; 1, mild or moderate hypokinesia; 2, severe hypokinesia; 3, akinesia; and 4, dyskinesia. A segment was defined as improved if the wall motion score decreased by at least 1 grade at the follow up scan. Myocardial oedema was defined as a mean signal intensity >2 standard deviation greater than that of remote myocardium by semiautomatic software detection on T2 W images and quantified as a percentage of total myocardium on matched slices [122]. Areas of LGE were graded in transmural extent (0, no LGE; 1, 1% to 25% LGE; 2, 26% to 50% LGE; 3,

51% to 75% LGE; and 4,>76% LGE) and quantified by use of computer-assisted planimetry on each of the short-axis images. Hyperenhanced pixels were defined as those with image intensities >5SD above the mean of image intensities in a remote myocardial region in the same image. A further region of infarct was quantified with image intensity as >2SD greater than remote myocardium. This was defined as the infarct at periphery with 5SD infarct size used to quantify the core infarct region. Infarct heterogeneity was defined as the region of difference between the periphery infarct (2SD infarct size) and the core infarct (5SD infarct size)[186]. Microvascular obstruction was visualized using LGE images and quantified by manual planimetry of hypoenhanced region surrounded by LGE in each short axis slice [207]. Myocardial Salvage was calculated as the difference between reversible myocardial injury (using T2W images to identify oedematous myocardium) and irreversible myocardial injury (as defined by 5SD infarct size on LGE images) [122].

Biochemical parameters

Cardiac enzymes (troponin, CK, CK-MB) and N-terminal B-type natriuretic peptide (NT-pro-BNP) were collected at pre-specified time points and sent to a central laboratory for processing. The main study utilized CK-MB AUC as its primary end point, however data on all cardiac enzymes was collected as part of their secondary end point. Curve fitting was performed by a central

laboratory (according to accepted methodologies to generate CK area under AUC and estimated peak, CK-MB AUC and peak, and cardiac troponin I estimated peak and AUC [208]. A subgroup analysis of efficacy was prespecified to be based upon infarct vessel flow as assessed by thrombolysis in myocardial infarction (TIMI) grade by the interventional physician. The two groups were TIMI grade 0 or 1 vs. TIMI grade 2 or 3 on angiography prior to primary PCI.

3.3 Statistical Analysis

Data for continuous variables are presented as medians (interquartile, IQ range), and categorical variables are presented as frequencies and percentages. Wilcoxon rank sum tests were used to evaluate differences in continuous variables between groups, and $\chi 2$ tests were used for categorical variables.

We evaluated the relationship between baseline markers of myocardial damage (CMR derived infarct size, myocardial salvage, microvascular obstruction and infarct heterogeneity; and biochemical markers including troponin I, CK, CK-MB) and absolute percentage change in LVEF at 90 days using linear regression. We also performed multiple linear regression analysis to determine the strongest association between LVEF at 90 days (late LVEF) and key CMR (infarct size, myocardial salvage, microvascular obstruction, infarct heterogeneity) and biochemical (CK-peak and AUC, CK-MB peak and

AUC and TnI-peak) parameters. We checked all variables for normality and log-transformed variables when necessary. All model residuals were also assessed for normality. We compared models using Akaike's and Schwarz's Bayesian information criteria (AIC and BIC respectively) and chose the model with the largest AIC and BIC.

We also sought to identify correlates of improvement in segmental myocardial contractility. Each myocardial segment was categorised as improving in contractility from baseline to day 90 (reduction in wall motion score of ≥ 1) or non-improving (no change or increment in wall motion score by ≥ 1). Logistic regression was used to identify factors associated with improved segmental contractility.

All statistical tests were 2-sided, and a p-value <0.05 was considered statistically significant. All analyses were undertaken using STATA software, Version 12 (Stata Corp, College Station, Texas).

3.4 Results

96 patients were enrolled in the study and 85 completed the 90 day follow-up, across 24 centres worldwide; see Table 3.1 for patient baseline characteristics. Patients were 63 ± 12 years of age, 77% male and median time from symptom onset to infusion of drug was 170 minutes (111, 226 minutes). Biochemical

analysis was performed at day 3 to 5 in 90/96 patients. Out of the 85 patients that had 90 day follow-up scan, 81 (95%) patients had LGE performed and 56 (66%) patients had adequate T2 weighted (T2W) imaging performed (i.e. myocardial salvage index, MSI calculated). A significant number of scans with T2 weighted imaging had breathing artefact, ghosting artefact or missing slices causing these images to be removed from further analysis. Furthermore, approximately 10 patients did not have T2 weighted imaging performed. Baseline characteristics are shown in Table 3.1. Compared to the main study cohort, patients in the CMR sub-study were similar in age, gender, Killip class, co-morbidities and time to treatment.

CMR findings

Cine CMR

The median LVEF was 56% (46, 63%) at baseline (day 3 to 5) and increased to 60% (49, 67%) at 90 days, $p<0.001$. LV end-diastolic volume index increased from 68mL/m^2 (57, 81mL/m^2) to 76mL/m^2 (66, 87mL/m^2) at 90 days, $p<0.001$ whilst LV end-systolic volume index improved from 29mL/m^2 (22, 41mL/m^2) to 28mL/m^2 (23, 41mL/m^2), $p=0.067$. LV mass decreased from 78g/m^2 (68, 88 g/m^2) to 65g/m^2 (56, 74 g/m^2), $p<0.001$ (Table 3.2)

LGE findings

The infarct characterization results are summarized in Table 3.2. Median Infarct size was 17.5g (10.1, 33.1g) which equated to 14% (7, 21%) of LV mass at day 3 to 5, and this reduced to 10.6g (5.3, 22g) which was 9% (5,17%) of LV mass at 90 days, $p<0.001$ in keeping with previously well recognized findings of infarct involution [92, 123]. Surprisingly this cohort had very little microvascular obstruction 0.8g (0, 1g) which was 1% of LV mass. None of the patients had persistent MVO at 90 days.

T2W and MSI findings

A third of our patients had inadequate quality of T2 weighted images. Ten patients did not have it performed at all. All images were assessed by 2 level 3 CMR consultants before being removed from further analysis. In all patients with myocardial oedema imaging available for analysis, a high T2 signal abnormality was observed in the infarct region yielding 100% sensitivity for visualizing injured myocardium. Predictably, the area at risk calculated using T2W imaging for myocardial oedema exceeded infarct size, 49.6g (41.2, 67.2g) which was 36% (29, 45%) of LV mass in the early scan. Myocardial Salvage (Area at risk – LGE infarct size) demonstrated significant amount of

myocardium which was potentially recoverable at 57% (36, 75%) in our patient cohort.

Predictors of Global LV function early (day 3 to 5) and late (90 days) following revascularisation for STEMI

There were strong correlations between LVEF (at both baseline and 90 days) and CMR indices of infarct measurement (Table 3.3). Amongst all the CMR parameters of infarct characterization, *infarct size as measured by late gadolinium enhancement (LGE-CMR) exhibited the strongest negative correlation with both early ($r=-0.7$, $p<0.001$) and late LVEF ($r=-0.7$, $p<0.001$),* (Figure 1). Infarct size normalized to LV mass also correlated with late LVEF, however it was weaker in correlation, $r = 0.5$, $p<0.001$. Other measurements such as MVO and infarct heterogeneity correlated better with LVEF at baseline, than at 90 days (Table 3.3).

Infarct transmurality after recent MI

Infarct transmurality was compared to the likelihood of improvement in regional wall motion at 90 days. Out of 1376 segments available for assessment, 1031 had normal wall motion or improved in contractility at the 90 day scan and 345 did not. When compared to the degree of transmurality,

we found that 96% of the segments with no LGE improved, 80% of segments with <25% of LGE, 71% of segments with 26-50% LGE, 28% of segments with 51-75% and 24% of segments with >75% LGE also improved (Figure 2). We found that for every increase in transmurality, the likelihood of a segmental improvement in regional wall motion was reduced (odds ratio, 0.33, 95% confidence intervals 0.30 – 0.38, $p < 0.001$).

Biochemical markers

Median biochemical markers performed at initial admission were; CKAUC 36786.2U*HR/L (14566, 70738.5), peak CK 1511U/L (562, 2951), peak CK-MB 227.5ng/mL (92.5, 424.4), CK-MB AUC 3989.7 U*HR/L (1723.7, 6430.2) and TnI peak 46.5μg/L (14.5, 133.4). All biochemical markers demonstrated significant inverse correlations with 90 day LVEF with similar results, CKAUC; r=-0.6, p<0.001, CK peak; r=-0.6, p<0.001, TnI peak; r=0.6, p<0.001, peak CK-MB; r=-0.6, p<0.001, CK-MB AUC r=-0.6, p<0.001. There were similar correlations between biochemical markers and LVEF at baseline. There was also a significant relationship between biochemical markers and infarct size as measured by CMR at day 3 to 5; (CKAUC; r=0.7, p<0.001, CK peak; r= 0.7, p<0.001, TnI peak; r=0.6, p<0.001, CK-MB peak; r=0.6, p<0.001 and CK-MB AUC r=0.5, p<0.001). NT-pro-BNP was performed at 90 days only; median 272pg/L (163, 692). There was a moderate correlation between NT-pro-BNP and LVEF at 90 days; r = -0.4, p<0.001.

Angiographic parameters

Nearly half of the patients presented with TIMI 0 flow; 45/96 (45.9%). The other TIMI group results were as follows: TIMI 1; 14/96 (14.6%), TIMI 2; 20/96 (20.8%), TIMI 3; 17/96 (17.7%). Majority of patients (94%) achieved TIMI 3 flow after intervention. TIMI flow at presentation had weak correlations with LVEF at baseline (r=0.2, p=0.04), 90 days (r=0.2, p=0.02) and infarct size by CMR (r=0.3, p=0.02).

Multivariate model

The multivariate regression model for 90 day LVEF incorporated clinical characteristics (age, time from symptom onset to PCI and Killip class), imaging (infarct size at day 3 to 5, infarct heterogeneity, MVO and MSI), and biomarker data (CK peak, CK-AUC, CK-MB peak, CK-MB AUC and TnI peak). Since several of the biomarker variables were collinear we chose the strongest predictor which was CK AUC for inclusion the model. In the best fitting model that was assessed using the AIC and BIC, only 2 variables independently predicted 90-day LVEF: baseline infarct size, infarct heterogenity (as expressed by LGE-CMR at day 3 to 5) and baseline LVEF (Table 3.4).

3.5 Discussion

The principal finding in our study was that late LVEF (at 90 days) post STEMI was best predicted by baseline LVEF and infarct size by CMR on day 3 to 5. We found that in a multi-vendor, multi-centre environment, performed at 24 sites, in 3 continents, the most robust CMR parameter for predicting 90 day LVEF following STEMI was infarct size rather than myocardial salvage, infarct heterogeneity or microvascular obstruction. Our findings have important implications for the future design of STEMI clinical trials that use CMR surrogate end-points to test effectiveness of new therapy.

Several non -CMR parameters including infarct territory [209], sum of ST segment elevation [210, 211], microvascular dysfunction [212, 213], time to reperfusion [214] and time to peak CK [215] are well recognized as significant correlates of LV function following STEMI. Additionally, in recent years CMR parameters have been extensively evaluated and found to be beneficial in predicting late LV function after STEMI. These parameters include infarct size using LGE, myocardial salvage, microvascular obstruction and infarct heterogeneity. Currently there are many CMR techniques available to assess myocardial infarction [216]. In our study, we were able to show that infarct size by LGE was superior to the other CMR parameters of infarct characterization, in a multi-site, multi-vendor setting.

CMR infarct characteristics to predict late LV remodelling

Multi-centre studies using CMR in STEMI populations are limited. The Assessment of Pexelizumab in Acute Myocardial Infarction (APEX-AMI) study which had a similar population basis to ours, evaluated CMR parameters (infarct size and microvascular obstruction) and biochemical markers to predict 3 month LVEF [217]. The study which was performed over 5 centres, found that infarct size, MVO and 24 hour NT-proBNP independently predicted late LVEF. Surprisingly we did not find that MVO independently predicted late LVEF which has been shown to be the case in single-centre studies [188, 207] as well as in APEX-AMI [217]. This may be explained by the fact, our study population had very little MVO as compared to the aforementioned studies. More recently, since our trial, a large cohort of STEMI patients enrolled in the (iv abiciximab versus ic abiciximab; AIDA-STEMI) trial compared CMR markers of myocardial injury including infarct size, myocardial salvage and MVO [218]. This study demonstrated that both infarct size and MVO provided independent and incremental prognostic value in addition to clinical risk scores and LVEF in predicting cardiovascular events. Indeed Eitel and colleagues found MVO to be the most potent predictor of cardiovascular outcomes. Our study did not find that MVO was an independent predictor and we feel this is largely due to small number of patients that demonstrated MVO.

Infarct size has shown to be superior to other CMR parameters in predicting late LV dysfunction in a single centre study performed by Larose and colleagues [219], in which salvageable myocardium and microvascular obstruction were also evaluated. Salvaged myocardium refers to region which is the difference between area at risk and irreversibly injured myocardium. It has shown utility in several studies in predicting late LV remodelling [181] and major adverse cardiac events [220]. However, these studies have largely been done in high volume, single centres with significant CMR expertise. When we assessed the performance of myocardial salvage measurements in a multi-vendor, multi-centre environment, myocardial salvage correlated moderately well with late LV function, yet failed to be an independent predictor on multi-variate analysis. This finding may be explained at least in part by the relative inexperience of the centres in performing the T2 technique when compared to the LGE technique. This is highlighted by the finding that a third of our cohort failed to have myocardial salvage index performed adequately, due to poor image quality.

We also found that infarct heterogeneity (measured using the LGE technique) was also independently predictive of late LV function. Previously infarct heterogeneity has been implicated in single centre studies to be related to increase in cardiovascular events and arrhythmia[186, 221]. As far as we are aware, it has not shown independent predictive value for late LV function. Indeed Yan et al. did not show any correlation between LVEF and infarct

heterogeneity. In patients with severe ischaemic cardiomyopathy, infarct heterogeneity has been shown to cause an increase in cardiovascular events[221]. It has been theorized, that this may potentially be due to increase risk of arrhythmia due to combination of 'alive' myocytes in the border of necrotic scar tissue. We propose that post revascularizton, over 3 months, some of the region of infarct heterogeneity may become completely necrotic and hence correlate with late LV function.

Similar to previous studies, we also found that regional functional recovery was related to degree of transmurality of infarct assessed in the acute period. Choi [87] and Beek [89] and colleagues performed early work done in this area, assessing the likelihood of segmental recovery and its relation to percentage transmurality. We found that nearly a quarter of our segments with >75% transmurality improved in RWM score, albeit still with residual dysfunction. This may be explained by tethering effect caused by improvement in contraction of viable segments adjacent to non-viable segments giving a false sense of overall improved contractility. Our results were in contrast to Choi (5%) and yet similar to Beek (25%). To our knowledge this is the first multi-vendor, multi-centre study to demonstrate this significant relationship between segmental recovery and degree of transmurality.

Biochemical markers

CMR, although increasing in clinical use worldwide, is still limited by expense, operator expertise and availability. Therefore, we compared how biochemical markers which are performed routinely would predict late LV function. Although CK, CK-MB and troponin have shown utility in risk stratifying STEMI patients [208, 222, 223], most of studies have not incorporated CMR assessment of infarct size. In our study all 3 biochemical markers had moderate univariate correlations with LVEF at 90 days; however they failed to add independent prognostic value when CMR assessment of infarct size was incorporated into the model. Furthermore, there was no difference between CK peak and AUC measurements when compared to infarct size by CMR. This has important implications for clinical feasibility and ease of data collection (i.e. single peak measurements rather than multiple measurements to perform curve fitting analysis for AUC generation).

Angiographic data

Although we found associations between TIMI flow and CMR infarct size and LVEF at baseline and 90 days, the correlations were weak. Pre-procedural TIMI flow has been shown to be in an independent predictor of mortality in

high risk populations following STEMI [224]. Ours was a small cohort and we feel that with larger numbers, these associations would have been stronger.

3.5.1 Study Limitations

We intended to compare all the CMR parameters used to characterize infarct including myocardial salvage, infarct heterogeneity, microvascular obstruction and infarct size. We found that 1/3 of our patients did not have myocardial salvage performed adequately due to site inexperience and hence might account for the fact that myocardial salvage was not an independent predictor of late LVEF on multivariate analysis. However we feel this is a "real world snapshot" of CMR worldwide, where some centres are not confident with their assessment of area at risk and myocardial salvage. One of the surprising findings was the lack of independent predictability of MVO and LVEF at 3 months. This may largely be due to the small number of patients and limited degree of MVO demonstrated in our cohort. Furthermore, our population had a significant number of patients with preserved ejection fraction. This may represent some form of selection bias, in which the more stable patients (preserved EF, likely less MVO, limited infarcts) were selected to participate in the CMR substudy.

3.6 Conclusion

In a multi-vendor, multi-centre trial of STEMI patients, CMR parameters of infarct characterization correlate well with late LV remodelling. Infarct size by the LGE technique and not myocardial salvage area remains the most robust predictor of LV functional recovery.

Table 3.1

Baseline characteristics

Variable	Overall trial Anterior cohort	Sub-study cohort	P-value
N	997	96	
Demographic			
Age, y	61±12	63±12	0.12
Male sex, %	80	77	
Clinical, (%, n)			
Prior coronary artery disease	16, 160	8, 8	0.05
Prior MI	11, 110	7, 7	0.03
Prior PCI	11, 110	4, 4	0.03
Prior congestive heart failure	1, 10	0, 0	1.0
History of Stroke	4, 40	2, 2	0.09
History of PVD	3, 30	1, 1	0.57
Diabetes –type I	1, 10	1, 1	0.17
Diabetes – type II	16, 160	8, 8	0.05
Hypertension	46, 459	42, 40	0.45
Hypercholesterolemia	33, 329	23, 22	0.05
Current Smokers	42, 419	39, 37	0.59
Presentation			
Time from symptom onset to PCI, minutes,	191 (143, 261)	170 (111,226)	
ST segment AUC, uv*minutes	6830 (4898,9599)	5807 (4397,8380)	
Pre PCI TIMI flow (%, n)			
0	50, 499	47, 45	0.91
1	11, 110	15, 14	
2	17, 169	21, 20	
3	21, 209	17, 16	
NA	2, 20	0, 0	
Systolic/Diastolic BP, mmHg,	136±22/81±14	129±19/76±10	< 0.01/ < 0.01
BMI	27 (24,30)	27 (24,30)	
Killip class, (%, n)			
1	91, 907	92, 88	0.82
2	7, 70	8, 8	
3	1, 10	0, 0	
4	0, 0	0, 0	
Adverse Events			
Death (%, n)	3, 30	3, 3	1.0
Congestive Heart failure (%, n)	9, 90	8	1.0
Arrhythmia (%, n)	2.5, 25	1, 1	0.7
Cardiogenic Shock (%, n)	3, 30	1, 1	0.5

Values are expressed as mean±sd or median (IQR). MI – myocardial infarction; PCI – percutaneous coronary intervention; PVD – peripheral vascular disease

Table 3.2

CMR characteristics

	Day 3 to 5 CMR		Day 90 CMR	
LVEDVI (mL/m2)	68 (57, 81)		76 (66, 87)	p<0.001
LVESVI (mL/m2)	29 (22, 41)		28 (23, 41)	p=0.067
LVEF (%)	56 (46, 63)		60 (49, 67)	p<0.001
LVMMI g/m^2	78 (68, 88)		65 (56, 74)	p<0.001
Area at risk (g, %)	49.6 (41.2,67.2)	36 (29,45)	-	-
Infarct size (g, %)	17.5 (10.1,33.1)	14 (6.7,21.4)	10.6 (5.3,22)	8.5 p<0.001 (4.6,16.6)
Infarct heterogeneity (g, %)	10.3 (4,17.9)	6 (2,10)	-	-
MVO (g, %)	0.8 (0, 2.1)	0 (0, 1)	-	-
Myocardial Salvage index (g, %)	25.1 (12,38.8)	57 (36,74)	-	-

Values are median (25th, 75th percentile)

Table 3.3

Univariate CMR predictors of Baseline and 90 day LVEF

Parameter	Baseline LVEF		90 day LVEF	
	R	p value	R	p value
Infarct Size	-0.7	<0.001	-0.7	<0.001
Infarct heterogeneity	-0.5	<0.001	-0.4	<0.001
Microvascular obstruction	-0.5	<0.001	-0.4	<0.001
Myocardial Salvage	0.4	<0.001	0.4	0.001

LVEF – left ventricular ejection fraction

Table 3.4

Univariate and multi-variate predictors of day 90 LVEF

Parameter	β coefficient	P value	Multivariate p value
Baseline LVEF	0.73	<0.001	0.015
CK AUC	-1.52e-06	<0.001	
CK peak	-0. 00004	<0.001	
TnI peak	-0.00001	<0.001	
CK-MB peak	-0.0003	<0.001	
Infarct Size (LGE-CMR)	-0.004	<0.001	<0.001
Microvascular obstruction	-0.016	<0.001	
Infarct heterogeneity	-0.004	0.003	0.014
Myocardial Salvage index	0.17	0.001	

LVEF – left ventricular ejection fraction; CK AUC – creatinine kinase area under the curve; CK-MB – creatinine kinase myocardial band; TnI – troponin I; LGE-CMR – late gadolinium enhanced cardiovascular magnetic resonance.

Figures

Figure 3.1

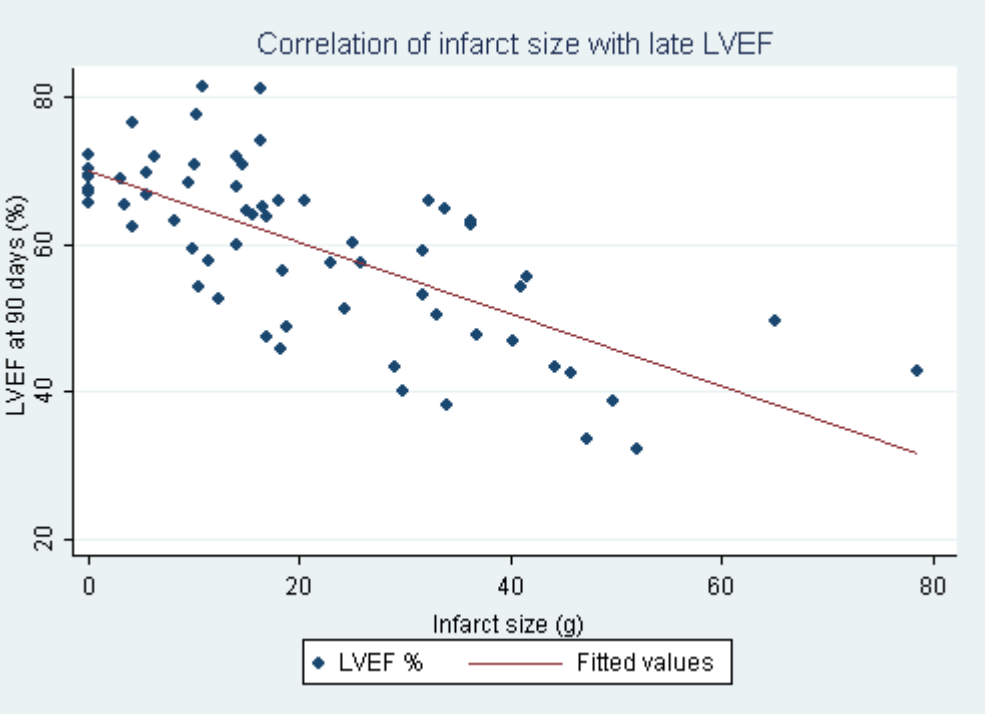

Demonstration of a negative linear correlation (r=-0.7) between infarct size by CMR and LVEF at 90 days.

Figure 3.2

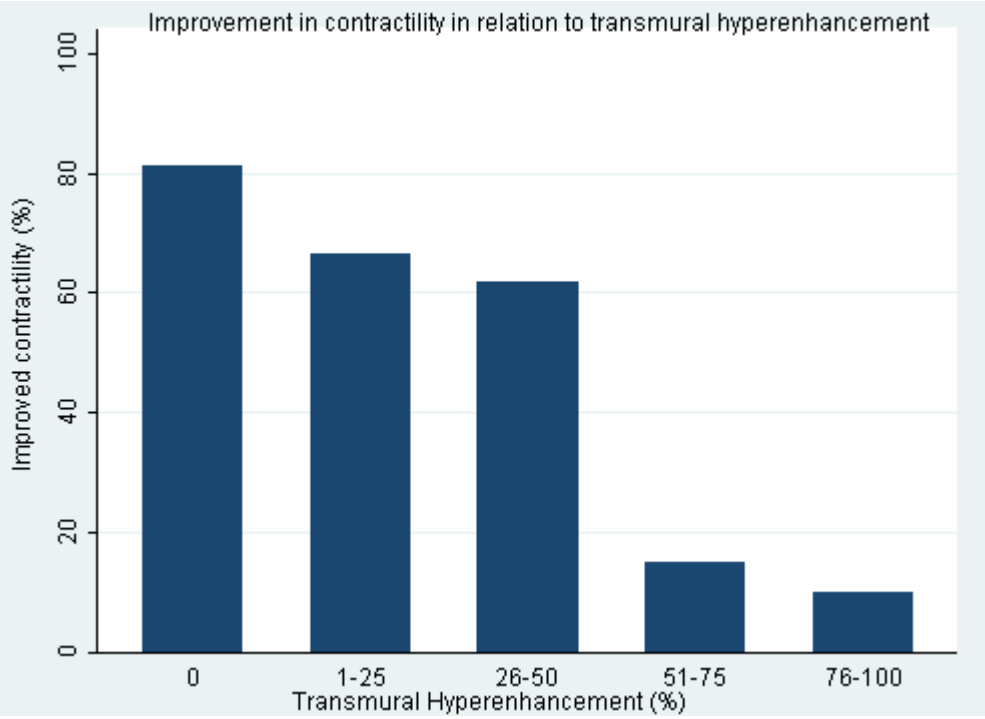

Relationship between transmural extent of hyperenhancement before revascularisation (day 3 to 5) and likelihood of increased regional function after revascularisation in all dysfunctional segments (at 90 days).

Chapter 4: Myocardial oxygenation in hibernating myocardium: insights from blood oxygen level dependent imaging pre and post revascularisation

4.1 Introduction

The term hibernating myocardium is traditionally defined as a "*result of reduced myocardial blood flow that causes impaired left ventricular function at rest and can be reversed by* revascularisation"[225]. The mechanisms underlying hibernating myocardium are controversial. Several studies, including our prior work using CMR quantitative perfusion, support the traditional view that under perfusion down-regulates local contractile performance [27, 29, 226, 227]. However recent studies have questioned this concept by demonstrating relatively normal regional perfusion in hibernating segments using Positron Emission Tomography [32, 33, 228], as well as normal oxidative metabolism using phosphorous magnetic resonance spectroscopy [229]. Yet, despite relatively normal resting perfusion, perfusion reserve has been found to be profoundly abnormal in hibernating segments [228, 230].

Blood oxygen level dependent cardiovascular magnetic resonance imaging relies on paramagnetic properties of deoxyhaemoglobin to non-invasively measure myocardial oxygenation. The net accumulation of deoxyhaemoglobin in the capillary blood leads to T2* shortening, which can

then be measured as regional signal loss in 'T2*-weighted' MR images. Initially validated in animal studies [137, 138], human studies have shown its utility in demonstrating the interplay between regional perfusion (using PET) and oxygenation in patients with coronary artery stenosis [116]. In addition, this technique has been recently evaluated with quantitative cardiovascular magnetic resonance perfusion in diagnosis of coronary artery disease [144], syndrome X [231], hypertension [232] and hypertrophic cardiomyopathy patients [233]. Measurement of myocardial oxygenation may provide understanding into the mechanisms underlying hibernating myocardium. Whether deoxygenation occurs at rest and/or stress in severely dysfunctional viable myocardium is unknown, and the simultaneous measurement of both myocardial perfusion and oxygenation in this setting has not yet been performed in clinical studies. Such a measurement would answer the question whether downregulation of myocardial oxygen demand in hibernating myocardium is sufficient to prevent deoxygenation at rest/stress.

Our aim was to use this non contrast method of measuring myocardial oxygenation to (1) examine whether deoxygenation occurs at stress/rest in dysfunctional 'viable myocardium' and (2) perform simultaneous measurement of CMR based first pass perfusion and oxygenation in viable myocardium. Our hypothesis was that hibernating myocardial segments will maintain myocardial oxygenation levels similar to those in remote normal myocardium both in stress and rest.

4.2 Methods

Study population: 15 patients with coronary artery disease and left ventricular dysfunction referred to surgical pre-admission clinic and agreed to participate in the study were recruited pre revascularisation. Inclusion criteria for CAD included 2 or 3 vessel disease diagnosed on coronary angiography. Alternatively single vessel disease patients could be included if there was significant stenosis (>70%) as assessed by the interventional cardiologist on visual inspection with matching regional LV dysfunction on echocardiography. LV dysfunction was diagnosed on 2D echocardiogram performed before revascularisation and included the following criteria: (1) moderate or severe regional LV dysfunction with regional LV dysfunction corresponding to the territory of significant stenosis on coronary angiography. CAD patients underwent imaging pre-revascularization and greater than 6 months post revascularization. A further 6 volunteers (healthy controls) from the community also underwent study protocol at 1 time point only.

Exclusion criteria were recent ST elevation myocardial infarction (within 3 months), contraindications to CMR (severe claustrophobia, metallic implants including pacemakers, defibrillators, cerebral aneurysms clips, ocular metallic deposits), contraindications to adenosine (second or third degree atrioventricular block, obstructive pulmonary disease, dipyridamole use) and contraindications to gadolinium (anaphylaxis, estimated glomerular filtration rate <60ml/min as calculated using Cockroft-Gaunt formula). Patients

underwent initial CMR imaging within 1 week prior to undergoing revascularisation.

CMR protocol

All subjects were asked to refrain from products that could counteract the effects of adenosine such as caffeinated drinks or methylxanthines for at least 24 hours before the CMR scan. Subjects provided written informed consent and the study was approved by the local ethics committee (ID: 31/09).

Each patient underwent CMR examination at 3-T (Trio, Siemens Medical Solutions, Erlangen, Germany) using an anterior 4-element phased-array coil and a posterior phased-array surface coil. From standard piloting, 3 long axis views (horizontal long axis, vertical long axis and left ventricular outflow tract) and short-axis cine images covering the left ventricle were acquired using a retrospective ECG-gated SSFP sequence (echo time, 1.5 ms; repetition time, 3 ms; flip angle, 60°). For BOLD imaging, patients were monitored by ECG, sphygmomanometry, and pulse oximetry. Six consecutive mid ventricular images were acquired from the same short axis slice using a T2-prepared ECG-gated SSFP sequence (echo time, 1.43 ms; repetition time, 2.86 ms; T2 preparation time, 40 ms; matrix, 168 x192; slice thickness, 8 mm; flip angle, 44°) at rest. If required, frequency scouting and shim adjustments were performed to minimize off resonance artifacts. For stress imaging, after

2 min of intravenous adenosine (140 μg/kg/min), 4 to 6 BOLD images were acquired in the same short-axis plane. Consecutive BOLD imaging slices are acquired commencing from 2 minutes to 5 minutes, until adenosine infusion was terminated. Immediately after stress BOLD imaging and prior to adenosine being terminated (4 to 5 minutes after commencing the adenosine infusion), first pass perfusion imaging was performed in the same short axis plane as for BOLD imaging, using an ECG-gated T1-weighted fast gradient echo sequence (echo time, 1.04 ms; repetition time, 2 ms; voxel size, 2.1 x 2.6 x 8 mm^3), and a peripheral bolus injection of a gadolinium-based contrast agent (Gadovist, Bayer) at 0.045mmol/kg followed by 15 mL flush at 6ml/s was injected. After 10 min, rest perfusion images were acquired without adenosine using the same sequence. For delayed enhancement imaging, an additional bolus of Gadovist (0.05 mmol/kg) was injected, and after 5 min, images were acquired in the 3 long axes and in the short axis plane to obtain coverage of the entire left ventricle using an ECG-gated T1-weighted segmented inversion recovery turbo fast low-angle shot sequence (echo time, 4.8 ms; voxel size, 1.4 x2.4 x8 mm; flip angle, 20°). The inversion time was adjusted to achieve optimal nulling of non infarcted myocardium.

Coronary angiography

Coronary angiography was performed based on institutional guidelines, using standard techniques and reported by the interventional cardiologist in charge

of the case. Based on these findings, the patients underwent appropriate revascularisation.

CMR analysis

All images were analyzed offline using (CMR circle-42 software, Calgary Canada). For BOLD analysis, endocardium and epicardium were manually traced and corrected for cardiac motion. The myocardium was sub-divided into 6 equiangular segments (anterior, anteroseptum, inferoseptum, inferior, inferolateral and anterolateral) based on the mid ventricular slice as per standard American heart association segmentation model [206]. Mean signal intensity was obtained from each segment at stress and rest and corrected for heart rate using previously published techniques [234]. The BOLD SI index was derived by dividing the change in SI from rest to stress by rest SI ([stress SI - rest SI]/rest SI). BOLD analysis was performed by a single operator (SKG, blinded to angiographic, functional, perfusion and LGE data).

For perfusion analysis, signal intensity curves were generated by tracing endocardium and epicardium contours and corrected for cardiac displacement. The myocardium was divided into 6 equiangular segments in a similar fashion to BOLD segmentation. A region of interest was placed within cavity of the left ventricle, excluding the myocardium and papillary muscles. Semi-quantitative perfusion analysis was performed as previously described [235]

and discussed in the methods section of this thesis. Because basal myocardial blood flow is closely related to the rate-pressure product (RPP), and index of left ventricular oxygen consumption, values for rest flow in each patient were also corrected for rate-pressure product [236]: Corrected Rest perfusion = (Rest perfusion/RPP) x 10^4. Myocardial Perfusion Reserve Index (MPRI) was calculated as the ratio of perfusion during adenosine-induced hyperemia to perfusion at rest corrected for RPP.

Regional wall motion was scored according to previous published criteria [92] by a blinded operator. Briefly, RWM was graded as 0, normal; 1, mild or moderate hypokinesia; 2, severe hypokinesia; 3, akinesia; and 4, dyskinesia. A segment was defined as improved if the wall motion score decreased by at least 1 grade at the follow up scan. For the purpose of this study, hibernating myocardium was defined as baseline RWM abnormality and improvement in RWM score post revascularisation of ≥ 1. All slices were matched for RWM, BOLD, perfusion and delayed enhanced imaging (Figure 4.1). Left ventricular volumes, mass and left ventricular ejection fraction were calculated and indexed to body surface area.

Angiographic analysis

Quantitative coronary angiography (QCA) was performed by single operators (JM) blinded to clinical information and CMR data. Diameters of reference

and stenotic coronary arteries were measured by a computer-assisted quantitative method (Quantcor Coronary Analysis, Siemens Medical Solutions). The contrast-filled catheter was used for image magnification calibration. All lesions in the main epicardial coronary arteries or their branches of greater than 2mm, were assessed for significance as the presence of stenosis >50% diameter. Each myocardial segment was assigned to a coronary artery territory according to standard criteria [206]. Collateral flow to the fully occluded vessel was graded using the Rentrop classification system [237].

4.3 Statistical Analysis

All analysis was performed using Stata version 13.0 (StataCorp, College Station, Texas). Differences in baseline characteristics between patients and controls were assessed using independent t-tests and chi-squared tests of association as appropriate. Differences in RPP at rest and under adenosine stress were assessed using paired t-tests. We assessed the effects of improvement in RWM and dysfunctional status at baseline on BOLD SI and MPRI using linear mixed effects models with a random intercept and adjustment for the 6 different segments and the study stage (pre or post revascularisation). Coronary artery disease patients were categorized according to whether or not they were dysfunctional at baseline and improved and in separate analysis as to whether or not they demonstrated improvement in RWM. Differences in means are described using beta coefficients with

standard errors from the mixed effects models. Univariate associations between BOLD SI and MPRI were assessed using Pearson correlations.

We also examined whether age, body surface area, cardiovascular risk factors (hypertension, diabetes mellitus, hypercholesterolemia, family history of coronary artery disease and smoking) were significantly associated with changes in BOLD SI after revascularisation by using risk factor x stage interaction terms. All significance tests were 2-sided and the type 1 error rate was chosen as $p<0.05$.

4.4 Results

Study population: Table 4.1 outlines the baseline characteristics of the participants. CAD patients had lower BOLD SI and MPRI as compared to normal volunteers. In addition, end diastolic volumes and end systolic volumes indexed were higher and ejection fraction lower in patients with CAD as compared to normal volunteers (Table 4.1). All CAD patients had baseline EF below the normal range (EF<55%) [238] and their indexed EDVI and ESVI were larger than reference standards. Furthermore, all CAD patients had cardiovascular risk factors (Table 4.2). None of volunteer patients had any history of previous CAD or cardiovascular risk factors. As expected changes were observed in the volumetric, functional, BOLD and perfusion indices post revascularisation (Table 4.3).

Pre revascularisation, the RPP at rest was 7721±1489 and increased to 11144 ± 2999 with stress (p=0.0002). Post revascularisation, RPP at rest was 8568±1915 and increased to 11001± 2143 with stress (p=0.005).

Regional and global left ventricular function pre and post revascularisation

Out of the 15 patients, 13 underwent coronary artery bypass grafting, whilst 2 underwent percutaneous coronary intervention; the latter in the left anterior descending artery (LAD). One patient refused follow up, due to illness. All CABG patients were fully revascularised and all received left internal mammary artery (LIMA) grafting. LVEF was reduced prior to revascularisation (47±10%). Post revascularisation, EF improved to 52±12% (p=0.012) at follow up. Overall there were 90 segments from 15 CAD patients. Pre-revascularisation, 66 out of 90 segments (74%), were dysfunctional (i.e. RWM≥1). At 8 months after revascularisation, 60 dysfunctional segments were available for analysis, from which 38 (63%) improved contraction by at least 1 grade.

Relationship between tissue oxygenation and perfusion

Normal volunteers

The mean overall BOLD SI for normal volunteers in our study was 12±3%. BOLD SI in normal volunteers that have been performed with the same sequence, on high field magnet such as our patients have ranged from 12% [144] to 17% [231]. All segments, except segment 5 had MPR values >1.5 (normal reference value)[239] (Table 4.1).

CAD patients

Relationship between coronary angiography and myocardial oxygenation and perfusion pre revascularisation

Overall there were 90 segments from 15 CAD patients. Of these, 68/90 (76%) were subtended by significant coronary artery stenosis. Fifty one segments had significant stenosis (QCA>50%) and 17 had significant stenosis with collaterals. Both BOLD signal intensity and MPR decreased in the presence of stenosis, r=0.2, p=0.08 and r=0.2, p=0.02 respectively (Figure 4.2).

Changes in myocardial oxygenation with adenosine stress pre and post revascularisation

Prior to revascularisation, the mean BOLD SI for the group was -3.2±16.4% and it improved to 2.7±13.1% after revascularisation (p=0.001). Importantly, there was a significant increase in BOLD SI in hibernating myocardial segments (β13.6±4.8, p=0.01) as opposed to those that were not hibernating (β 6.4, 5.7±6.8, p=0.26) (figure 3). Baseline BOLD SI did not differ between the two groups (p=0.33). This indicates that the improvement observed in BOLD SI in hibernating myocardial segments is potentially driven by revascularisation.

In multivariate analysis there was no significant association between BOLD SI and global LV function post revascularisation (p=0.13). However, there was a significant association between BOLD SI and end systolic volume indexed to body surface area (β=-0.13±0.16, p=0.04) after adjustment for segment and RWM improvement.

In multivariate analysis that assessed the effects of cardiovascular risk factors on improvement in BOLD, there was a significant interaction between hypercholesterolemia, hypertension and a trend towards diabetes mellitus and stage, i.e. patients with hypercholesterolemia were less likely to demonstrate a rise in BOLD SI after revascularisation than those without

hypercholesterolemia (β=-13.3±5.7, p=0.02). Similarly, patients with hypertension and diabetes were also less likely to demonstrate a rise in BOLD SI after revascularisation than those without (β-12.5±4.1, p=0.002) and (β-8.4±4.5, p=0.06) respectively.

Changes in perfusion with adenosine stress pre and post revascularisation

There was a significant increase in the myocardial perfusion ratio (MPR) after revascularisation (β=0.5±0.09, p<0.001). MPR increased in hibernating segments; (β=0.32±0.14, p=0.02), however it also showed a trend towards increase in segments that were not hibernating, (β=0.32±0.19, p=0.09). BOLD SI and MPR were significantly correlated (r=0.31, p=0.001). In multivariate analysis, MPR was not associated with improvement in hibernating myocardial segments (β=-0.03±0.0.08, p=0.72).

Late gadolinium enhancement

There were minimal segments with full thickness scar in hibernating myocardium (8/84, 9.5%) whilst the majority of segments had no hyperenhancement (n=66/84, 79%). The significant relationship between BOLD SI and hibernating myocardium remained after excluding segments with scar (i.e. >75% hyperenhancement) (β =12.5±5.5, p=0.03).

4.5 Discussion

BOLD CMR provides valuable insights into the pathophysiology of CAD. Hibernating myocardial segments demonstrate deoxygenation at stress. Although myocardial perfusion reserve improves in hibernating segments after revascularisation, it also showed improvement in segments that were not hibernating. There was an expected weak correlation between BOLD SI and MPRI. These findings would suggest that myocardial oxygenation is impaired in hibernating myocardium.

Potential mechanisms of chronic LV dysfunction

Reduced perfusion as assessed by ^{13}N-labeled ammonia in context of preserved fluorodeoxyglucose (FDG) uptake led to the concept of perfusion-metabolism mismatch [225, 240]. In addition, histological evidence suggests that contractile elements of myocytes are depleted with increased glycogen deposition [228], yet whether cellular metabolism is impaired is unknown. Animal models evaluating flow, oxygen consumption and metabolism indicate that hibernating myocardium retains metabolic and contractile reserve despite reductions in flow, function and resting oxygen consumption [241]. This adaptive down regulation is thought to provide potential for the hibernating

myocardium to maintain cellular metabolism, without development of ischaemia. However, later PET studies have challenged this theory by demonstrating preserved resting myocardial blood flow [32, 34]. In addition, animal work demonstrated reduced function in ameroid-induced stenosis reflecting cumulative myocardial stunning rather than primary deficit in coronary blood flow [242]. Furthermore, although resting myocardial blood flow has always remained controversial, there is no doubt that coronary flow reserve is reduced in hibernating myocardium [243]. In this situation, myocardial ischaemia may develop when there is a small increase in oxygen demand [244]. Our study provides some evidence to support this hypothesis. We were able to demonstrate that in patients with significant hibernating myocardium (74% segments), coronary flow reserve is reduced (i.e. reduced myocardial perfusion ratio). Furthermore, we also exhibited that oxygenation is reduced (i.e. reduced BOLD SI). Post revascularisation, there was a significant improvement in myocardial perfusion reserve and myocardial oxygenation. We propose that the reduced BOLD signal in hibernating myocardium during stress, reflects **development of ischaemia.** This is largely due to reduced myocardial perfusion reserve. We were not able to perform absolute quantification of myocardial blood flow. Selvanayagam and colleagues have previously shown reduction in myocardial blood flow at rest using quantification first pass perfusion [29]. In addition, work by the same group in coronary artery disease demonstrated reduction in BOLD SI and myocardial blood flow in myocardium subtended by significant coronary

artery stenosis, however these were all in patients with normal LV systolic function [144]. In our population (hibernating myocardium and reduced LV function), there is an increase in myocardial perfusion reserve post revascularisation. Hence, we propose that there is potential reversal of this ischemic state (rise in BOLD SI) in segments that improve in their regional wall motion abnormality.

Using an invasive animal model, Fallavolita and colleagues demonstrated down regulation of myocardial oxygen consumption at rest, however preserved ability of hibernating myocardium to increase oxygen consumption in response to stress. This occurred without development of ischaemia as reflected by normal myocardial lactate extraction and coronary venous pH [241]. This is in contrast to our patients that demonstrated increased deoxyhaemoglobin following vasodilator stress and hence had a drop in BOLD SI. There may be some important differences in our methodologies to account for this. Firstly Fallavolita utilizing an animal model evaluated regional hibernating myocardium segments only (i.e. by instrumenting LAD stenosis). Therefore, this animal model of regional hibernation may not have the same degree of deoxygenation as our patients with 2 or 3 vessel disease. Secondly, their stress was performed in the context of atrial pacing, whilst ours involved vasodilator stress, therefore direct comparison into the degree of deoxygenation/ischemia cannot be compared. Finally the methodology to measure ischaemia itself differed, with the former study using myocardial

lactate whilst ours uses deoxyhaemoglobin. In a normal functioning cell, when anaerobic metabolism occurs, lactate may remain in the cell and accumulate, be used by aerobic cells to reconvert to pyruvate or leach into the blood stream. It is not until anaerobic threshold is reached, that the blood lactic acid suddenly rises and is likely detectable. We propose that the measured myocardial lactate in this study may not have reached the threshold required to be significantly detectable. Whilst measuring deoxygenation directly bypasses some of the concerns around the varied way in which lactate is dealt with by the cells. When evaluating patients that exhibit changes in BOLD SI, it is important to appreciate that the observed changes reflect alterations in predominantly the venous compartment of the capillary bed and therefore do not represent actual cell (cardiomyocyte). Yet the oxygenation of the capillary blood directly reflects the balance of oxygen supply and demand and hence can be understood as a direct marker of tissue oxygenation.

Furthermore, it has been shown that BOLD imaging can be used to detect microcirculatory changes. This was specifically evaluated in patients with hypertension and hypertrophic cardiomyopathy [232, 233]. In addition to significant epicardial coronary artery stenosis, our patients also had co-morbidities such as hypertension. Therefore in addition to reduced BOLD SI secondary to epicardial coronary artery stenosis, microvascular dysfunction may have also contributed to the increased levels of deoxyhaemoglobin observed in our cohort.

We feel our patients reflect an accurate model of chronic ischaemic LV dysfunction. Previous studies have often separated reversibly or irreversibly injured myocardium, or presence and absence of collaterals. As expected for hibernating myocardium, most of our patients did not show evidence of significant previous myocardial infarction. Only 10% of our patients had full-thickness scar. Importantly BOLD SI continued to demonstrate a significant relationship in hibernating myocardium, even when segments with full-thickness scar were removed. In addition, up to 20% of segments were subtended by coronary artery stenosis with collaterals. Hence, although our findings may differ to some of the previous PET based studies, we feel they showcase a representative group of chronic ischaemic LV dysfunction patients that have a combination of predominantly hibernating myocardium, with some degree of scar. In these patients, a rise in myocardial oxygenation was noted after being revascularised.

PET reflects myocardial oxygen uptake, whilst BOLD examines the rate of cellular oxygenation in the heart. In animal models MRI methods of oxygen consumption and rest (i.e. myocardial blood flow, myocardial oxygen consumption and fractional oxygen extraction) have been found to have good correlation with PET as the gold standard [140]. Importantly, at the cellular level, it is believed that hibernating myocardium is spared from biological ischemia (preserved lactate levels), yet physiologically ischaemic [245]. Our

study provides further insight into the theory, that hibernating myocardium is at least physiologically an ischemic state. We demonstrated reduced BOLD SI in hibernating segments. Furthermore BOLD SI improved after revascularisation, particularly in segments that were hibernating. On the basis of such findings, we propose that hibernating myocardium results from recurring episodes of stress ischemia which may cause repetitive and therefore chronic stunning.

4.5.1 Study limitations

Our study numbers are small, hence these findings need to be replicated in larger numbers. In addition, we could not perform absolute quantification of myocardial blood flow which would have provided simultaneous measurement of oxygenation and resting blood flow. CMR first pass perfusion has found resting blood flow using absolute quantification, to be reduced in hibernating segments [29]. We were only able to show impairment in myocardial perfusion reserve using semi-quantitative perfusion analysis confirming previous work done. Hence, we can only postulate that the observed decline in BOLD SI seen in our patients is due to reduction in MPR and as this improves post revascularisation, the oxygenation also improves.

The use of a single mid ventricular slice for BOLD imaging is a further weakness of our study. Our patients had multiple coronary artery stenosis and

it is possible that some contribution of distal vessels to the overall BOLD signal intensity may have been missed by evaluating the mid ventricular SI only. In future studies, multi-slice imaging with parallel imaging techniques and artifact reduction methods [246, 247] may improve further utility of BOLD measurement in this population.

4.5.2 Conclusion

The noninvasive assessment of myocardial oxygenation by BOLD imaging offers valuable insights into the pathophysiology of hibernating myocardium. Although preliminary, our results indicate that the BOLD response is impaired in hibernating myocardium and that oxygenation is not down regulated in these myocardial segments.

Table 4.1 Study subjects characteristics

	Pre-revascularisation	Normal Volunteers	P value
Demographics			
Age	65±8	46±9	0.0002
Male (n,%)	15, 100	3,50	0.02
Height (cm)	175±7	170±11	0.09
Weight (kg)	87±18	73±7	0.05
Body surface area (m^2)	2.0±0.2	1.9±0.1	0.05
BOLD SI (segment), %			
1	-0.5±15.2	12.9±6.7	0.03
2	-1.0±9.5	12.4±7.5	0.0006
3	-3.9±17.5	10.8±9.9	0.05
4	-8.7±18.9	16.2±7.8	0.003
5	-3.8±18.9	6.3±8.0	0.1
6	-1.2±11.3	12.8±13.2	0.04
MPR (segment)			
1	0.8±0.4	1.8±1.0	0.002
2	0.9±0.3	1.7±0.8	0.002
3	0.7±0.2	1.6±0.9	0.001
4	0.7±0.3	1.9±0.7	<0.001
5	0.7±0.3	1.4±0.2	<0.001
6	0.8±0.4	2.0±1.0	0.0004
Rate pressure product Rest	7721±1489	9274±1516	0.02
Stress	11144±2999	11803±903	0.3
Volumetric Indices EDV indexed ml/m2	101±25	71±8	0.006
ESV indexed ml/m2	56±24	23±7	0.002
SV indexed ml/m2	45±11	50±6	0.2
EF (%)	47±11	68±7	0.0002
Myocardial mass indexed g/m2	72±16	54±9	0.01

Table 4.2 CAD patients risk factors and medications

Risk Factors (n,%)		**Medications**	
Smoker (ex or current)	10, 66	Aspirin	15, 100
Hypertension	8, 53	B-Blockers	12, 80
Hypercholesterolemia	13, 86	ACE/ARB inhibitors	11, 73
Diabetes Mellitus	4, 26	Statins	14, 93
Family history	4, 26	Ca channel blockers	2, 13

Table 4.3 CAD patients pre and post revascularisation

Volumetric Indices	Pre-revascularisation	Post revascularisation	
Ejection Fraction (%)	47±10	52±11	p<0.001
End-diastolic volume indexed ml/m^2	101±24	91±26	p<0.001
End-systolic volume indexed ml/m^2	56±23	48±25	p<0.001
Stroke volume indexed ml/m^2	45±11	46±12	p=0.2
Myocardial mass indexed g/m^2	72±15	68±14	p<0.001
BOLD SI (%)	-3.2±16.4	2.7±13.1	p<0.001
MPR	0.8±0.3	1.2±0.4	p<0.001

Figure 4.1

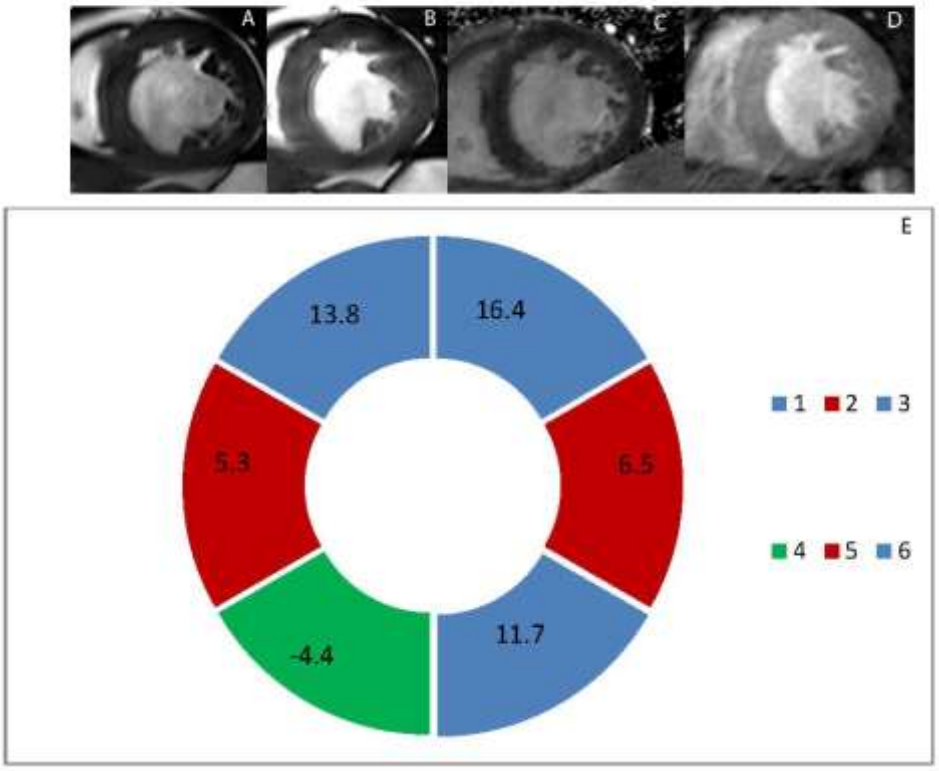

Mid ventricle short axis end-diastole phase of cine image in part A, end-systolic phase in part B, late gadolinium image in part C, and blood oxygen level dependent (BOLD) image in part D, with pictorial representation of BOLD Signal intensity (SI) in part E, in a 56 year old patient with significant circumflex (Cx) and right coronary (RCA) disease and 50% mid left anterior descending (LAD) lesion, following stress imaging. Segment 1 and 6 represent LAD artery territory and show positive BOLD SI (16.4% and 13.8%), 2 and 3 represent Cx with reduced BOLD SI in comparison (6.5% and 11.7%) and 4 and 5 represent RCA showing significantly reduced BOLD SI (-4.4%, 5.3%).

Figure 4.2

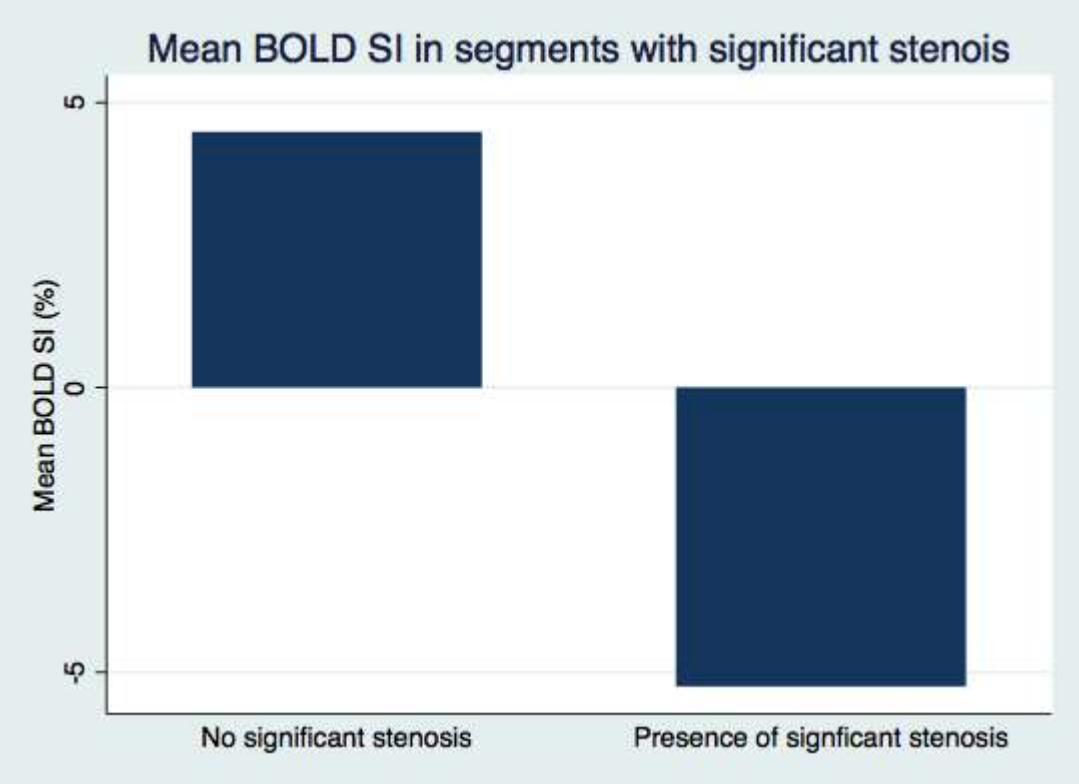

Bar graph shows pre revascularisation mean BOLD signal intensity based on presence/absence of significant stenosis.

Figure 4.3

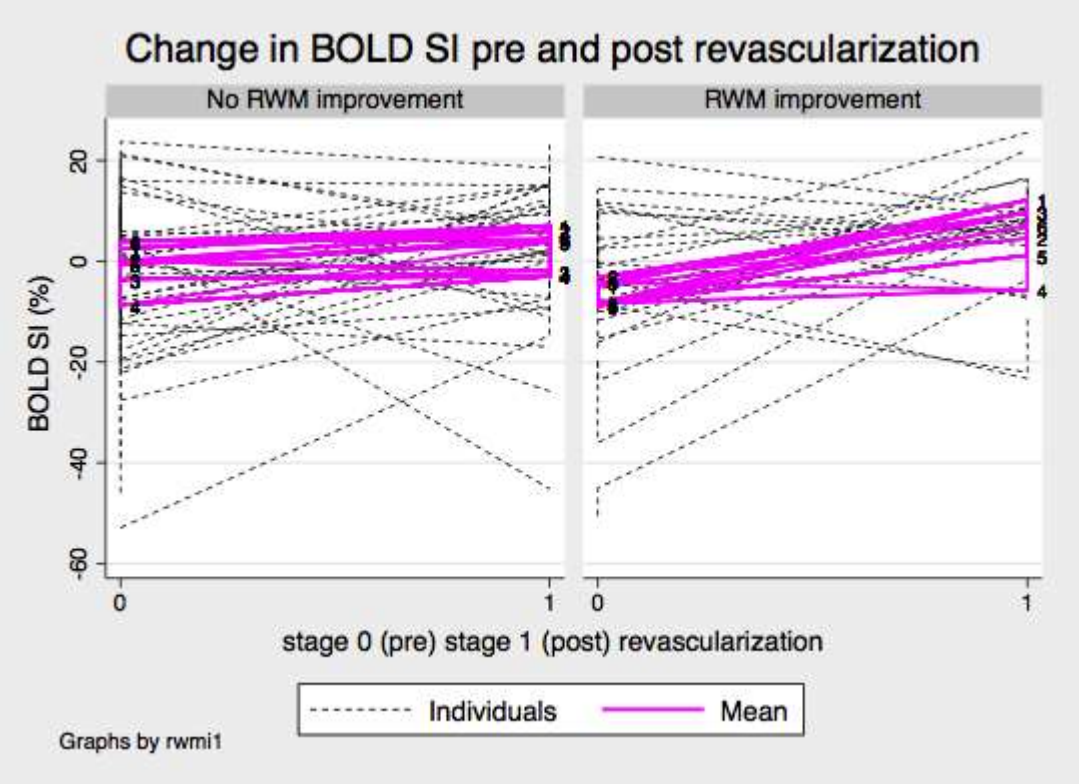

Line graph demonstrating individual and mean change in BOLD signal intensity before and after revascularisation (stage 0 and 1 respectively), depending upon whether they showed an improvement in regional wall motion score.

Figure 4.4

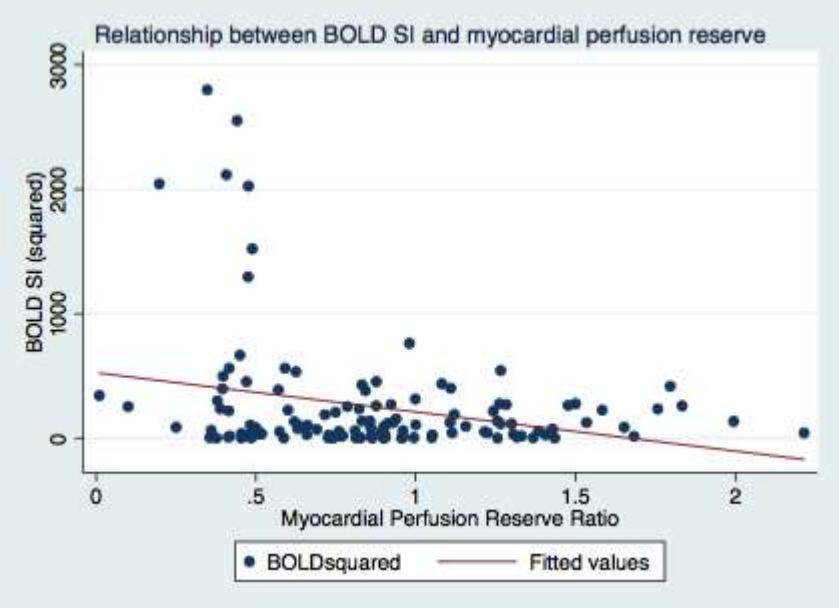

This graph displays correlation between BOLD signal intensity and myocardial perfusion ratio. The solid line is derived from a simple linear correlation after transforming the BOLD SI to BOLD SI squared. The individual blue dots represent BOLD SI and myocardial perfusion reserve in the same segment. Spearman's correlation was 0.3, p=0.01.

Chapter 5: Left ventricular effects of Anthracycline and Trastuzumab chemotherapy: a prospective, multi-centre study using novel cardiac imaging and biochemical markers

5.1 Introduction

Prolongation of survival resulting from cancer treatment has resulted in cardiac toxicity becoming the main determinant of quality of life, and in some cases premature mortality. For some patients with early stage breast cancer, a patient is more likely to die from heart disease than cancer [248]. Although, trastuzumab (Tr) related cardiotoxicity (CTX) is considered reversible, left ventricular dysfunction has been noted in up-to a third of patients in studies administered trastuzumab after anthracyline (A) based chemotherapy, [249-252] or trastuzumab alone [253]. The prediction of CTX in this setting is highly desirable so that alternative treatment strategies can be explored or potentially preventative maneuvers (such as angiotensin-converting enzyme inhibition) can be instituted.

Cardiovascular magnetic resonance offers the ability to non-invasively evaluate cardiac structure and function with unrivalled precision [74-77]. It remains the gold standard for accurate and reproducible assessment of left and right ventricular volumes and function. Furthermore, CMR tissue

characterization with myocardial oedema imaging allows detection of reversible myocardial injury, whilst late gadolinium imaging can detect myocardial scar and irreversible myocardial injury [82, 86, 122]. Meanwhile, speckle-tracking strain echocardiographic imaging represents an important emerging analysis technique that has shown promise in the sensitive evaluation of myocardial function and substrate [164].

The aim of this study was to use these novel imaging approaches to characterize serial LV structural remodelling and functional change following A and/or Tr and explore likely mechanisms. Our primary hypothesis was that LV functional impairment occurs early and persists into 12 months in patients following A or Tr, and this relates to the degree of myocardial oedema seen during chemotherapy. Our secondary hypotheses were that (1) the early functional changes detected by CMR correspond to changes seen in global longitudinal strain (GLS) and (2) late LV functional changes are associated with abnormalities in diastolic function.

5.2 Methods

From August 2010 to October 2012 inclusive, 48 female patients with early or metastatic breast cancer, from three Adelaide Oncology Centres were prospectively recruited into the study. All patients were planned to receive

adjuvant chemotherapy with A and/or Tr (not concurrently). In the metastatic disease group, the patients were required to be chemo-naïve for 5 years and not have received previous A or Tr. Exclusion criteria included age less than 18 years, previous diagnosis of coronary artery disease, cardiomyopathy, severe valvular heart disease or myocarditis. In addition, patients with permanent pacemakers, implantable cardioverter defibrillators or glomerular filtration rate (GFR) of <30/mL/min were excluded from participation. Participants underwent transthoracic echocardiography (TTE), CMR, biochemical markers and clinical evaluation pre-treatment and at 1, 4 and 12 months post-treatment. All patients provided written informed consent to the study protocol (24/10), which was approved by the clinical research and ethics committee of each participating institution, and conforms to the Declaration of Helsinki.

5.2.1 Cardiac magnetic resonance imaging

CMR was performed with a 1.5 T scanner (Area, Siemens, Erlangen, Germany). Transverse images were acquired with an inversion recovery prepared, dark blood HASTE sequence (repetition time [TR] 0518 600 ms, echo time [TE] 26ms, 6 mm slice thickness, 1.8 mm interslice gap, matrix 256x 104). Cine breathold balanced steady-state free precession sequence (TR 42 ms, TE1.2 ms, fractional anisotropy 70°, 6 mm slice thickness, matrix 192x174) was used to acquire 4 chamber, 2 chamber and LVOT views and

subsequently these images were used to plan the short-axis images that encompassed the entire LV from the base to the apex (stack of 10 sequential short-axis slices). To evaluate myocardial oedema, dark blood T2-weighted turbo spin echo short-axis images were obtained (TR 1,800 to 2,100 ms, TE 74 ms, 8 mm slice thickness, 4 mm interslice gap, matrix 256x175) at 3 short axis slices representing basal, mid and apical myocardium. Late gadolinium enhancement (LGE) images were obtained after 6 min of 0.1 mmol/kg injection of gadolinium (Gd-DTPA, Gadovist, Bayer, Germany) with a T1-weighted inversion recovery-prepared multislice true fast imaging with steady-state precession sequence with magnitude and phase-sensitive reconstruction. Images were acquired sequentially in the short axis, followed by horizontal and vertical long-axis images (TR 700 ms, TE 1.0 ms, fractional anisotropy 40°, 8 mm slice thickness, 1.6 mm interslice gap, matrix 192x144).

5.2.2 Cardiac Magnetic Resonance Analysis

Functional data was assessed using the cine images. Endocardium and epicardium were contoured using standard criteria previously published [254]. End-diastolic (EDV) and end-systolic volumes (ESV) were measured from which LV stroke volume (SV), ejection fraction and myocardial mass (MM) were calculated. All parameters were indexed to body surface area. Chemotherapy mediated toxicity was defined in our study as a decline in LVEF by 10% from baseline at 12 months as is considered clinically significant [255]. Myocardial oedema assessment was performed using the

Lake Louise Criteria [129]. Briefly, endocardium and epicardium were contoured on 3 short axis dark blood T2-weighted turbo spin echo images and an area of interest was selected in the latissimus dorsi muscle to generate a myocardial:skeletal muscle (M:Sk) signal intensity ratio (Figure 1). A global ratio of ≥2.0 in any SA slice was considered significant as previously published [129], and this was assessed at 1 and/or 4 months following commencement of chemotherapy. LGE analysis was performed visually by 2 independent observers and graded as present/absent in each short axis slice. Analysis was performed with dedicated computer software (CMR42, Release 4.0.0, Circle Cardiovascular Imaging, Calgary, Alberta, Canada).

5.2.3 Transthoracic Echocardiography

TTE was performed using GE Vivid 7 platform (General Electric, Milwaukee, Wisconsin). Images were performed with patients in the left lateral decubitus position, in standard parasternal and apical views. A minimum of 3 consecutive cardiac cycles were recorded for each image. Data was stored digitally for subsequent analysis. All grey scale images were acquired with frame rates between 60 to 80 frames per second. Transmitral blood flow velocities (E and A wave) were measured by pulse wave Doppler at the mitral valve leaflet tips. E' was measured off-line using color-coded tissue Doppler imaging (TDI) as the peak septal mitral annular tissue velocity in early diastole. LV strain profiles were derived by speckle tracking of grey-scale

images as previously described to determine global LV longitudinal strain score [256].

Blood Samples

Venous blood samples were collected and immediately centrifuged for 10 minutes at 1000(x g), and the serum aliquoted and stored at -80°C for batch analysis. Amino-terminal pro brain natriuretic peptide (NT-pro-BNP), high sensitive troponin T (hs-tnt) and high sensitive C reactive protein (hs-crp) concentrations were analyzed at baseline, 1 month and 4 months.

5.3 Statistical Analysis

Continuous variables are presented as mean± SD (where normally distributed) or median (inter-quartile range) and compared between groups at baseline using analysis of variance or the Kruskal-Wallis test as appropriate. Categorical data are summarized as frequencies and percentages, and compared using the χ^2 or Fisher's exact test.

For repeated-measures analysis of outcome variables of interest (indexed LV and EFs), mixed effects modeling was employed. The significance of predictor

variables (GLS, M:Sk ratio, hypertension, diabetes, hypercholesterolemia, smoking, family history, biochemical markers (NT-pro-BNP, hs-CRP and hs-tnt)) of interest was evaluated by including them in a mixed effects model as part of an interaction term with subjects' visit time (i.e. baseline vs. follow-up). If this predictor-time interaction term was significant, it implied that the candidate predictor variable's influence on the outcome variable was time-dependent. Post hoc testing was then performed to determine whether the candidate predictor variable's influence on the outcome variable was significant at both baseline and follow-up visit. All statistical tests were 2-sided, and a p-value <0.05 was considered statistically significant.

Observer reproducibility of parameters was assessed using the approach of Bland and Altman. All analyses were undertaken using STATA software, Version 12 (Stata Corp, College Station, Texas).

5.4 Results

5.4.1 Patient Characteristics

Forty-eight women (mean age 55 ± 10 years) requiring A and/or Tr containing chemotherapy regimens for breast cancer were enrolled from August 2010 to October 2012. Two patients were excluded due to detection of undiagnosed cardiomyopathy on baseline investigations in one and refusal to follow-up after baseline investigations in the other. Hence, 46 patients proceeded with the study (42, early breast cancer) and (4, metastatic breast cancer), receiving 3 to 6 cycles of epirubicin at 100mg/m2 or 3 to 6 cycles of doxorubicin at 50mg/m2, and/or trastuzumab in combination with taxanes or on its own with a loading dose of 8mg/kg followed by 6mg/kg every 21 days for 12 months (Figure 2). The clinical details are summarized in Table 5.1.

5.4.2 CMR parameters

Among 46 patients, 3 patients refused CMR due to claustrophobia. From the remaining 43 patients, functional assessment was feasible in all patients, myocardial oedema imaging in 40/43 patients (93%) and late gadolinium imaging for scar assessment was feasible in 40/43 (93%); in the remainder, gadolinium could not be administered at 4 months owing to inability to obtain intravenous access.

LV function

Significant functional changes were seen in the LV from baseline to 4 months. These changes persisted at 12 months (Table 5.2). At 4 months, immediately after completion of A or completion of 6 cycles of Tr, 21% patients (9/43) showed a decline in LVEF by >10%. By 12 months, 27% (7/26) of the cohort examined had persistent LV dysfunction, however none had LVEF below the normal range (<55%) [254].

T2W- short term inversion recovery (STIR) and LGE imaging findings

A substantial number of patients had increases in myocardial oedema following commencement of chemotherapy and this effect persisted to 4 months (Table 5.3). We found that 14/43 (33%) of patients had M:Sk ratio ≥2.0 at 1 month and 21/43 (49%) of patients had M:Sk ratio of ≥2.0 at 1 or 4 months following commencement of chemotherapy. One patient developed new sub-epicardial hyperenhancement suggestive of myocardial fibrosis in the Tr group at 4 months following therapy (figure 3).

5.4.3 Echocardiographic parameters

2D strain was feasible in 2405 out of 2772 segments (86%), owing to image quality. MV E:A, deceleration time and MV E:E' was performed in 100% of patients in whom the data was collected.

Diastolic function as measured by mitral valve (MV) E:A, MV deceleration and MV E:E prime (MV E:E') showed no significant change at 12 months (table 5.4). In addition, there was no significant change in E' prime with time. We did see significant decrease in GLS magnitude from baseline to 4 months (-21.4±2.5 to -19.5±2.0, p value < 0.001), with incomplete improvement at 12 months (-20.1±2.6, p value 0.01).

5.4.4 Biochemical markers

NT-pro-BNP did not change from baseline to 4 months. Significant changes were seen in hs-crp and hs-tnt at 1 and 4 months after commencement of therapy (table 5.4). Six patients had hs-tnt values greater than 15ng/L which is the upper limits of normal in our laboratory.

5.4.5 Correlation of myocardial oedema with functional data

Although increase in myocardial oedema and subsequent decline in LV function was observed post chemotherapy, we could not demonstrate that these two parameters were related.

Correlation of biochemical markers and echo parameters with CMR functional data

Early drop in GLS either at 1 or 4 months was not predictive of adverse LV or remodelling and subsequent drop in EF at 12 months. Biochemical markers: Increase in pro-BNP, hs-tnt or hs-crp levels did not predict a change in LV ESVI and EF.

Correlation of cardiovascular risk factors and functional data

Hypertension ($p=0.01$) and smoking ($p=0.05$) had significant association with adverse remodelling and decline in LVEF whilst age, family history, hypercholesterolemia and diabetes had no significant correlations. However,

the former two failed to predict deterioration in LV function depending on whether patients had a background of these risk factors.

Inter-observer variability

Bland-Altman analysis was performed to assess inter-observer variability of functional parameters (Table 5.5). This analysis exhibited good inter-observer agreement. Inter-observer 95% limits of agreement for GLS agreement at our institution was 1.6% (-1.8 to 5%) [257].

5.5 Discussion

Our principal findings show that: (1) significant functional changes detected by CMR occur early in the LV, and that these changes persist at 12 months. (2) These CMR functional changes are accompanied by significant change in GLS measured echocardiographically and biochemical markers such as hs-tnt and hs-crp. (3) A third of our patients showed an increase in myocardial oedema at 1 month and nearly half showed an increase at 1 or 4 months. None of our parameters allowed us to predict which patients would deteriorate in their LV function.

The cardiotoxicity of anthracylines and trastuzumab is well known, although most of the clinical studies evaluating this have been retrospective. To the best of our knowledge, ours is the first study to serially evaluate in a prospective manner, the effects of contemporary breast cancer chemotherapy regimens, on both early and late LV function using state of the art CMR and advanced echocardiographic techniques. Our results indicate that mild LV functional changes occur early, after commencing A or Tr therapy with subsequent decrease in ejection fraction of 3% at 1 month and 5% by 4 months. Reductions in LVEF of up to 5.5% have been detected by radionuclide ventriculography in a lymphoma population with doxorubicin doses of 200mg/m2 (similar to what our patients had received by cycle 4). At similar doses, echocardiography had failed to detect a significant change in LVEF. Only at doses of 500mg/m2 (far greater than what our cohort was given) was a similar significant change detected in LVEF by 2D echocardiography [258]. Multiple other studies have also shown that serial monitoring of LV function with cardiac imaging can detect early subtle cardiac dysfunction [166, 259-263]. None have elucidated a potential mechanism for the early cardiac changes observed. It is widely recognized that anthracylines lead to myocyte loss due to damage by toxic free radicals[38], and subsequent development of intracellular oedema [264]. Available imaging parameters to evaluate this hypothesis are limited, and relying on routine cardiac biopsies in all patients with chemotherapy CTX is associated with increased risk. Our results suggest that one of the likely

mechanisms for the sub-clinical LV dysfunction detected in prior studies may be chemotherapy induced myocardial inflammation. Significantly increased myocardial oedema were observed in almost half our patients, although we were not able to conclusively link deterioration in LV function with those that displayed the greatest increase in myocardial oedema. The relationship between myocardial oedema and deterioration in LV function following anthracylines, was first explored by Wassmuth et al. using the contrast enhanced method in myocardial oedema imaging by CMR [36]. In this study, significant deterioration in LV EF was noted in patients that exhibited positive myocardial oedema. Our results were less conclusive, likely owing to milder changes in LVEF in our cohort, differing methodologies of measuring myocardial oedema and the time interval of when patients were scanned following chemotherapy.

Despite seeing significant myocardial oedema and deterioration in LV function, we were surprised not to see evidence of significant myocardial necrosis (in acute scans) or replacement myocardial fibrosis (in 12 month scan), especially in the trastuzumab group. Previously Fallah-Rad evaluated patients receiving both A and Tr sequentially with serial echocardiography and CMR at baseline and then 12 months [265]. They found cardiomyopathy rates (EF drop by 10% and below lower limits of normal) in 25% of their cohort at 6 months and all of these patients demonstrated myocardial fibrosis by 12 months. Even though we also had nearly a quarter of the patients demonstrate

LVEF decline by 10%, none were below the lower limits of normal (LLN). Furthermore majority of our patients received either A or Tr which is in contrast to the Fallah-Rad group in which they received both agents sequentially. This may explain the low incidence of myocardial fibrosis observed in our group. Although myocardial oedema imaging was performed in Fallah-Rad group, it was only performed at baseline and then at 12 months following completion of chemotherapy. Furthermore, they do not report on any T2 changes and hence we cannot compare this to our group.

The functional changes observed by CMR in our study were corroborated by changes in global longitudinal strain. Strain by 2D echocardiography has shown promise in several studies evaluating LV dysfunction following chemotherapy [166, 167, 265]. We found that GLS decline peaked at 4 months post chemotherapy and remained relatively stable over 12 months. This was in keeping with the pattern of LV dysfunction detected by CMR in our cohort.

In addition to the functional changes observed in the left ventricle, we found that biochemical markers also increased with chemotherapy, particularly hs-tnt and hs-crp. Biochemical markers such as NT-pro-BNP, hs-tnt and hs-crp have found to be elevated after administration of anthracyclines in previous studies [62, 266]. Cardinale showed that troponin I measurements can rise after high

dose chemotherapy including use of anthracyclines and subsequent treatment of these patients with angiotensin converting enzymes may be able to prevent development of CTX [267]. On the other hand, our assay utilized hs-tnt and we found significant changes occurred in hs-tnt with increasing chemotherapy cycles, including 6 patients in whom the results were greater than 15ng/ml which is considered the upper limits of normal in our assay. Yet in contrast to the Cardinale study, rises in hs-tnt in our group did not predict a decline in LV function. There are 2 plausible explanations for this discrepancy. In comparison to the Cardinale group, our measurements were not performed within 72 hours of patients receiving chemotherapy and hence we may have missed the peak. Second, although hs-tnt changes were significant, they were not substantial enough to cause significant irreversible injury and hence adverse LV remodelling. This was supported by the absence of significant myocardial necrosis or replacement fibrosis in our cohort. Elevated cardiac troponin concentrations have been shown to identify patients at higher risk of mortality and adverse cardiovascular outcomes [268]. Our patients only exhibited mild declines in their LVEF, despite showing elevations in hs-tnt. Importantly, our follow up is limited to 12 months and whether these patients will go onto to develop more severe LV dysfunction and/or clinical heart failure in the future remains to be seen. We found that NT-pro-BNP did not significantly change in our cohort with increasing doses of chemotherapy and subsequent decline of LV function. There is some heterogeneity in the literature published evaluating NT-pro-BNP in this setting [175, 262, 265],

however direct comparison may not be possible as chemotherapy regime differed when compared to our cohort. Furthermore, it is likely that even though we had changes in LVEF (mean decline 6% at 12 months), the magnitude did not warrant changes in NT-pro-BNP.

5.5.1 Study Limitations

Our study showed development of myocardial oedema and decline in LV function occurs following chemotherapy. However we could not demonstrate that rise in myocardial oedema early would predict a decline in LV function and this is most likely due to limited study numbers. A larger population with longer follow-up would be necessary to substantiate these findings. Additionally whether T1 mapping, a technique utilized for assessment of diffuse fibrosis would be useful in this population requires further study. Furthermore our population included patients receiving anthracyclines or trastuzumab with only 4 patients receiving both agents sequentially.

5.6 Conclusion

Modern breast cancer chemotherapeutic regimens result in minimal persisting LV dysfunction and irreversible myocardial injury at 12 months. One of the potential mechanisms may be myocardial inflammation. Further evaluation is

required to correlate this with the observed ventricular changes seen and why in some patients, the function continues to deteriorate after completion of therapy despite the absence of irreversible injury.

Table 5.1

Baseline clinical demographics (n=46)

Age (y)	55±10
Body Surface Area (m^2)	1.8±0.2
Stage, n (%) Early Metastatic	 42 (91) 4 (9)
Anthracycline, n (%) Doxorubicin % Epirubicin % Trastuzumab, n (%) Both, n (%)	27 (59) 22 78 15 (33) 4 (9)
Radiotherapy, n (%) Left sided % Right sided %	22 (48) 45 55
Diabetes Mellitus, n (%)	8 (17)
Hypertension, n (%)	9 (20)
Hypercholesterolemia, n (%)	15 (33)
Smoking, n (%) Ex-smoker % Current %	25 (54) 84 16
Family history of ischaemic heart disease, n (%)	6 (13)

Table 5.2

Left ventricular functional changes following chemotherapy

	LVEDVI (mL/m2)	**LVESVI (mL/m2)**	**LVEF (%)**	**LVMMI (g/m2)**
Baseline (n=43)	63.4±11.8	18.1±6.3	71.9±6.3	47.1±9.1
1 month (n=41)	64.8±11.4	20.4±6.4**	68.8±6.3**	49.5±8.6
4 months (n=42)	65.4±11.3	22.1±7.0**	66.7±6.7**	46.4±8.4
12 months (n=26)	70.7±14.0**	24.8±9.6**	65.9±7.0**	41.2±7.3

Data are presented as mean±sd. LVEDVI – left ventricular end-diastolic volume indexed. LVESVI – left ventricular end-systolic volume indexed. LVEF – left ventricular ejection fraction. LVMMI – left ventricular myocardial mass indexed. .

*p<0.05 for comparison with baseline (repeated measures analysis)

**p<0.001 for comparison with baseline (repeated measures analysis)

Table 5.3

Change in Myocardial Oedema with chemotherapy

Time Point	Myocardial to skeletal muscle signal intensity ratios		
	Basal Myocardium	Mid Myocardium	Distal Myocardium
Baseline	1.3±0.3	1.4±0.2	1.5±0.3
1 month	1.4±.4, p=0.02	1.6±0.5, p=0.002	1.8±0.4, p=0.001
4 months	1.3±0.5, p=0.65	1.6±0.3, p= 0.05	1.8±0.4, p=0.003

Myocardial to Skeletal muscle signal intensity ratios were generated in three slices (basal, mid and distal) myocardium by contouring the myocardium and skeletal muscle and comparing the relative signal intensities as described previously [129]. Changes were compared to pre chemotherapy (baseline) ratios at 1 month and 4 months.

Table 5.4

Echocardiographic and Biochemical markers following commencement of chemotherapy

	GLS (%)	MV E:A ratio	MV deceleration time (ms)	E:E' ratio	NT-pro-BNP (pg/mL)	hs-TnT (ng/L)	hs-CRP (mg/L)
Baseline (n=46)	-21.4±2.6	1.2±0.5	216.8±41.2	8.9±2.5	68 (47-104)	3 (3-4)	2.1 (0.8-3.9)
1 month (n=42)	-20.7±2.4	1.1±0.5	216.6±38.9	8.3±2.6	53 (31-88)	4 (3-6)	3.7 (1.1-7.2)
4 months (n=43)	-19.5±2.0**	1.2±0.5	208.5±44.9	9.1±2.7	67 (37-109)	6 (3-14)**	3.7 (1-10)*
12 months (n=28)	-20.1±2.6	1.2±0.5	219.5±43.6	7.8±2.9			

Data are presented as mean±sd or median with interquartile range in parenthesis, at baseline and then follow-up at subsequent time points. GLS – global longitudinal strain. MV – mitral valve. TAPSE – tricuspid annular systolic plane excursion. NT-pro-BNP – amino peptide of brain naturietic peptide. Hs-TnT – high sensitivity troponin T. Hs-CRP – high sensitivity C reactive protein.

*$p<0.05$ for comparison with baseline (repeated measures analysis)

**$p<0.001$ for comparison with baseline (repeated measures analysis)

Table 5.5

Inter-observer variability for Cardiovascular Magnetic Resonance Parameters

Parameter	**Bland Altman 95% LOA**
LVEDV	-3.3 to 3.1Ml
LVESV	-0.5 to 1.4Ml
LVEF	-1.1 to 0.3%

See Table 5.2 for abbreviations

Figures

Figure 5.1

Demonstration of myocardial: skeletal muscle ratio for measurement of myocardial oedema

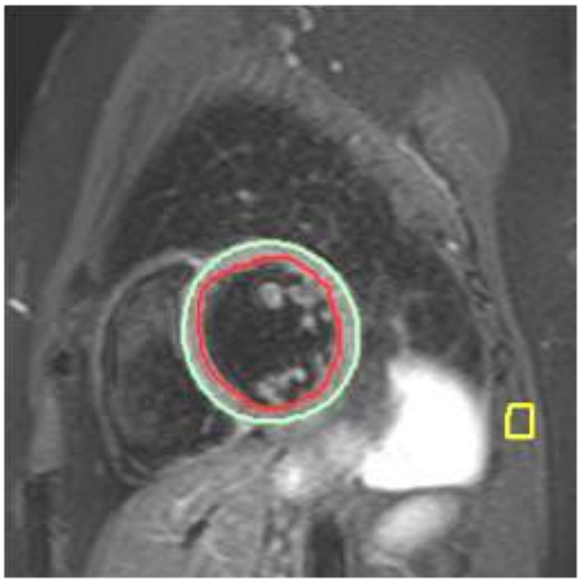

Mid ventricular short axis endocardium (red contour) and epicardium (green contour) in T2 W – short term inversion recovery (STIR) images and contour in the latissimus dorsi muscle (yellow contour) are demonstrated. Relative signal intensities in the myocardium are compared to the skeletal muscle to generate a myocardial to skeletal muscle signal intensity ratio.

Figure 5.2

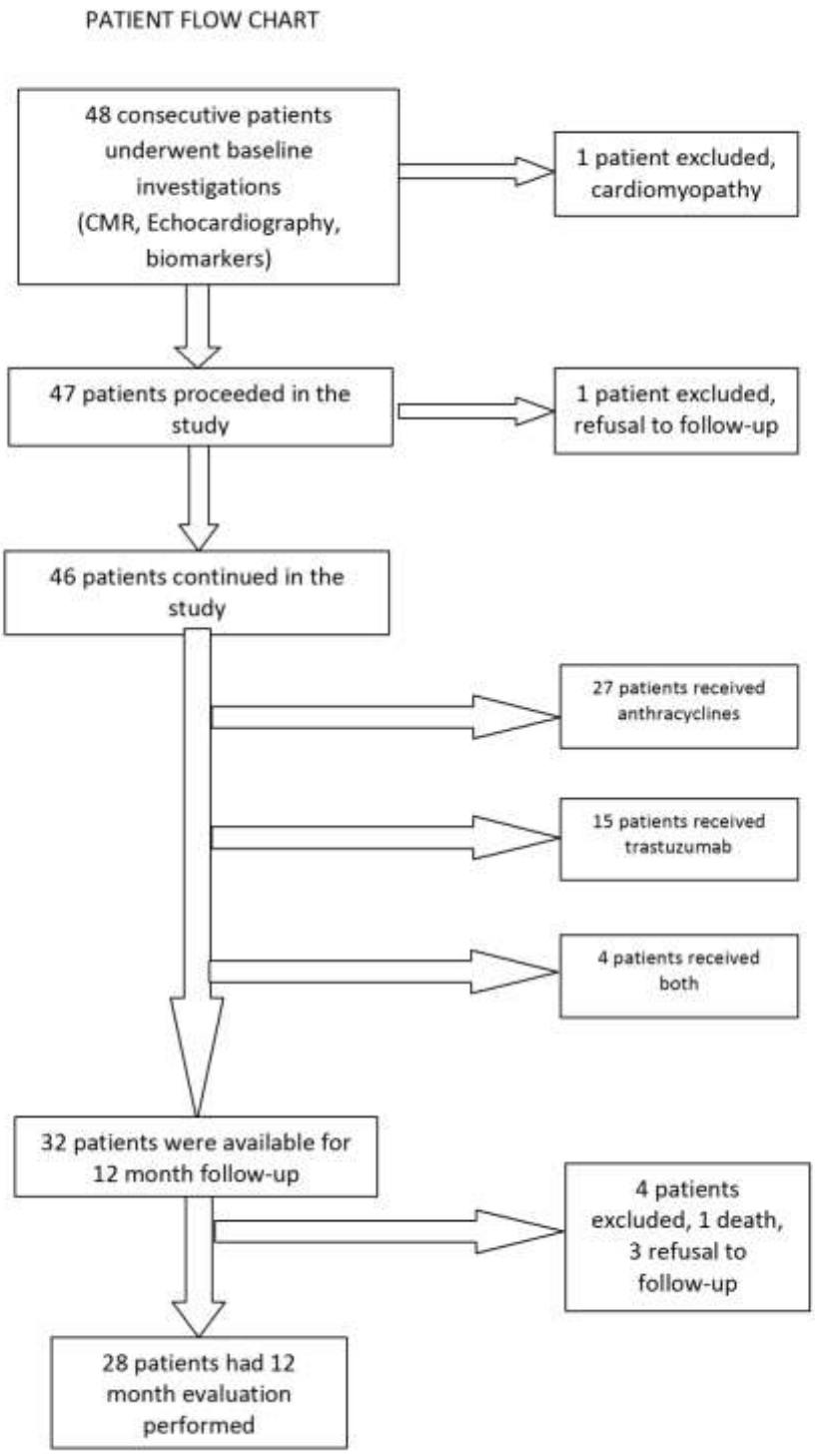
PATIENT FLOW CHART
48 consecutive patients underwent baseline investigations (CMR, Echocardiography, biomarkers)
1 patient excluded, cardiomyopathy
47 patients proceeded in the study
1 patient excluded, refusal to follow-up
46 patients continued in the study
27 patients received anthracyclines
15 patients received trastuzumab
4 patients received both
32 patients were available for 12 month follow-up
4 patients excluded, 1 death, 3 refusal to follow-up
28 patients had 12 month evaluation performed

Figure 5.3 Development of Late gadolinium enhancement in patient on trastuzumab

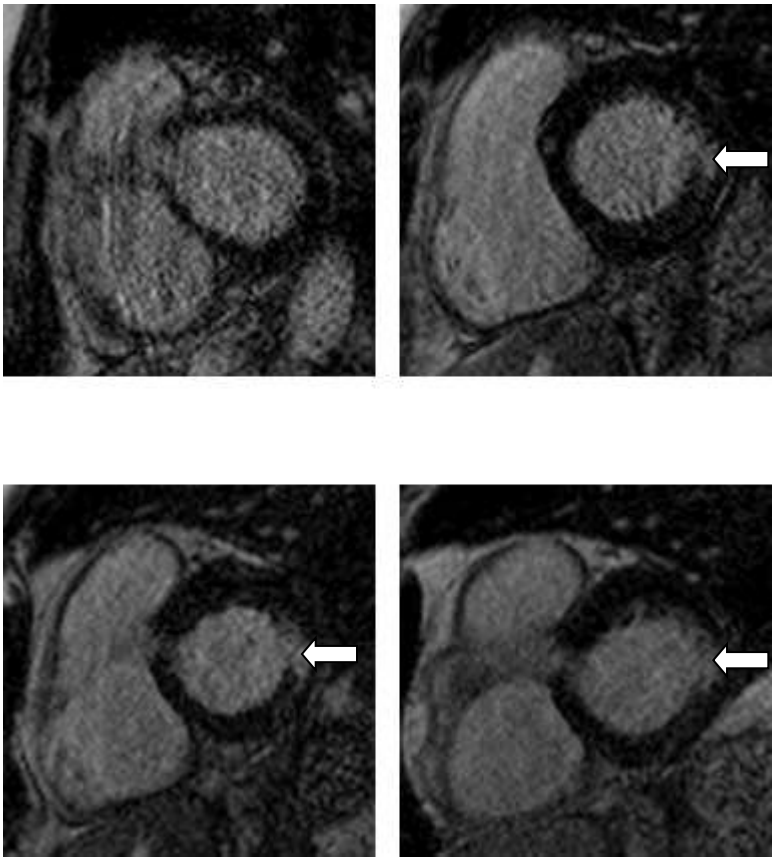

Late gadolinium enhanced imaging in a basal short axis slice demonstrating development of hyperenhancement (white arrowheads) in the lateral wall in the same patient at 4 different time points. Baseline (A), 1 month (B), 4 months (C), 12 months (D).

Chapter 6: Right ventricular effects of Anthracycline and Trastuzumab chemotherapy: a prospective, multi-centre study using cardiovascular magnetic resonance and biochemical markers

6.1 Introduction

Chemotherapy cardiotoxicity is defined as decline in left ventricular function by >10% and/or < lower limits of normal (EF<55%). This is largely based on evidence from adjuvant trials with trastuzumab and led to the recommendations of baseline and on-treatment cardiac function [255]. Furthermore, existing evidence on chemotherapy cardiotoxicity has emphasized the LV, with a relative paucity of literature on its RV effects. The importance of RV function as a predictor of outcome is well established in heart failure patients [168, 169], yet its significance in chemotherapy CTX remains uncertain.

Traditional imaging modalities for serial monitoring of cardiac function such as gated heart pool scans do not evaluate the RV. Alternatively echocardiographic measurement of RV is difficult due to the complicated geometry of the right ventricle. Cardiovascular magnetic resonance (CMR) offers the ability to non-invasively evaluate cardiac structure and function with unrivalled precision [74-77]. It remains the gold standard for accurate and

reproducible assessment of left and right ventricular volumes and function. Furthermore, CMR tissue characterization with myocardial oedema imaging allows detection of reversible myocardial injury, whilst late gadolinium imaging can detect myocardial scar and irreversible myocardial injury [82, 86, 122].

The aim of this study was to use these novel imaging approaches to characterize serial RV structural remodelling and functional change following A and/or Tr and explore likely mechanisms. Our group had previously demonstrated that current chemotherapy regimens for treatment of breast cancer, cause mild effects on the LV (chapter 5). We utilized the same cohort of patients collecting information on the RV including CMR volumes, function and echocardiographic assessment with tricuspid annular plane systolic excursion (TAPSE). Our primary hypothesis was that, despite the mild LV functional impairment observed, we may see more pronounced effects of these drugs on the RV.

6.2 Methods

The methodology for this study has been detailed in chapter 5. In brief, we evaluated 48 female patients with early or metastatic breast cancer, who were planned to receive adjuvant chemotherapy with A and/or Tr (not

concurrently). In the metastatic disease group, the patients were required to be chemo-naïve for 5 years and not have received previous A or Tr. Standard exclusion criteria and contraindications to CMR were excluded. All patients provided written informed consent to the study protocol (24/10), which was approved by the clinical research and ethics committee of each participating institution, and conforms, to the Declaration of Helsinki.

6.2.1 Cardiac magnetic resonance imaging

The CMR protocol was this study has been detailed in chapter 5. With regards to the right ventricle standard long axis images were used to plan the short-axis images that encompassed the entire LV and RV from the base to the apex (stack of 10 sequential short-axis slices). To evaluate myocardial oedema, dark blood T2-weighted turbo spin echo short-axis images were obtained (TR 1,800 to 2,100 ms, TE 74 ms, 8 mm slice thickness, 4 mm interslice gap, matrix 256x175) at 3 short axis slices representing basal, mid and apical myocardium. Late gadolinium enhancement (LGE) images were obtained after 6 min of 0.1 mmol/kg injection of gadolinium (Gd-DTPA, Gadovist, Bayer, Germany) with a T1- weighted inversion recovery-prepared multislice true fast imaging with steady-state precession sequence with magnitude and phase-sensitive reconstruction.

6.2.2 Cardiac Magnetic Resonance Analysis

Functional data was assessed using the cine images. RV EDV and end ESV were contoured and subsequent RV SV and EF were calculated. All parameters were indexed to body surface area. Chemotherapy mediated toxicity was defined in our study as a decline in EF by 10% from baseline at 12 months as is considered clinically significant [255]. Details regarding analysis methods for myocardial oedema and late gadolinium enhancement are described in chapter 5. In short, myocardial oedema assessment was performed using the Lake Louise Criteria [129]. A global ratio of $\geq$2.0 in any SA slice was considered significant as previously published [129], and this was assessed at 1 and/or 4 months following commencement of chemotherapy. LGE analysis was performed visually by 2 independent observers and graded as present/absent in each short axis slice. Analysis was performed with dedicated computer software (CMR42, Release 4.0.0, Circle Cardiovascular Imaging, Calgary, Alberta, Canada).

6.3 Statistical Analysis

Continuous variables are presented as mean± SD (where normally distributed) or median (inter-quartile range) and compared between groups at baseline using analysis of variance or the Kruskal-Wallis test as appropriate.

Categorical data are summarized as frequencies and percentages, and compared using the χ^2 or Fisher's exact test.

For repeated-measures analysis of outcome variables of interest (indexed RV and EFs), mixed effects modeling was employed. The significance of predictor variables (M:Sk ratio, hypertension, diabetes, hypercholesterolemia, smoking, family history) of interest was evaluated by including them in a mixed effects model as part of an interaction term with subjects' visit time (i.e. baseline vs. follow-up). If this predictor-time interaction term was significant, it implied that the candidate predictor variable's influence on the outcome variable was time-dependent. Post hoc testing was then performed to determine whether the candidate predictor variable's influence on the outcome variable was significant at both baseline and follow-up visit. All statistical tests were 2-sided, and a p-value <0.05 was considered statistically significant.

Observer reproducibility of parameters was assessed using the approach of Bland and Altman. All analyses were undertaken using STATA software, Version 12 (Stata Corp, College Station, Texas).

6.4 Results

6.4.1 Patient Characteristics

Forty-eight women (mean age 55 ± 10 years) requiring A and/or Tr containing chemotherapy regimens for breast cancer were enrolled from August 2010 to October 2012. Two patients were excluded due to detection of undiagnosed cardiomyopathy on baseline investigations in one and refusal to follow-up after baseline investigations in the other. Hence, 46 patients proceeded with the study (42, early breast cancer) and (4, metastatic breast cancer), receiving 3 to 6 cycles of epirubicin at 100mg/m2 or 3 to 6 cycles of doxorubicin at 50mg/m2, and/or trastuzumab in combination with taxanes or on its own with a loading dose of 8mg/kg followed by 6mg/kg every 21 days for 12 months (Figure 2, chapter 5). The clinical details are summarized in Table 5.1 (chapter 5).

6.4.2 RV function

Significant functional changes were seen in the RV from baseline to 4 months. Specifically, 23% patients (10/43) showed RV dysfunction (i.e. EF drop by 10%) at 4 months. These changes mirrored the drop in EF observed in the left ventricle. However, in contrast to the LV where the EF stabilized after the

first 4 months, the RV showed continued decline in EF with 46% (12/26) having a drop in their EF of 10%. In distinction to the LV changes, 83% (10/12) of these patients had RVEF below the lower limits of normal (LLN).

6.4.3 T2W- short term inversion recovery (STIR) and LGE imaging findings

A substantial number of patients had increases in myocardial oedema following commencement of chemotherapy and this effect persisted to 4 months (Table 6.3). We found that 14/43 (33%) of patients had M:Sk ratio ≥2.0 at 1 month and 21/43 (49%) of patients had M:Sk ratio of ≥2.0 at 1 or 4 months following commencement of chemotherapy. One patient developed new sub-epicardial hyperenhancement suggestive of myocardial fibrosis in the Tr group at 4 months following therapy.

6.4.4 Correlation of myocardial oedema with functional data

Although increase in myocardial oedema and subsequent decline in LV function was observed post chemotherapy (Table 5.3, chapter 5), we could not demonstrate that these two parameters were related. In contrast, when we specifically evaluated the patients that had significant myocardial oedema (global T2 ratio ≥2.0) in at least one short axis slice, we found that there was a

significant relationship between those with increased T2 ratios and lower RVEF at 12 months (EF 48.2±8.3 versus 55.8±8.0, p= 0.02).

6.4.5 Correlation of cardiovascular risk factors and functional data

With regards to the RV, hypertension ($p < 0.001$) and diabetes ($p = 0.02$) had significant associations with RVEF, nonetheless did not predict a decline in RV function at subsequent time points.

6.4.6 Inter-observer variability

Bland-Altman analysis was performed to assess inter-observer variability of functional parameters (Table 6.2).

6.5 Discussion

Our principal findings show, that despite mild changes in the LV, more significant and persistent changes occur in the RV. In addition, we found that those patients that had significant LV myocardial oedema at 1 or 4 months post-chemotherapy showed persistent RV dysfunction at 12 months.

In contrast to the relatively mild LV effects, we found that almost half of our cohort had impairments in RV function at 12 months when assessed by CMR, the gold standard technique for this measurement. Although to our knowledge no prior study has examined the effect of trastuzumab on the RV using CMR, our results support previous work by Barendswaard et al. using radionuclide ventriculography in patients receiving anthracyclines [269]. Furthermore, in our cohort LV function remained stable after the initial decline at 4 months, whereas the RV continued to deteriorate in function at 12 months. We hypothesize that the thinner structure of the RV, with fewer number of myofibrils makes it more susceptible to damage by chemotoxins. This was supported by the significant relationship between early myocardial oedema and decline in RV function at 12 months. We were not able to demonstrate the same significance with LV function. A potential reason maybe that the overall changes in myocardial oedema were mild, leaving the thinner RV susceptible, yet the LV with its greater number of myofibrils relatively preserved. In addition our follow up is limited at 12 months, and further deterioration in LV function may be elucidated if these patients were reimaged some years later.

The importance of RV function in predicting outcome of heart failure patients has been established previously [168, 169]. Yet it is not a chamber that can be easily imaged by standard techniques especially echocardiography owing to its unique geometry. Hence, surrogate markers of RV function utilizing echocardiography were recently evaluated in patients receiving multiple

chemotherapeutic agents, including anthracyclines. Tanindi et al. found that echocardiographic indices such as tricuspid annular plane systolic excursion and RV fractional area change showed significant changes in the acute setting (within 2 cycles), however they were sub-clinical [175]. Our study also showed early subtle changes in RV systolic function. In comparison Tanindi et al. did not have any long term follow up and we found that by 12 months, a significant portion of our patients had declined RVEF to below LLN. Whether the changes observed in the RV in our cohort are precursor to developing LV cardiomyopathy or a separate pathological process remains to be confirmed. Our study highlights, that routine RV assessment following chemotherapy should be incorporated as part of assessment of chemotherapy CTX.

6.6 Conclusion

In contrast to the LV effects, RV effects as detected by cardiovascular magnetic resonance, occur early and persist at 12 months in a significant number of patients. These RV changes seem to correlate to the rates of myocardial oedema, which is a likely surrogate of A/Tr chemotherapy induced myocardial inflammation.

Table 6.1

	LVEF (%)	**RVEDVI (mL/m2)**	**RVESVI (mL/m2)**	**RVEF (%)**
Baseline (n=43)	71.9±6.3	65.1±13.4	24.6±7.2	62.5±6.9
1 month (n=41)	68.8±6.3**	67.6±14.4	27.8±7.4*	58.9±5.8*
4 months (n=42)	66.7±6.7**	66.4±12.2	28.5±7.1**	57.2±6.4**
12 months (n=26)	65.9±7.0**	69.6±12.0*	32.9±8.1**	52.8±8.8**

Data are presented as mean±sd. RVEDVI – left ventricular end-diastolic volume indexed. RVESVI – left ventricular end-systolic volume indexed. LVEF – left ventricular ejection fraction. RVEF – right ventricular ejection fraction.

*$p<0.05$ for comparison with baseline (repeated measures analysis)

**$p<0.001$ for comparison with baseline (repeated measures analysis)

Table 6.2

Inter-observer variability for Cardiovascular Magnetic Resonance Parameters

Parameter	**Bland Altman 95% LOA**
RVEDV	-0.9 to 3.2mL
RVESV	-1.2 to 2.4mL
RVEF	-1.9 to 1.5%

See Table 6.1 for abbreviations.

Chapter 7 Early and late changes in markers of aortic remodelling with breast cancer therapy

7.1 Introduction

Anthracylines and trastuzumab are commonly used for the treatment of breast cancer and are well recognized for their potential for cardiotoxicity. These agents can cause injury to the LV myocardium, reduction in global ventricular function and lead to clinical heart failure (HF) [59, 249, 253, 270, 271]; both early and late after administration, however the exact mechanism remains unclear. Anthracyclines induce generation of toxic oxygen free radicals, which can potentially lead to cardiovascular injury. The heart in particular is significantly susceptible to oxidative stress. Trastuzumab, responsible for inhibiting HER 2 protein, blocks repair pathways, which leaves the myocardium vulnerable to injury and failure to repair efficiently.

Negative arterial remodelling (reflected by changes in aortic stiffness such as rise in pulse wave velocity and decline in distensibility) has been linked to increase in cardiovascular (CV) events [272, 273]. Indeed, presence of increased aortic stiffness is an independent predictor of all cause mortality in patients with hypertension [147, 274]. Increase in aortic stiffness has been implicated as one of the potential mechanisms for the observed CV morbidity in chemotherapy, particularly when combined with other CV risk factors such

as hypertension, diabetes and age [272-274]. Although changes in aortic compliance and stiffness following anthracylines have been evaluated, little is known whether these changes reverse after cessation of therapy. Furthermore, the effects of trastuzumab on aortic compliance and stiffness remain unstudied. Our aim was therefore to study the acute (within 1 and 4 months) and late (at 14 months) effects of anthracyclines and trastuzumab on aortic compliance and stiffness in patients undergoing treatment for breast cancer.

7.2 Methods

Patients were eligible for enrolment if they had early or metastatic breast cancer, and had chemotherapy with anthracylines and/or trastuzumab prescribed (although not concurrently). In the metastatic disease group, the patients were required to be chemotherapy-naïve for 5 years and not to have received either of these drugs previously. Exclusion criteria included age less than 18 years, previous diagnosis of coronary artery disease, cardiomyopathy, severe valvular heart disease or myocarditis. In addition, patients with permanent pacemakers, implantable cardioverter defibrillators or glomerular filtration rate (GFR) of <30/mL/min were excluded from participation. All patients provided written informed consent to the study protocol (24/10), which was approved by the clinical research and ethics committee of each participating institution, and conforms to the Declaration of Helsinki.

7.2.1 Study procedures

Using our initial cohort of breast cancer chemotherapy patients, we amended our original protocol to perform CMR derived assessment of aortic remodelling. From July 2011 to October 2012 inclusive, 29 female patients from 3 oncology centres in Adelaide were prospectively recruited into the study. Participants underwent clinical evaluation and cardiovascular magnetic resonance, pre-treatment and at 1, 4 and 14 months post-treatment. This cohort was followed up later than the original cohort to give at least 1 month after finishing the trastuzumab therapy. Furthermore, 12 women from the community, age (54±13) underwent baseline CMR investigations including aortic pulse wave velocity, aortic distensibility, aortic stiffness and LV function.

7.2.2 Cardiovascular magnetic resonance imaging

CMR was performed with a 1.5 T scanner (Aera, Siemens, Erlangen, Germany). Transverse and sagittal images were acquired with a dark blood HASTE sequence (repetition time [TR] 600 ms, echo time [TE] 33ms, 6 mm slice thickness, 1.8 mm interslice gap, matrix 256x 151). Cine breathold balanced steady-state free precession sequence (TR 48 ms, TE 1.2 ms, fractional anisotropy 70°, 7 mm slice thickness, matrix 192x 156) was used to

acquire 4 chamber, 2 chamber and LVOT views and subsequently these images were used to plan the short-axis images that encompassed the entire LV from the base to the apex (stack of 8- 10 sequential short-axis slices). Using transverse and sagittal HASTE localizers, cine images of the ascending and proximal descending aorta were acquired in the sagittal plane and then axial cross sectional images were planned to determine the maximum and minimum aortic lumen area for the ascending aorta and proximal descending aorta. A nonferromagnetic brachial blood pressure cuff was applied to record BP during the aortic cross-sectional image acquisitions. Phase-contrast cardiovascular magnetic resonance (PC-CMR) images were performed according to previous published techniques (10), in the same plane to determine pulse wave velocity in AA and PDA. PC-CMR imaging parameters included a 34- to 36-cm field of view, a 256x192 matrix, a TR 23ms repetition time, a 3- to 5-ms echo time, a 15- to 20-degree flip angle, an 8-mm thick slice, and a through plane velocity encoding of 150 cm/sec.

To evaluate myocardial oedema, dark blood T2-weighted turbo spin echo short-axis images were obtained (TR 1,800 to 2,100 ms, TE 74 ms, 8 mm slice thickness, 2 mm interslice gap, matrix (256x175) at 3 short axis slices representing basal, mid and apical myocardium.

7.2.3 CMR image analysis

7.2.3.1 Aortic remodelling

All images were analyzed offline using CMR-42 software. Using the cine image, the aortic lumen was magnified 400 to 800% and manually traced to determine the maximum and minimum area. Ascending and proximal descending aorta distensibility (Figure 1), and pulse wave velocity through the thoracic aorta was determined using previously published criteria (Figure 2) [275, 276]. Specifically, pulse wave velocity (m/s) was calculated as the ratio of distance between levels and time difference between arrivals of the pulse wave at these levels. The pulse wave was considered to "arrive" at a certain level when the mean velocity reached half of its maximum value.

The stiffness index was calculated as follows:

$$\frac{\ln\left(SBP/DBP\right)}{Change\ in\ cross\text{-}sectional\ area}$$

where SBP is systolic blood pressure, DBP is diastolic blood pressure, change in cross sectional area is the difference between maximum and minimum area at arterial vessel of interest.

7.2.3.2 LV volumes, function and mass

Functional data was assessed using the cine images. Endocardium and epicardium were contoured using standard criteria previously published [254]. End-diastolic and end-systolic volumes were measured from which LV stroke volume; ejection fraction and myocardial mass were calculated.

7.2.3.4 Myocardial Oedema

Endocardium and epicardium were contoured on 3 short axis dark blood T2-weighted turbo spin echo images and an area of interest was selected in the latissimuslatissimus dorsi muscle to generate a myocardial:skeletal muscle signal intensity ratio. A global ratio of $\geq$2.0 in any SA slice was considered significant as previously published [129], and this was assessed at 1 and/or 4 months following commencement of chemotherapy.

7.3 Statistical Analysis

Continuous variables are presented as mean± SD (where normally distributed) or median (25^{th}-75^{th} percentile) and compared between groups at baseline using analysis of variance or the Kruskal-Wallis test as appropriate. Categorical data are summarized as frequencies and percentages, and compared using the χ^2 or Fisher's exact test.

For repeated-measures analysis of outcome variables of interest (distensibility and stiffness index of ascending and proximal descending aorta; and pulse wave velocity from ascending to proximal descending aorta), mixed effects modeling was employed. The significance of predictor variables (baseline LV EF, M:Sk ratio, hypertension, diabetes, hypercholesterolemia, smoking, family history of ischaemic heart disease, pulse pressure, systolic blood pressure, age, body surface area, use of anthracycline, trastuzumab, left sided radiotherapy)) of interest was evaluated by including them in a mixed effects model as part of an interaction term with subjects' visit time (i.e. baseline vs. follow-up). If this predictor-time interaction term was significant, it implied that the candidate predictor variable's influence on the outcome variable was time-dependent. Post hoc testing was then performed to determine whether the candidate predictor variable's association with the outcome variable was significant at both baseline and follow-up visit. All statistical tests were 2-sided, and a p-value <0.05 was considered statistically significant.

Observer reproducibility of parameters was assessed in 12 patients using the approach of Bland and Altman. All analyses were undertaken using STATA software, Version 12 (Stata Corp, College Station, Texas).

7.4 Results

Twenty-nine women (mean age 54±11 years) requiring anthracycline and/or trastuzumab containing chemotherapy regimens for breast cancer were enrolled from July 2011 to October 2012. Two patients were excluded due to detection of undiagnosed cardiomyopathy on baseline investigations in one and refusal to follow-up after baseline investigations in the other. Hence, 27 patients proceeded with the study (25, early breast cancer) and (2, metastatic breast cancer), receiving 3 to 6 cycles of epirubicin at 100mg/m2 or 3 to 6 cycles of doxorubicin at 50mg/m2, and/or trastuzumab in combination with taxanes or on its own with a loading dose of 8mg/kg followed by 6mg/kg every 21 days for 12 months. Five patients (3 in the anthracycline group and 2 in the trastuzumab group) received left sided radiotherapy as part of their treatment regime. The control group (volunteers) had similar cardiovascular risk factors as our study group (table1) and no previous history of malignancy or chemotherapy.

7.4.1 Baseline parameters

Specifically, 5 patients had a history of hypertension, for which 1 received angiotensin converting enzyme inhibitors. No new medications were begun during the course of the study period. Functional and aortic pulse wave velocity CMR imaging was feasible in all 27 cancer patients, aortic distensibility calculation was feasible in 26/27 (96%) patients and myocardial

oedema imaging was feasible in 26/27 (96%) patients. We found no difference in pulse wave velocity or distensiblity at the ascending and proximal descending aorta between pre-treatment study patients and volunteers (Table 7.1).

7.4.2 Aortic remodelling measurements

Significant changes were observed in aortic distensibility and pulse wave velocity at 4 months (Table 7.2). While the pulse wave velocity increased, paralleled decrease was seen in aortic distensibility at the ascending aorta (Figure 3). Furthermore, improvement was noted in pulse wave velocity at 14 months, yet, aortic distensibility at the ascending aorta failed to demonstrate a significant return to normal. At the proximal descending aorta, only significant changes were observed in distensibility from pre-chemotherapy to 14 months When evaluating aortic stiffness, we found marginal increases at the ascending aorta from 5.9±0.6 to 6.1±0.7 within 1 month, $p=0.005$ to 6.4±0.6 at 4 months, $p<0.001$. In comparison, aortic stiffness measured at the proximal descending aorta only showed significant change at 14 months, at which point it had increased from 5.9±0.6 to 6.4±0.5, $p=0.002$.

We examined whether baseline age, body surface area, pulse pressure, systolic blood pressure, myocardial oedema, LVEF, co-morbidities (hypertension, diabetes mellitus, hypercholesterolemia and smoking), use of anthracylines,

trastuzumab or left sided radiotherapy were significantly associated with change in pulse wave velocity over time. We found that baseline patient age, pulse pressure and systolic blood pressure were predictive of change in pulse wave velocity. The older the patient, the more they demonstrated an increase in pulse wave velocity with time (age-time interaction p=0.004). The wider the pulse pressure and higher the systolic blood pressure, the greater the increase in pulse wave velocity with time (pulse pressure-time interaction p = 0.002 and systolic blood pressure-time interaction p=0.04).

We were able to demonstrate similar relationships between aortic distensibility at the ascending aorta and body surface area, systolic blood pressure and pulse pressure. Patients with increased body surface area, had greater reduction in aortic distensibility at the ascending aorta with time (body surface area-time interaction p=0.001). Furthermore, higher systolic blood pressure was associated with greater reduction in distensibility (systolic blood pressure-time interaction p = 0.001) and a trend towards interaction between pulse pressure and distensibility at the ascending aorta were also established (pulse pressure-time interaction p=0.08). **Importantly, we found that significant interaction between patients that received anthracylines (n=14) and aortic distensibility at the ascending aorta (anthracycline-time interaction p = 0.02).** Therefore, in comparison to the group that did not receive anthracyclines, patients with anthracycline exposure had a greater reduction in aortic distensibility in the ascending aorta with time, p=0.005 at 1 month,

$p<0.001$ at 4 months and $p=0.009$ at 12 months. In the anthracycline group, aortic distensibility at the ascending aorta decreased from 9.2±2.8 to 6.8±2.5 $10^{-3}mmHg^{-1}$ at 14 months. In contrast, in the trastuzumab group, the distensibility changed from 6.7±4.0 to 7.1±2.2 $10^{-3}mmHg^{-1}$.

With respect to the aortic distensibility of the proximal descending aorta, a trend was observed between aortic distensibility and pulse pressure (pulse pressure-time interaction $p=0.06$).

7.4.3 LV function

There were no significant differences in LV volumes, mass or EF between study patients at baseline and normal volunteers (Table 7.1). Significant LV functional changes were seen among cancer patients from baseline to 4 months. These changes persisted at 14 months (Table 7.2). At 4 months, immediately after completion of anthracylines or completion of 6 cycles of trastuzumab, 27% patients (7/26) showed a decline in LVEF by >10%. By 14 months, 19% (5/26) of the cohort examined had persistent LV dysfunction, however none had LVEF below the normal range (<55%) [254].

7.4.4 T2W- short term inversion recovery (STIR) findings

A substantial number of patients had increases in myocardial oedema following commencement of chemotherapy and this effect persisted to 4

months. We found that 8/26 (31%) of patients had M:Sk ratio ≥2.0 at 1 month or 4 months following commencement of chemotherapy. None of the patients had M:Sk ratios of ≥2.0 at 14 months.

7.5 Discussion

Our principal findings show that significant changes in aortic stiffness occur early (within 4 months), of commencement of chemotherapy. At 14 months; 1 month after completion of trastuzumab and 10 months after completion of anthracyclines, only pulse wave velocity remained reduced suggesting potential return of aortic stiffness measurements to baseline. This was mirrored in measurements of overall aortic stiffness which increased acutely at the ascending aorta and returned to baseline by 14 months, although the latter was not significant. All parameters (pulse wave velocity, aortic distensibility and aortic stiffness) remained elevated at the proximal descending aorta at 14 months.

Aortic stiffness changes have been demonstrated acutely with anthracylines, yet whether these return to normal or remain persistently elevated is not evident from previous work. Chaosuwannakit and colleagues demonstrated significantly increased pulse wave velocity and parallel decrease in aortic distensibility in patients receiving anthracyline chemotherapy as measured by CMR [275]. These changes were evaluated over 4 months and were greater in

magnitude than seen in our study. However whether they remained persistently elevated or returned to baseline was not demonstrated in this study as they did not report a 12 month follow up. In comparison, an ultrasound based study evaluated patient pre anthracycline chemotherapy, and 6 months post and showed lasting elevations in aortic stiffness and decrease in aortic compliance, suggesting persistent negative arterial remodelling at least to 6 months post anthracycline therapy [277]. We did not demonstrate persistent changes in all our parameters of aortic stiffness. Specifically, aortic pulse wave velocity decreased at the 14 month mark, although not to baseline. In addition, significant increase aortic stiffness was only demonstrated at 1 and 4 month mark, with values returning to baseline at 14 months.

We hypothesize that acute changes in aortic stiffness parameters following chemotherapy with anthracycline or trastuzumab, are reversible. One of the potential reasons that we were not able to demonstrate return of all our CMR parameters to baseline, may be related to the fact that half our patients received anthracyclines, whilst the other half were given trastuzumab. We found significant interaction between aortic distensibility at the ascending aorta and anthracylines. Therefore, in the group of patients that received anthracyclines, the changes in aortic distensibility at ascending aorta were significant and greater at each stage, showing an acute decline and then an attempt to return to baseline at 14 months. We propose that in our overall group, most of the changes observed were driven by patients receiving

anthracylines and that trastuzumab doesn't cause significant changes in negative arterial remodelling. This may explain why the magnitude of overall changes in our group were smaller than work by Chaosuwannakit and colleagues who predominantly only evaluated anthracyclines. This group had average increases in pulse wave velocity of 5.9ms, whilst ours were half that amount.

In a large study of hypertensive patients, it was demonstrated that an absolute pulse wave velocity of 11.3ms was associated with a 1.5 times increased odds ratio of cardiovascular mortality over 9 years [147]. The mean pulse wave velocity in our group was $8.2 \pm 4.1\ ms^{-1}$ at the end of 14 months and only 23% of our patients had pulse wave velocity greater than $11.3ms^{-1}$ at that time point. Furthermore none of our patients dropped their LVEF below normal at 14 months. Whether our patients represent a group which by far had limited abnormalities in pulse wave velocities and hence our likely to remain free of significant cardiovascular mortality is unclear. There are some distinct differences between the two studies. Firstly this initial study performed by Laurent and colleagues evaluated a stable cohort of hypertensive patients, whilst ours examined pulse wave velocity following administration of potentially cardiotoxic drugs. Secondly, the methodologies utilized differed, with Laurent employing carotid-femoral pulse wave velocity, whilst ours was measured between ascending and proximal descending aorta using MRI. In addition, the study authors found that, at an absolute pulse wave velocity of

11.3 ms^{-1}, their odds ratio of cardiovascular risk increased. Their events developed over 9 years whilst our follow up is limited to 14 months. This large study of 1980 patients did not find that their annual mean pulse wave velocity values changed. In contrast we found increases within the year, albeit following administration of a potentially cardiotoxic insult. We have shown that at 14 months following the toxic insult, the pulse wave velocity is stabilizing or even regressing towards baseline. Hence, we propose that the pulse wave velocity at 14 months may represent the degree of aortic stiffness our patients are now subject to and therefore act as a guide to the cardiovascular risk they may face in the future.

The mechanism by which chemotherapy or hormonal therapy agents cause negative arterial remodelling remains unclear. Anthracyclines in particular have been extensively evaluated and are thought to cause an increase in oxidative stress due to production of toxic oxygen free radicals [59, 270]. This in turn leads to structural changes in the vascular matrix and interferes with endothelin regulation of vascular tone, thereby increasing aortic stiffness. Doxorubicin has been demonstrated to suppress endothelin production, which in turn may make the myocytes susceptible to apoptosis [278].

Trastuzumab on the other hand is a recombinant DNA-derived monoclonal antibody that binds to extracellular domain of the Her2 protein in breast cancer cells. Its cardiotoxicity is due to its effect in nulling the beneficial effects of

erbB2 derived repair pathways in the heart. This specifically impacts how myocytes responds to stress. Experimental animal work using trastuzumab and high dose radiation has been shown to demonstrate greater effect on vessel relaxation and electron microscopic evidence of endothelial damage on thoracic aorta [279]. Our patients showed greater decline in aortic distensiblity in the anthracycline group rather than the trastuzumab group. This may potentially reflect the acute endothelial derived insult of the anthracyclines. Whilst the patients that received trastuzumab potentially require accumulation of further toxicity and failure of repair processes, to have similar changes in markers of aortic stiffness. Long-term follow up of these patients may clarify whether trastuzumab on its own causes limited effects, or with time, do they mirror similar changes in aortic stiffness as seen with anthracylines.

7.5.1 Limitations

Our study has a number of limitations. Firstly our patient numbers are small and hence our findings need to be replicated in larger multi-centre studies. Secondly, we did not follow up our control group over similar time period as our study patients. We only had baseline comparisons which showed no differences in our study patients and volunteers. Therefore, it is theoretically possible, that these changes are due to time (14 month older patient), rather than chemotherapy. Against this are the lack of difference between baseline characteristics of study patients and normal volunteers. Furthermore, previous

studies have evaluated normal volunteers and found no difference in pulse wave velocity and distensibility over 4 months [275]. Recently, evaluation of the Multi-Ethnic study of atherosclerosis (MESA) cohort, showed absolute changes in pulse wave velocity of 1 ms^{-1} over 10 years in a normal cohort [280]. Hence it is unlikely that the temporal changes seen in the Anthracycline group are due to time. Finally, as our proposed changes in aortic distensibility may have been driven by endothelin derived effect, we should have specifically evaluated flow mediated dilatation after reactive hyperemia, to better elucidate the etiology of changes observed in our study patients.

7.6 Conclusion

Acute changes are observed in pulse wave velocity and distensiblity at the ascending aorta following contemporary breast cancer chemotherapy. These changes reverse a year after chemotherapy is discontinued. Anthracyclines have more severe effects on arterial remodelling than trastuzumab therapy.

Table 7.1

Baseline characteristics of study and volunteer populations

Variable	Study population	Volunteer population	P-value
N	27	12	
Demographic			
Age, y	54±11	54±13	0.47
BSA, m^2	1.8±0.2	1.8±0.1	0.49
Co-morbidities			
Diabetes	4,	0, 0	0.29
Hypertension	5,	4,	0.42
Hypercholesterolemia	10,	3,	0.71
Smokers – current	2,	2,	0.57
Smokers - ex	11	4,	0.73
Family history of CAD	7	1	0.39
Clinical			
Systolic/Diastolic BP, mmHg	115±17/68±11	122±14/73±9	0.13/0.08
Pulse pressure, mmHg	48±11	49±14	0.41
Parameters			
Aortic pulse wave velocity, m/s	6.8±3.2	7.5±2.8	0.25
Aortic distensibility – AA, $10^{-3}mmHg^{-1}$	8.1±3.6	8.4±3.1	0.37
Aortic distensibility – PDA, $10^{-3}mmHg^{-1}$	7.8±4.4	8.6±3.8	0.30
Aortic stiffness – AA	5.8±0.6	6.1±1.0	0.12
Aortic stiffness - PDA	5.9±0.6	6.1±0.6	0.16
Ejection Fraction, %	72±5	71±7	0.30
Myocardial mass indexed, g/m^2	46.1±8.9	46.1±8.8	0.50

Table 7.2

Changes in aortic stiffness, LV function and myocardial oedema with time

Parameter	Pulse wave velocity (m/s)	AA Aortic distensibility (10^{-3}mmHg^{-1})	PDA Aortic distensibility (10^{-3}mmHg^{-1})	LVEF (%)	Myocardial Mass (g/m^2)
Pre-treatment	6.8±3.2	8.1±3.6	7.8±4.4	72±5	46.1±8.9
1 month f/u	7.8±4.3	6.0±3.2*	6.4±3.3	68±6**	47.4±8.4
4 months f/u	8.9±6.4*	5.7±3.2**	6.6±4.1	66±7**	46.8±7.9
12 months f/u	8.2±4.2*	6.9±2.3	4.9±1.6*	67±7**	44.9±7.6

AA – ascending aorta, PDA – proximal descending aorta, LVEF – Left ventricular ejection fraction, f/u – follow up. * represent p valves <0.05 and ** represent p values < 0.001.

Figure 7.1 Evaluation of Aortic Distensibility

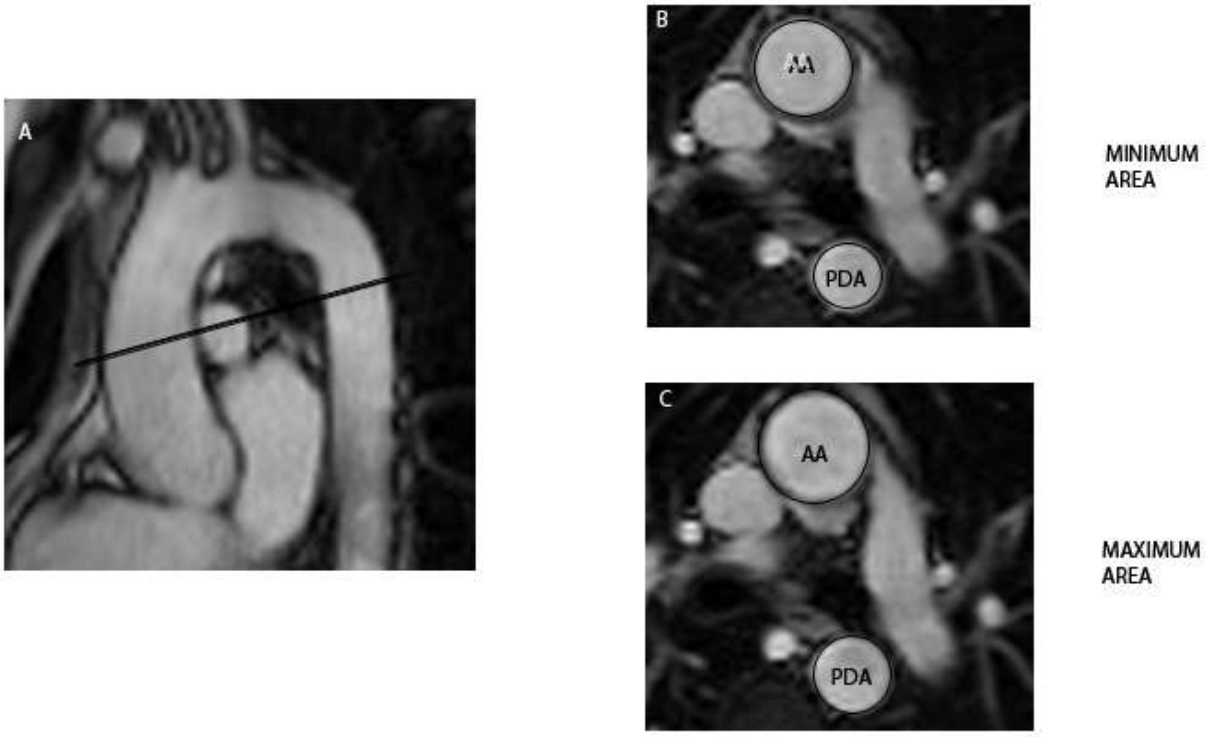

The aorta was demonstrated in a sagittal plane (A) and cross sectional images were planned at the level of the middle pulmonary artery (solid black line) to generate ascending aorta (AA) and proximal descending aorta (PDA). Image B and C represent the minimum and maximum areas in AA and PDA, the difference between the two and aortic pulse pressure, were subsequently used to calculate aortic distensibility at AA and PDA.

Figure 7.2 Pulse wave velocity transit time from ascending aorta to proximal descending aorta

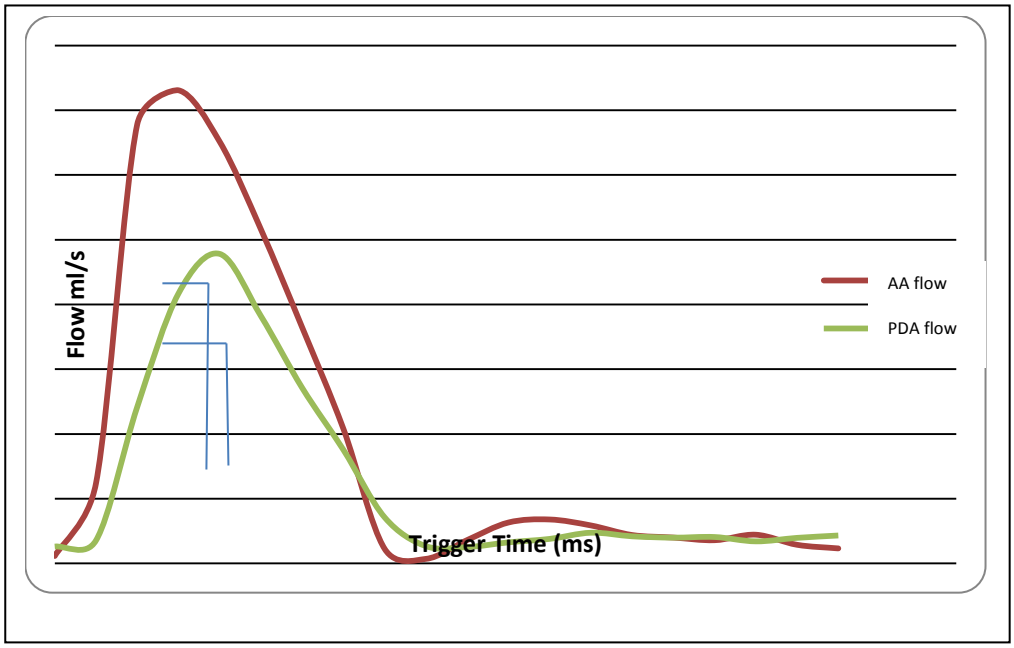

Velocity time curves of the ascending aorta (AA flow) and proximal descending aorta (PDA flow) were generated. Transit time of the flow wave (red horizontal line) was computed on the basis of time to reach 50% of the upstroke velocity at AA and PDA (blue * and # respectively). Pulse wave velocity was calculated by dividing the distance between ascending and descending thoracic aorta by the transit time of the flow wave.

Figure 7.3

Changes in pulse wave velocity and aortic distensibility with time

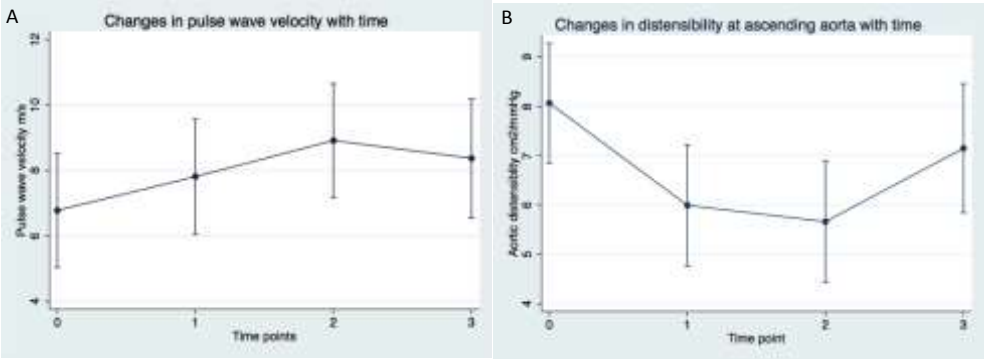

Graph represents the change in mean (blue dots) with standard deviation (graph bars) pulse wave velocity (A) and distensibility at the ascending aorta (B) for the overall group at time point 0 (pre-therapy), time point 1 (1 month after commencement of therapy), time point 2 (4 months after therapy) and time point 3 (12 months after therapy).

Chapter 8 Final Discussion

This thesis has explored the complex relationships between myocardial injury and adverse outcome. Importantly, it has aimed to define the temporal pattern that follows insult to the observed change. Furthermore it has evaluated imaging biomarkers that may elucidate potential mechanisms of injury. The value of this work stems from early identification of prospective reversible myocardial injury. It clinically tackles three pathological states, acute ischaemic injury, chronic ischaemic left ventricular dysfunction and non-ischaemic cardiomyopathy. We used a clinical model of acute ischaemic injury that is most commonly seen and has the greatest clinical burden – anterior ST elevation myocardial infarction. We evaluated it in a clinical trial setting where time to reperfusion and symptoms were known. This thesis also examines the interplay between perfusion and oxygenation to identify markers of improvement post revascularisation in chronic ischaemic cardiomyopathy. Finally, it details a pattern of non-ischemic cardiomyopathy, to identify temporal relationships and potential mechanisms that may be responsible for the observed cardiovascular morbidity and mortality seen in these patients.

8.1 Acute ischaemic injury

Survivors of an acute myocardial event face substantial risk of further complications including death, repeat infarction, heart failure and arrhythmias. One of the important determinants of survival is LV function following infarct. Chapter 3 detailed the clinical study in STEMI patients following primary PCI and administration of delcasterib (a protein kinase 2 inhibitor) designed to limit reperfusion injury. Our study involved a sub-population of 90 patients, which examined markers of infarct characterization in these patients to evaluate best predictors of predicting late LV function. Studies conducted so far have examined CMR markers of ischaemic injury such as myocardial salvage, infarct size, microvascular obstruction, area at risk and infarct heterogeneity in single centres. Ours was the first study to explore these markers and their predictive value in a STEMI cohort in a multi-centre environment, depicting the most robust method in a 'real world' population. We performed CMR early post intervention (day 3 to 5) and at 3 months. Our aim was to use CMR markers measured early to possibly predict adverse LV remodelling and function at follow up. We found that infarct size as measured by the late gadolinium enhancement technique was the most vigorous marker in predicting late LV function (i.e. 3 months post infarct). Particularly, this technique was superior to myocardial salvage and microvascular obstruction, both of which have independently been demonstrated to predict LV function. This may possibly be related to the fact that 1/3 of our patients failed to have

adequate assessment of area at risk and hence myocardial salvage. However, we felt this represented an accurate picture of 'real world' CMR assessment of acute ischemic injury, where some centres do not adequately perform this more recent and possibly less familiar technique. This has important implications for assessing and risk stratifying patients following STEMI.

8.2 Chronic ischaemic cardiomyopathy

Chapter 4 was designed to evaluate patients with hibernating myocardium. We aimed to address some of the controversies regarding the potential mechanisms in this pathological state that have existed for decades. The traditional definition of hibernating myocardium was based on the widely held belief, that this was a protective state of myocardium as a result of chronic underperfusion. Several PET studies had demonstrated preserved metabolism and reduced perfusion in these patients. However, over the years this notion has largely been challenged by demonstration of normal resting perfusion. Although resting perfusion remained controversial, it was largely agreed that perfusion reserve (changes when myocardium is stressed) is reduced. This leads to a reduction in the oxygen supply, yet what happens to the oxygen demand has not been adequately explored. Our technique of Blood oxygen level dependent CMR allowed measurement of the de/oxygenation of the venous compartment of capillary bed, hence directly reflecting tissue oxygenation. We evaluated 15 patients pre revascularisation and median of 8

months post revascularisation. Majority of our patients underwent coronary artery bypass grafting. We studied oxygenation via BOLD CMR and myocardial perfusion ratio through semiquantiative perfusion assessment. Interestingly we found that these patients exhibited significant deoxygenation prior to revascularisation and indeed this improved post revascularisation. This was particularly significant in myocardium that was dysfunctional pre and improved post revascularisation (i.e. hibernating myocardium). As expected, our patients showed significant reduction in myocardial perfusion reserve. However, we found that deoxygenation rather than reduction in myocardial perfusion reserve more accurately related to subjects that improved in their regional wall motion at follow up. This study provides valuable insight into the potential mechanism behind this reversible state of contractile recovery.

8.3 Non-ischaemic cardiomyopathy

The third clinical study outlined in chapters 5-7 evaluated a model of non-ischaemic cardiomyopathy. The temporal pattern of injury can be difficult to define in non-ischaemic cardiomyopathy, particularly as the onset is insidious. Chemotherapy is unique in this manner, as it allows measurement of baseline (i.e. pre insult) LV function and hence description of the temporal changes observed. This allowed us to evaluate some of the early and hence potential reversible changes that may occur in this population soon after the

administration of potentially cardiotoxic agents. Anthracyclines traditionally have formed the mainstay of chemotherapy regimes in several malignancies. Their initial use since the 1970's led to the discovery that large doses of these drugs can lead to a cardiomyopathy. Although rates of cardiomyopathy have now decreased due to chemotherapy doses being limited, a significant proportion of patients still develop abnormalities in LV function. The concern is that often this may occur years later and present in an insidious manner. As they are utilized in paediatric malignancies, there is still a substantial adult population developing cardiomyopathy. We wanted to examine these drugs in an adult malignancy population. We chose breast cancer patients, to study effects of anthracylines as well as trastuzumab. The latter agent inhibits action of the HER 2 protein that has implications for the adequate function of repair pathways in the heart. It is also recognized to cause cardiomyopathy and is considered largely reversible upon cessation of the drug.

In chapters 5 and 6, the effects of these drugs on the LV and RV respectively are described. Patients were examined at four time points, pre-treatment, 1 month, 4 months and 12-14 months post therapy. In these patients, LV function declined by 5% at 4 months and then stabilized. A substantial number of patients showed increases in myocardial oedema and decline in global longitudinal strain, all are considered to represent early, potentially reversible changes. However, our work could not demonstrate that the patients that showed this early change were the ones who demonstrated more

severe functional LV changes at 12 months. In contrast, RV function displayed more severe and persistent decline over the follow up period. In addition, our work showed that the patients that demonstrated early LV myocardial oedema were more likely to subsequently show RV function decline at follow up. Whether these drugs lead to a particular RV cardiomyopathy, or whether the RV decline is a precursor to later LV deterioration remains to be seen. The importance of RV function has been established in heart failure patients. It remains to be seen what significance it has in chemotherapy patients. Finally, in chapter 7 we studied aortic stiffness which has shown importance in predicting cardiovascular events in several population cohorts including patients with hypertension. We wanted to evaluate whether changes in aortic stiffness occur and whether they are persistent or reverse following administration of these drugs. Our study revealed increased aortic stiffness following administration of these agents, and upon cessation, some of the markers of aortic stiffness improved. However, in patients that received anthracyclines, these markers remained abnormal at long term follow up (14 months). Considering the importance of aortic stiffness in predicting cardiovascular mortality, our research suggests that patients that received trastuzumab are likely subject to lower cardiovascular risk than patients that received anthracyclines.

Chapter 9 Future Directions

Although the observations made in the course of this thesis have yielded some understanding of the mechanisms underlying the pathogenesis and perpetuation of acute and chronic LV dysfunction, and early and late changes in chemotherapy cardiotoxicity, they have led to further questions, some of which are outlined in this chapter.

The finding in Chapter 3 that infarct size was the most robust marker for predicting late LV function in STEMI patients suggests that it should form part of the routine evaluation in these patients. The value of such a strategy would aim to identify early reperfusion/revascularisation tools. The ideal test of the merits of this approach would be to randomly assign patients to therapies based on infarct size assessment, and subsequently compare outcomes. Furthermore, several of the new therapy trials often use CMR infarct size as a surrogate marker to show benefit. However, there is a still a need for outcome based studies based on changed treatment as a result of CMR, particularly with regards to device therapy.

In contrast to the significant understanding that exists in patients with acute myocardial infarction, the mechanisms behind chronic myocardial infarction

remain contentious. This thesis has outlined some of the controversies in hibernating myocardium. Chapter 4 summarized the significance of myocardial oxygenation and its role in evaluating patients that improved in contractility after revascularisation. The development of non-invasive techniques to accurately quantify myocardial flow and oxygenation simultaneously may enable identification of myocardium that is likely to improve post revascularisation. The recent controversies with regards to myocardial viability and its role in revascularisation itself could be better addressed with evaluation of the interplay between perfusion and oxygenation. This requires larger trials to be conducted using assessment of oxygenation and perfusion with the aim to identify 'reversible LV dysfunction'. In addition, whether therapy was tailored to these changes results in improved LV function post revascularisation remains to be seen.

This thesis examined early changes that occur following administration of potentially cardiotoxic agents. Although this research demonstrated increase in myocardial oedema and its importance in predicting RV decline, it was unable to reach such a conclusion for LV function. One of the potential reasons regarding this finding may be due to the follow up being terminated at 14 months. These patients may not have had the time to develop LV dysfunction and hence follow up of these patients at 5 years, with evaluation of cardiovascular outcome may shed light into the degree to which these patients develop LV cardiomyopathy. Furthermore, in addition to early

identification, more work needs to be done to target these early changes observed, with therapy, and potentially alleviate development of cardiomyopathy. Finally, this thesis provided initial insight into the role aortic stiffness may play in this population. However, the temporal relationship between changes observed in aortic stiffness and development of cardiovascular outcomes may take years to develop. Hence these patients should be followed up, to assess the utility of these early changes of aortic stiffness in predicting their long term cardiovascular outcome.

Bibliography

1. Cohn, J.N., *Structural basis for heart failure. Ventricular remodeling and its pharmacological inhibition.* Circulation, 1995. **91**(10): p. 2504-7.
2. Kanoh, M., et al., *Significance of myocytes with positive DNA in situ nick end-labeling (TUNEL) in hearts with dilated cardiomyopathy: not apoptosis but DNA repair.* Circulation, 1999. **99**(21): p. 2757-64.
3. Steenbergen, C., et al., *Alterations in apoptotic signaling in human idiopathic cardiomyopathic hearts in failure.* Am J Physiol Heart Circ Physiol, 2003. **284**(1): p. H268-76.
4. Wencker, D., et al., *A mechanistic role for cardiac myocyte apoptosis in heart failure.* J Clin Invest, 2003. **111**(10): p. 1497-504.
5. Jennings, R.B., et al., *Myocardial necrosis induced by temporary occlusion of a coronary artery in the dog.* Arch Pathol, 1960. **70**: p. 68-78.
6. Reimer, K.A., M.M. Rasmussen, and R.B. Jennings, *Reduction by propranolol of myocardial necrosis following temporary coronary artery occlusion in dogs.* Circ Res, 1973. **33**(3): p. 353-63.
7. Fishbein, M.C., D. Maclean, and P.R. Maroko, *The histopathologic evolution of myocardial infarction.* Chest, 1978. **73**(6): p. 843-9.
8. Yellon, D.M. and G.F. Baxter, *Protecting the ischaemic and reperfused myocardium in acute myocardial infarction: distant dream or near reality?* Heart, 2000. **83**(4): p. 381-7.
9. Ambrosio, G. and I. Tritto, *Reperfusion injury: experimental evidence and clinical implications.* Am Heart J, 1999. **138**(2 Pt 2): p. S69-75.
10. Kloner, R.A. and R.B. Jennings, *Consequences of brief ischemia: stunning, preconditioning, and their clinical implications: part 1.* Circulation, 2001. **104**(24): p. 2981-9.
11. Kloner, R.A. and R.B. Jennings, *Consequences of brief ischemia: stunning, preconditioning, and their clinical implications: part 2.* Circulation, 2001. **104**(25): p. 3158-67.
12. Braunwald, E. and R.A. Kloner, *The stunned myocardium: prolonged, postischemic ventricular dysfunction.* Circulation, 1982. **66**(6): p. 1146-9.
13. Park, J.L. and B.R. Lucchesi, *Mechanisms of myocardial reperfusion injury.* Ann Thorac Surg, 1999. **68**(5): p. 1905-12.
14. Patel, M.R., et al., *Pexelizumab and infarct size in patients with acute myocardial infarction undergoing primary percutaneous coronary Intervention: a delayed enhancement cardiac magnetic resonance substudy from the APEX-AMI trial.* JACC Cardiovasc Imaging, 2010. **3**(1): p. 52-60.
15. Bates, E., et al., *Intracoronary KAI-9803 as an adjunct to primary percutaneous coronary intervention for acute ST-segment elevation myocardial infarction.* Circulation, 2008. **117**(7): p. 886-96.
16. Piot, C., et al., *Effect of cyclosporine on reperfusion injury in acute myocardial infarction.* N Engl J Med, 2008. **359**(5): p. 473-81.

17. Atar, D., et al., *Effect of intravenous FX06 as an adjunct to primary percutaneous coronary intervention for acute ST-segment elevation myocardial infarction results of the F.I.R.E. (Efficacy of FX06 in the Prevention of Myocardial Reperfusion Injury) trial.* J Am Coll Cardiol, 2009. **53**(8): p. 720-9.
18. Heyndrickx, G.R., et al., *Depression of regional blood flow and wall thickening after brief coronary occlusions.* Am J Physiol, 1978. **234**(6): p. H653-9.
19. Anderson, J.L., et al., *A randomized trial of intracoronary streptokinase in the treatment of acute myocardial infarction.* N Engl J Med, 1983. **308**(22): p. 1312-8.
20. Sheehan, F.H., et al., *Advantages and applications of the centerline method for characterizing regional ventricular function.* Circulation, 1986. **74**(2): p. 293-305.
21. Topol, E.J., et al., *Regional wall motion improvement after coronary thrombolysis with recombinant tissue plasminogen activator: importance of coronary angioplasty.* J Am Coll Cardiol, 1985. **6**(2): p. 426-33.
22. Bolli, R., *Mechanism of myocardial "stunning".* Circulation, 1990. **82**(3): p. 723-38.
23. Bolli, R., *Myocardial 'stunning' in man.* Circulation, 1992. **86**(6): p. 1671-91.
24. Schinkel, A.F., et al., *How many patients with ischemic cardiomyopathy exhibit viable myocardium?* Am J Cardiol, 2001. **88**(5): p. 561-4.
25. Auerbach, M.A., et al., *Prevalence of myocardial viability as detected by positron emission tomography in patients with ischemic cardiomyopathy.* Circulation, 1999. **99**(22): p. 2921-6.
26. Bonow, R.O., *The hibernating myocardium: implications for management of congestive heart failure.* Am J Cardiol, 1995. **75**(3): p. 17A-25A.
27. Gewirtz, H., et al., *Positron emission tomographic measurements of absolute regional myocardial blood flow permits identification of nonviable myocardium in patients with chronic myocardial infarction.* J Am Coll Cardiol, 1994. **23**(4): p. 851-9.
28. Shivalkar, B., et al., *Only hibernating myocardium invariably shows early recovery after coronary revascularization.* Circulation, 1996. **94**(3): p. 308-15.
29. Selvanayagam, J.B., et al., *Resting myocardial blood flow is impaired in hibernating myocardium: a magnetic resonance study of quantitative perfusion assessment.* Circulation, 2005. **112**(21): p. 3289-96.
30. Conversano, A., et al., *Delineation of myocardial stunning and hibernation by positron emission tomography in advanced coronary artery disease.* Am Heart J, 1996. **131**(3): p. 440-50.

31. Maki, M., et al., *Glucose uptake in the chronically dysfunctional but viable myocardium.* Circulation, 1996. **93**(9): p. 1658-66.
32. Gerber, B.L., et al., *Myocardial blood flow, glucose uptake, and recruitment of inotropic reserve in chronic left ventricular ischemic dysfunction. Implications for the pathophysiology of chronic myocardial hibernation.* Circulation, 1996. **94**(4): p. 651-9.
33. Marinho, N.V., et al., *Pathophysiology of chronic left ventricular dysfunction. New insights from the measurement of absolute myocardial blood flow and glucose utilization.* Circulation, 1996. **93**(4): p. 737-44.
34. Vanoverschelde, J.L., et al., *Mechanisms of chronic regional postischemic dysfunction in humans. New insights from the study of noninfarcted collateral-dependent myocardium.* Circulation, 1993. **87**(5): p. 1513-23.
35. Shen, Y.T., et al., *Inotropic reserve and histological appearance of hibernating myocardium in conscious pigs with ameroid-induced coronary stenosis.* Basic Res Cardiol, 1996. **91**(6): p. 479-85.
36. Wassmuth, R., et al., *Subclinical cardiotoxic effects of anthracyclines as assessed by magnetic resonance imaging-a pilot study.* Am Heart J, 2001. **141**(6): p. 1007-13.
37. Ewer, M.S., et al., *Reversibility of trastuzumab-related cardiotoxicity: new insights based on clinical course and response to medical treatment.* J Clin Oncol, 2005. **23**(31): p. 7820-6.
38. Sparano, J.A., D.L. Brown, and A.C. Wolff, *Predicting cancer therapy-induced cardiotoxicity: the role of troponins and other markers.* Drug Saf, 2002. **25**(5): p. 301-11.
39. Economics, A., *The shifting burden of cardiovascular disease in Australia,* N.H. Foundation, Editor. 2005.
40. Felker, G.M., L.K. Shaw, and C.M. O'Connor, *A standardized definition of ischemic cardiomyopathy for use in clinical research.* J Am Coll Cardiol, 2002. **39**(2): p. 210-8.
41. Haas, F., et al., *Preoperative positron emission tomographic viability assessment and perioperative and postoperative risk in patients with advanced ischemic heart disease.* J Am Coll Cardiol, 1997. **30**(7): p. 1693-700.
42. Beanlands, R.S., et al., *F-18-fluorodeoxyglucose PET imaging alters clinical decision making in patients with impaired ventricular function.* Am J Cardiol, 1997. **79**(8): p. 1092-5.
43. Allman, K.C., et al., *Myocardial viability testing and impact of revascularization on prognosis in patients with coronary artery disease and left ventricular dysfunction: a meta-analysis.* J Am Coll Cardiol, 2002. **39**(7): p. 1151-8.
44. Beanlands, R.S., et al., *F-18-fluorodeoxyglucose positron emission tomography imaging-assisted management of patients with severe left ventricular dysfunction and suspected coronary disease: a randomized,*

controlled trial (PARR-2). J Am Coll Cardiol, 2007. **50**(20): p. 2002-12.
45. Cleland, J.G., et al., *The Heart Failure Revascularisation Trial (HEART).* Eur J Heart Fail, 2011. **13**(2): p. 227-33.
46. Bonow, R.O., et al., *Myocardial Viability and Survival in Ischemic Left Ventricular Dysfunction.* N Engl J Med, 2011.
47. Abraham, A., et al., *18F-FDG PET imaging of myocardial viability in an experienced center with access to 18F-FDG and integration with clinical management teams: the Ottawa-FIVE substudy of the PARR 2 trial.* J Nucl Med, 2010. **51**(4): p. 567-74.
48. Felker, G.M., et al., *The spectrum of dilated cardiomyopathy. The Johns Hopkins experience with 1,278 patients.* Medicine (Baltimore), 1999. **78**(4): p. 270-83.
49. Baum, M., *Polychemotherapy for early breast cancer.* Lancet, 1998. **352**(9139): p. 1554.
50. Jensen, B.V., *Cardiotoxic consequences of anthracycline-containing therapy in patients with breast cancer.* Semin Oncol, 2006. **33**(3 Suppl 8): p. S15-21.
51. Kaklamani, V.G. and W.J. Gradishar, *Epirubicin versus doxorubicin: which is the anthracycline of choice for the treatment of breast cancer?* Clin Breast Cancer, 2003. **4 Suppl 1**: p. S26-33.
52. Hershman, D.L. and T. Shao, *Anthracycline cardiotoxicity after breast cancer treatment.* Oncology (Williston Park), 2009. **23**(3): p. 227-34.
53. Roul, G., C. Cohen, and A. Lieber, *[Anthracycline-induced cardiomyopathy]*. Presse Med, 2009. **38**(6): p. 987-94.
54. Sliwkowski, M.X., et al., *Nonclinical studies addressing the mechanism of action of trastuzumab (Herceptin).* Semin Oncol, 1999. **26**(4 Suppl 12): p. 60-70.
55. Yakes, F.M., et al., *Herceptin-induced inhibition of phosphatidylinositol-3 kinase and Akt Is required for antibody-mediated effects on p27, cyclin D1, and antitumor action.* Cancer Res, 2002. **62**(14): p. 4132-41.
56. Bianco, A.R., *Targeting c-erbB2 and other receptors of the c-erbB family: rationale and clinical applications.* J Chemother, 2004. **16 Suppl 4**: p. 52-4.
57. Arnould, L., et al., *Trastuzumab-based treatment of HER2-positive breast cancer: an antibody-dependent cellular cytotoxicity mechanism?* Br J Cancer, 2006. **94**(2): p. 259-67.
58. van Dalen, E.C., et al., *Different dosage schedules for reducing cardiotoxicity in cancer patients receiving anthracycline chemotherapy.* Cochrane Database Syst Rev, 2006(4): p. CD005008.
59. Singal, P.K. and N. Iliskovic, *Doxorubicin-induced cardiomyopathy.* N Engl J Med, 1998. **339**(13): p. 900-5.
60. Lee, K.F., et al., *Requirement for neuregulin receptor erbB2 in neural and cardiac development.* Nature, 1995. **378**(6555): p. 394-8.

61. Crone, S.A., et al., *ErbB2 is essential in the prevention of dilated cardiomyopathy.* Nat Med, 2002. **8**(5): p. 459-65.
62. Feola, M., et al., *Cardiotoxicity after anthracycline chemotherapy in breast carcinoma: effects on left ventricular ejection fraction, troponin I and brain natriuretic peptide.* Int J Cardiol, 2011. **148**(2): p. 194-8.
63. Lehmann, E.D., et al., *Non-invasive assessment of cardiovascular disease in diabetes mellitus.* Lancet, 1997. **350 Suppl 1**: p. SI14-9.
64. Von Hoff, D.D., et al., *Risk factors for doxorubicin-induced congestive heart failure.* Ann Intern Med, 1979. **91**(5): p. 710-7.
65. Swain, S.M., F.S. Whaley, and M.S. Ewer, *Congestive heart failure in patients treated with doxorubicin: a retrospective analysis of three trials.* Cancer, 2003. **97**(11): p. 2869-79.
66. Pinder, M.C., et al., *Congestive heart failure in older women treated with adjuvant anthracycline chemotherapy for breast cancer.* J Clin Oncol, 2007. **25**(25): p. 3808-15.
67. Ryberg, M., et al., *New insight into epirubicin cardiac toxicity: competing risks analysis of 1097 breast cancer patients.* J Natl Cancer Inst, 2008. **100**(15): p. 1058-67.
68. Bristow, M.R., et al., *Clinical spectrum of anthracycline antibiotic cardiotoxicity.* Cancer Treat Rep, 1978. **62**(6): p. 873-9.
69. Perez, E.A., et al., *Cardiac safety analysis of doxorubicin and cyclophosphamide followed by paclitaxel with or without trastuzumab in the North Central Cancer Treatment Group N9831 adjuvant breast cancer trial.* J Clin Oncol, 2008. **26**(8): p. 1231-8.
70. Hundley, W.G., et al., *Magnetic resonance imaging determination of cardiac prognosis.* Circulation, 2002. **106**(18): p. 2328-33.
71. Bloch, F., *Nuclear Induction.* Physical Review online archive, 1946. **70**(7-8): p. 460-474.
72. Purcell, E., *Resonance Absorption by Nuclear Magnetic Moments in a Solid.* :Physical Review Online Archive, 1946. **69**: p. 37-38.
73. Bellenger, N.G., et al., *Comparison of left ventricular ejection fraction and volumes in heart failure by echocardiography, radionuclide ventriculography and cardiovascular magnetic resonance; are they interchangeable?* Eur Heart J, 2000. **21**(16): p. 1387-96.
74. Debatin, J.F., et al., *Cardiac ejection fraction: phantom study comparing cine MR imaging, radionuclide blood pool imaging, and ventriculography.* J Magn Reson Imaging, 1992. **2**(2): p. 135-42.
75. Bellenger, N.G., et al., *Reduction in sample size for studies of remodeling in heart failure by the use of cardiovascular magnetic resonance.* J Cardiovasc Magn Reson, 2000. **2**(4): p. 271-8.
76. Sakuma, H., et al., *Evaluation of left ventricular volume and mass with breath-hold cine MR imaging.* Radiology, 1993. **188**(2): p. 377-80.
77. Wintersperger, B.J., et al., *Single breath-hold real-time cine MR imaging: improved temporal resolution using generalized autocalibrating partially parallel acquisition (GRAPPA) algorithm.* Eur Radiol, 2003. **13**(8): p. 1931-6.

78. Cwajg, J.M., et al., *End-diastolic wall thickness as a predictor of recovery of function in myocardial hibernation: relation to rest-redistribution T1-201 tomography and dobutamine stress echocardiography.* J Am Coll Cardiol, 2000. **35**(5): p. 1152-61.
79. Baer, F.M., et al., *Dobutamine magnetic resonance imaging predicts contractile recovery of chronically dysfunctional myocardium after successful revascularization.* J Am Coll Cardiol, 1998. **31**(5): p. 1040-8.
80. Krittayaphong, R., et al., *Comparison of cardiovascular magnetic resonance of late gadolinium enhancement and diastolic wall thickness to predict recovery of left ventricular function after coronary artery bypass surgery.* J Cardiovasc Magn Reson, 2008. **10**: p. 41.
81. Rehwald, W.G., et al., *Myocardial magnetic resonance imaging contrast agent concentrations after reversible and irreversible ischemic injury.* Circulation, 2002. **105**(2): p. 224-9.
82. Kim, R.J., et al., *Relationship of MRI delayed contrast enhancement to irreversible injury, infarct age, and contractile function.* Circulation, 1999. **100**(19): p. 1992-2002.
83. Klein, C., et al., *Assessment of myocardial viability with contrast-enhanced magnetic resonance imaging: comparison with positron emission tomography.* Circulation, 2002. **105**(2): p. 162-7.
84. Wagner, A., et al., *Contrast-enhanced MRI and routine single photon emission computed tomography (SPECT) perfusion imaging for detection of subendocardial myocardial infarcts: an imaging study.* Lancet, 2003. **361**(9355): p. 374-9.
85. Simonetti, O.P., et al., *An improved MR imaging technique for the visualization of myocardial infarction.* Radiology, 2001. **218**(1): p. 215-23.
86. Kim, R.J., et al., *Myocardial Gd-DTPA kinetics determine MRI contrast enhancement and reflect the extent and severity of myocardial injury after acute reperfused infarction.* Circulation, 1996. **94**(12): p. 3318-26.
87. Choi, K.M., et al., *Transmural extent of acute myocardial infarction predicts long-term improvement in contractile function.* Circulation, 2001. **104**(10): p. 1101-7.
88. Gerber, B.L., et al., *Accuracy of contrast-enhanced magnetic resonance imaging in predicting improvement of regional myocardial function in patients after acute myocardial infarction.* Circulation, 2002. **106**(9): p. 1083-9.
89. Beek, A.M., et al., *Delayed contrast-enhanced magnetic resonance imaging for the prediction of regional functional improvement after acute myocardial infarction.* J Am Coll Cardiol, 2003. **42**(5): p. 895-901.
90. Dall'armellina, E., et al., *Dynamic changes of edema and late gadolinium enhancement after acute myocardial infarction and their*

relationship to functional recovery and salvage index. Circ Cardiovasc Imaging, 2011. **4**(3): p. 228-36.
91. Kim, R.J., et al., *The use of contrast-enhanced magnetic resonance imaging to identify reversible myocardial dysfunction.* N Engl J Med, 2000. **343**(20): p. 1445-53.
92. Selvanayagam, J.B., et al., *Value of delayed-enhancement cardiovascular magnetic resonance imaging in predicting myocardial viability after surgical revascularization.* Circulation, 2004. **110**(12): p. 1535-41.
93. White, H.D., et al., *Left ventricular end-systolic volume as the major determinant of survival after recovery from myocardial infarction.* Circulation, 1987. **76**(1): p. 44-51.
94. Rizzello, V., et al., *Opposite patterns of left ventricular remodeling after coronary revascularization in patients with ischemic cardiomyopathy: role of myocardial viability.* Circulation, 2004. **110**(16): p. 2383-8.
95. Pegg, T.J., et al., *Prediction of global left ventricular functional recovery in patients with heart failure undergoing surgical revascularisation, based on late gadolinium enhancement Cardiovascular Magnetic Resonance.* J Cardiovasc Magn Reson, 2010. **12**: p. 56.
96. Pennell, D.J., et al., *Magnetic resonance imaging during dobutamine stress in coronary artery disease.* Am J Cardiol, 1992. **70**(1): p. 34-40.
97. Fayad, Z.A., T.J. Connick, and L. Axel, *An improved quadrature or phased-array coil for MR cardiac imaging.* Magn Reson Med, 1995. **34**(2): p. 186-93.
98. Geskin, G., et al., *Quantitative assessment of myocardial viability after infarction by dobutamine magnetic resonance tagging.* Circulation, 1998. **98**(3): p. 217-23.
99. Bogaert, J., et al., *Functional recovery of subepicardial myocardial tissue in transmural myocardial infarction after successful reperfusion: an important contribution to the improvement of regional and global left ventricular function.* Circulation, 1999. **99**(1): p. 36-43.
100. Saito, I., S. Watanabe, and Y. Masuda, *Detection of viable myocardium by dobutamine stress tagging magnetic resonance imaging with three-dimensional analysis by automatic trace method.* Jpn Circ J, 2000. **64**(7): p. 487-94.
101. Kaandorp, T.A., et al., *Head-to-head comparison between contrast-enhanced magnetic resonance imaging and dobutamine magnetic resonance imaging in men with ischemic cardiomyopathy.* Am J Cardiol, 2004. **93**(12): p. 1461-4.
102. Lauerma, K., et al., *Multimodality MR imaging assessment of myocardial viability: combination of first-pass and late contrast enhancement to wall motion dynamics and comparison with FDG PET-initial experience.* Radiology, 2000. **217**(3): p. 729-36.

103. Wellnhofer, E., et al., *Magnetic resonance low-dose dobutamine test is superior to SCAR quantification for the prediction of functional recovery.* Circulation, 2004. **109**(18): p. 2172-4.
104. Bove, C.M., et al., *Dobutamine response and myocardial infarct transmurality: functional improvement after coronary artery bypass grafting--initial experience.* Radiology, 2006. **240**(3): p. 835-41.
105. Motoyasu, M., et al., *Prediction of regional functional recovery after acute myocardial infarction with low dose dobutamine stress cine MR imaging and contrast enhanced MR imaging.* J Cardiovasc Magn Reson, 2003. **5**(4): p. 563-74.
106. Jerosch-Herold, M., N. Wilke, and A.E. Stillman, *Magnetic resonance quantification of the myocardial perfusion reserve with a Fermi function model for constrained deconvolution.* Med Phys, 1998. **25**(1): p. 73-84.
107. Larsson, H.B., et al., *Myocardial perfusion modeling using MRI.* Magn Reson Med, 1996. **35**(5): p. 716-26.
108. Wang, L., et al., *Coronary risk factors and myocardial perfusion in asymptomatic adults: the Multi-Ethnic Study of Atherosclerosis (MESA).* J Am Coll Cardiol, 2006. **47**(3): p. 565-72.
109. Christian, T.F., et al., *Absolute myocardial perfusion in canines measured by using dual-bolus first-pass MR imaging.* Radiology, 2004. **232**(3): p. 677-84.
110. Cullen, J.H., et al., *A myocardial perfusion reserve index in humans using first-pass contrast-enhanced magnetic resonance imaging.* J Am Coll Cardiol, 1999. **33**(5): p. 1386-94.
111. Nandalur, K.R., et al., *Diagnostic performance of stress cardiac magnetic resonance imaging in the detection of coronary artery disease: a meta-analysis.* J Am Coll Cardiol, 2007. **50**(14): p. 1343-53.
112. Lerakis, S., et al., *Prognostic value of adenosine stress cardiovascular magnetic resonance in patients with low-risk chest pain.* J Cardiovasc Magn Reson, 2009. **11**: p. 37.
113. Lo, K.Y., et al., *Prognostic value of adenosine stress myocardial perfusion by cardiac magnetic resonance imaging in patients with known or suspected coronary artery disease.* QJM, 2011. **104**(5): p. 425-32.
114. Jahnke, C., et al., *Prognostic value of cardiac magnetic resonance stress tests: adenosine stress perfusion and dobutamine stress wall motion imaging.* Circulation, 2007. **115**(13): p. 1769-76.
115. Hundley, W.G., et al., *Utility of fast cine magnetic resonance imaging and display for the detection of myocardial ischemia in patients not well suited for second harmonic stress echocardiography.* Circulation, 1999. **100**(16): p. 1697-702.
116. Karamitsos, T.D., et al., *Relationship between regional myocardial oxygenation and perfusion in patients with coronary artery disease: insights from cardiovascular magnetic resonance and positron emission tomography.* Circ Cardiovasc Imaging, 2010. **3**(1): p. 32-40.

117. Jekic, M., et al., *Cardiac function and myocardial perfusion immediately following maximal treadmill exercise inside the MRI room.* J Cardiovasc Magn Reson, 2008. **10**: p. 3.
118. Cury, R.C., et al., *Diagnostic performance of stress perfusion and delayed-enhancement MR imaging in patients with coronary artery disease.* Radiology, 2006. **240**(1): p. 39-45.
119. Klem, I., et al., *Improved detection of coronary artery disease by stress perfusion cardiovascular magnetic resonance with the use of delayed enhancement infarction imaging.* J Am Coll Cardiol, 2006. **47**(8): p. 1630-8.
120. Hazlewood, C.F., et al., *Nuclear magnetic resonance transverse relaxation times of water protons in skeletal muscle.* Biophys J, 1974. **14**(8): p. 583-606.
121. Aletras, A.H., et al., *Retrospective determination of the area at risk for reperfused acute myocardial infarction with T2-weighted cardiac magnetic resonance imaging: histopathological and displacement encoding with stimulated echoes (DENSE) functional validations.* Circulation, 2006. **113**(15): p. 1865-70.
122. Friedrich, M.G., et al., *The salvaged area at risk in reperfused acute myocardial infarction as visualized by cardiovascular magnetic resonance.* J Am Coll Cardiol, 2008. **51**(16): p. 1581-7.
123. Ingkanisorn, W.P., et al., *Gadolinium delayed enhancement cardiovascular magnetic resonance correlates with clinical measures of myocardial infarction.* J Am Coll Cardiol, 2004. **43**(12): p. 2253-9.
124. Selvanayagam, J.B., et al., *Troponin elevation after percutaneous coronary intervention directly represents the extent of irreversible myocardial injury: insights from cardiovascular magnetic resonance imaging.* Circulation, 2005. **111**(8): p. 1027-32.
125. Wisenberg, G., et al., *Serial nuclear magnetic resonance imaging of acute myocardial infarction with and without reperfusion.* Am Heart J, 1988. **115**(3): p. 510-8.
126. Higgins, C.B., et al., *Nuclear magnetic resonance imaging of acute myocardial infarction in dogs: alterations in magnetic relaxation times.* Am J Cardiol, 1983. **52**(1): p. 184-8.
127. Garcia-Dorado, D., et al., *Analysis of myocardial oedema by magnetic resonance imaging early after coronary artery occlusion with or without reperfusion.* Cardiovasc Res, 1993. **27**(8): p. 1462-9.
128. Abdel-Aty, H., et al., *Delayed enhancement and T2-weighted cardiovascular magnetic resonance imaging differentiate acute from chronic myocardial infarction.* Circulation, 2004. **109**(20): p. 2411-6.
129. Friedrich, M.G., et al., *Cardiovascular magnetic resonance in myocarditis: A JACC White Paper.* J Am Coll Cardiol, 2009. **53**(17): p. 1475-87.
130. Pauling, L. and C.D. Coryell, *The Magnetic Properties and Structure of Hemoglobin, Oxyhemoglobin and Carbonmonoxyhemoglobin.* Proc Natl Acad Sci U S A, 1936. **22**(4): p. 210-6.

131. Fieno, D.S., et al., *Myocardial perfusion imaging based on the blood oxygen level-dependent effect using T2-prepared steady-state free-precession magnetic resonance imaging.* Circulation, 2004. **110**(10): p. 1284-90.
132. Friedrich, M.G., et al., *Blood oxygen level-dependent magnetic resonance imaging in patients with stress-induced angina.* Circulation, 2003. **108**(18): p. 2219-23.
133. Wacker, C.M., et al., *Susceptibility-sensitive magnetic resonance imaging detects human myocardium supplied by a stenotic coronary artery without a contrast agent.* J Am Coll Cardiol, 2003. **41**(5): p. 834-40.
134. Atalay, M.K., et al., *Oxygenation in the rabbit myocardium: assessment with susceptibility-dependent MR imaging.* Radiology, 1993. **189**(3): p. 759-64.
135. Li, D., et al., *Myocardial signal response to dipyridamole and dobutamine: demonstration of the BOLD effect using a double-echo gradient-echo sequence.* Magn Reson Med, 1996. **36**(1): p. 16-20.
136. Li D, O.W., Gropler RJ., *Magnetic resonance assessment of myocardial oxygenation.* Cardiovascular magnetic resonance, ed. P.D. Manning W. 2001, Philadelphia: Churchill Livingstone.
137. Zheng, J., et al., *Dynamic estimation of the myocardial oxygen extraction ratio during dipyridamole stress by MRI: a preliminary study in canines.* Magn Reson Med, 2004. **51**(4): p. 718-26.
138. Vohringer, M., et al., *Oxygenation-sensitive CMR for assessing vasodilator-induced changes of myocardial oxygenation.* J Cardiovasc Magn Reson, 2010. **12**: p. 20.
139. McCommis, K.S., et al., *Myocardial blood volume is associated with myocardial oxygen consumption: an experimental study with cardiac magnetic resonance in a canine model.* JACC Cardiovasc Imaging, 2009. **2**(11): p. 1313-20.
140. McCommis, K.S., et al., *Quantification of regional myocardial oxygenation by magnetic resonance imaging: validation with positron emission tomography.* Circ Cardiovasc Imaging, 2010. **3**(1): p. 41-6.
141. Reeder, S.B., et al., *Simultaneous noninvasive determination of regional myocardial perfusion and oxygen content in rabbits: toward direct measurement of myocardial oxygen consumption at MR imaging.* Radiology, 1999. **212**(3): p. 739-47.
142. Atalay, M.K., et al., *Cardiac susceptibility artifacts arising from the heart-lung interface.* Magn Reson Med, 2001. **45**(2): p. 341-5.
143. Reeder, S.B., et al., *In vivo measurement of T*2 and field inhomogeneity maps in the human heart at 1.5 T.* Magn Reson Med, 1998. **39**(6): p. 988-98.
144. Arnold, J.R., et al., *Myocardial oxygenation in coronary artery disease: insights from blood oxygen level-dependent magnetic resonance imaging at 3 tesla.* J Am Coll Cardiol, 2012. **59**(22): p. 1954-64.

145. Mitchell, G.F., et al., *Sphygmomanometrically determined pulse pressure is a powerful independent predictor of recurrent events after myocardial infarction in patients with impaired left ventricular function. SAVE investigators. Survival and Ventricular Enlargement.* Circulation, 1997. **96**(12): p. 4254-60.
146. Franklin, S.S., et al., *Is pulse pressure useful in predicting risk for coronary heart Disease? The Framingham heart study.* Circulation, 1999. **100**(4): p. 354-60.
147. Laurent, S., et al., *Aortic stiffness is an independent predictor of all-cause and cardiovascular mortality in hypertensive patients.* Hypertension, 2001. **37**(5): p. 1236-41.
148. Abhayaratna, W.P., et al., *Characteristics of left ventricular diastolic dysfunction in the community: an echocardiographic survey.* Heart, 2006. **92**(9): p. 1259-64.
149. Raunso, J., et al., *Prognostic importance of a restrictive transmitral filling pattern in patients with symptomatic congestive heart failure and atrial fibrillation.* Am Heart J, 2009. **158**(6): p. 983-8.
150. Bess, R.L., et al., *Technical aspects of diastology: why mitral inflow and tissue Doppler imaging are the preferred parameters?* Echocardiography, 2006. **23**(4): p. 332-9.
151. Vanoverschelde, J.L., et al., *Left ventricular filling in dilated cardiomyopathy: relation to functional class and hemodynamics.* J Am Coll Cardiol, 1990. **15**(6): p. 1288-95.
152. Pinamonti, B., et al., *Restrictive left ventricular filling pattern in dilated cardiomyopathy assessed by Doppler echocardiography: clinical, echocardiographic and hemodynamic correlations and prognostic implications. Heart Muscle Disease Study Group.* J Am Coll Cardiol, 1993. **22**(3): p. 808-15.
153. Giannuzzi, P., et al., *Doppler-derived mitral deceleration time of early filling as a strong predictor of pulmonary capillary wedge pressure in postinfarction patients with left ventricular systolic dysfunction.* J Am Coll Cardiol, 1994. **23**(7): p. 1630-7.
154. Yamamoto, K., et al., *Determination of left ventricular filling pressure by Doppler echocardiography in patients with coronary artery disease: critical role of left ventricular systolic function.* J Am Coll Cardiol, 1997. **30**(7): p. 1819-26.
155. Lotrionte, M., et al., *Temporal changes in standard and tissue Doppler imaging echocardiographic parameters after anthracycline chemotherapy in women with breast cancer.* Am J Cardiol, 2013. **112**(7): p. 1005-12.
156. Nagueh, S.F., et al., *Doppler tissue imaging: a noninvasive technique for evaluation of left ventricular relaxation and estimation of filling pressures.* J Am Coll Cardiol, 1997. **30**(6): p. 1527-33.
157. Kasner, M., et al., *Utility of Doppler echocardiography and tissue Doppler imaging in the estimation of diastolic function in heart failure*

with normal ejection fraction: a comparative Doppler-conductance catheterization study. Circulation, 2007. **116**(6): p. 637-47.
158. Ommen, S.R., et al., *Clinical utility of Doppler echocardiography and tissue Doppler imaging in the estimation of left ventricular filling pressures: A comparative simultaneous Doppler-catheterization study.* Circulation, 2000. **102**(15): p. 1788-94.
159. Heimdal, A., et al., *Real-time strain rate imaging of the left ventricle by ultrasound.* J Am Soc Echocardiogr, 1998. **11**(11): p. 1013-9.
160. Urheim, S., et al., *Myocardial strain by Doppler echocardiography. Validation of a new method to quantify regional myocardial function.* Circulation, 2000. **102**(10): p. 1158-64.
161. Amundsen, B.H., et al., *Noninvasive myocardial strain measurement by speckle tracking echocardiography: validation against sonomicrometry and tagged magnetic resonance imaging.* J Am Coll Cardiol, 2006. **47**(4): p. 789-93.
162. Langeland, S., et al., *Experimental validation of a new ultrasound method for the simultaneous assessment of radial and longitudinal myocardial deformation independent of insonation angle.* Circulation, 2005. **112**(14): p. 2157-62.
163. Gjesdal, O., et al., *Global longitudinal strain measured by two-dimensional speckle tracking echocardiography is closely related to myocardial infarct size in chronic ischaemic heart disease.* Clin Sci (Lond), 2007. **113**(6): p. 287-96.
164. Reisner, S.A., et al., *Global longitudinal strain: a novel index of left ventricular systolic function.* J Am Soc Echocardiogr, 2004. **17**(6): p. 630-3.
165. Cho, G.Y., et al., *Global 2-dimensional strain as a new prognosticator in patients with heart failure.* J Am Coll Cardiol, 2009. **54**(7): p. 618-24.
166. Jurcut, R., et al., *Strain rate imaging detects early cardiac effects of pegylated liposomal Doxorubicin as adjuvant therapy in elderly patients with breast cancer.* J Am Soc Echocardiogr, 2008. **21**(12): p. 1283-9.
167. Ho, E., et al., *Subclinical anthracycline- and trastuzumab-induced cardiotoxicity in the long-term follow-up of asymptomatic breast cancer survivors: a speckle tracking echocardiographic study.* Heart, 2010. **96**(9): p. 701-7.
168. Di Salvo, T.G., et al., *Preserved right ventricular ejection fraction predicts exercise capacity and survival in advanced heart failure.* J Am Coll Cardiol, 1995. **25**(5): p. 1143-53.
169. Ghio, S., et al., *Independent and additive prognostic value of right ventricular systolic function and pulmonary artery pressure in patients with chronic heart failure.* J Am Coll Cardiol, 2001. **37**(1): p. 183-8.
170. Ghio, S., et al., *Prognostic usefulness of the tricuspid annular plane systolic excursion in patients with congestive heart failure secondary*

to idiopathic or ischemic dilated cardiomyopathy. Am J Cardiol, 2000. **85**(7): p. 837-42.
171. Meluzin, J., et al., *Prognostic importance of various echocardiographic right ventricular functional parameters in patients with symptomatic heart failure.* J Am Soc Echocardiogr, 2005. **18**(5): p. 435-44.
172. Harada, K., et al., *Comparison of the right ventricular Tei index by tissue Doppler imaging to that obtained by pulsed Doppler in children without heart disease.* Am J Cardiol, 2002. **90**(5): p. 566-9.
173. Vogel, M., et al., *Validation of myocardial acceleration during isovolumic contraction as a novel noninvasive index of right ventricular contractility: comparison with ventricular pressure-volume relations in an animal model.* Circulation, 2002. **105**(14): p. 1693-9.
174. Kowalski M, K.T., Jamal F, D'Hooge J, Weidemann F, Rademakers F et al. , *Can natural strain and strain rate quantify regional myocardial deformation? A study in healthy subjects.* Ultrasound Med Biol, 2001. **27**(8): p. 1087-1097.
175. Tanindi, A., et al., *Assessment of right ventricular functions during cancer chemotherapy.* Eur J Echocardiogr, 2011. **12**(11): p. 834-40.
176. Grover, S., D.P. Leong, and J.B. Selvanayagam, *Evaluation of left ventricular function using cardiac magnetic resonance imaging.* J Nucl Cardiol, 2011. **18**(2): p. 351-65.
177. Lonborg, J., et al., *Myocardial area at risk and salvage measured by T2-weighted cardiovascular magnetic resonance: reproducibility and comparison of two T2-weighted protocols.* J Cardiovasc Magn Reson, 2011. **13**: p. 50.
178. Petersen, S.E., et al., *Functional and structural vascular remodeling in elite rowers assessed by cardiovascular magnetic resonance.* J Am Coll Cardiol, 2006. **48**(4): p. 790-7.
179. Marcus, J.T., et al., *The influence of through-plane motion on left ventricular volumes measured by magnetic resonance imaging: implications for image acquisition and analysis.* J Cardiovasc Magn Reson, 1999. **1**(1): p. 1-6.
180. Karamitsos, T.D., et al., *Operator induced variability in left ventricular measurements with cardiovascular magnetic resonance is improved after training.* J Cardiovasc Magn Reson, 2007. **9**(5): p. 777-83.
181. Masci, P.G., et al., *Myocardial salvage by CMR correlates with LV remodeling and early ST-segment resolution in acute myocardial infarction.* JACC Cardiovasc Imaging, 2010. **3**(1): p. 45-51.
182. Kim, R.J., et al., *Performance of delayed-enhancement magnetic resonance imaging with gadoversetamide contrast for the detection and assessment of myocardial infarction: an international, multicenter, double-blinded, randomized trial.* Circulation, 2008. **117**(5): p. 629-37.
183. Sievers, B., et al., *Rapid detection of myocardial infarction by subsecond, free-breathing delayed contrast-enhancement*

cardiovascular magnetic resonance. Circulation, 2007. **115**(2): p. 236-44.
184. Amado, L.C., et al., *Accurate and objective infarct sizing by contrast-enhanced magnetic resonance imaging in a canine myocardial infarction model.* J Am Coll Cardiol, 2004. **44**(12): p. 2383-9.
185. Beek, A.M., et al., *Quantification of late gadolinium enhanced CMR in viability assessment in chronic ischemic heart disease: a comparison to functional outcome.* J Cardiovasc Magn Reson, 2009. **11**: p. 6.
186. Yan, A.T., et al., *Characterization of the peri-infarct zone by contrast-enhanced cardiac magnetic resonance imaging is a powerful predictor of post-myocardial infarction mortality.* Circulation, 2006. **114**(1): p. 32-9.
187. !!! INVALID CITATION !!!
188. Nijveldt, R., et al., *Functional recovery after acute myocardial infarction: comparison between angiography, electrocardiography, and cardiovascular magnetic resonance measures of microvascular injury.* J Am Coll Cardiol, 2008. **52**(3): p. 181-9.
189. Wiesmann, F., et al., *Global impairment of brachial, carotid, and aortic vascular function in young smokers: direct quantification by high-resolution magnetic resonance imaging.* J Am Coll Cardiol, 2004. **44**(10): p. 2056-64.
190. Oliver, J.J. and D.J. Webb, *Noninvasive assessment of arterial stiffness and risk of atherosclerotic events.* Arterioscler Thromb Vasc Biol, 2003. **23**(4): p. 554-66.
191. O'Rourke, M.F., et al., *Clinical applications of arterial stiffness; definitions and reference values.* Am J Hypertens, 2002. **15**(5): p. 426-44.
192. Silber, H.A., et al., *Why is flow-mediated dilation dependent on arterial size? Assessment of the shear stimulus using phase-contrast magnetic resonance imaging.* Am J Physiol Heart Circ Physiol, 2005. **288**(2): p. H822-8.
193. Baer, F.M., et al., *Head to head comparison of dobutamine-transoesophageal echocardiography and dobutamine-magnetic resonance imaging for the prediction of left ventricular functional recovery in patients with chronic coronary artery disease.* Eur Heart J, 2000. **21**(12): p. 981-91.
194. Baer, F.M., et al., *Comparison of low-dose dobutamine-gradient-echo magnetic resonance imaging and positron emission tomography with [18F]fluorodeoxyglucose in patients with chronic coronary artery disease. A functional and morphological approach to the detection of residual myocardial viability.* Circulation, 1995. **91**(4): p. 1006-15.
195. Gunning, M.G., et al., *Comparison of 201Tl, 99mTc-tetrofosmin, and dobutamine magnetic resonance imaging for identifying hibernating myocardium.* Circulation, 1998. **98**(18): p. 1869-74.
196. Sayad, D.E., et al., *Dobutamine magnetic resonance imaging with myocardial tagging quantitatively predicts improvement in regional*

function after revascularization. Am J Cardiol, 1998. **82**(9): p. 1149-51, A10.
197. Sandstede, J.J., et al., *Detection of myocardial viability by low-dose dobutamine Cine MR imaging.* Magn Reson Imaging, 1999. **17**(10): p. 1437-43.
198. Trent, R.J., et al., *Dobutamine magnetic resonance imaging as a predictor of myocardial functional recovery after revascularisation.* Heart, 2000. **83**(1): p. 40-6.
199. Dendale, P.A., et al., *Low-dosage dobutamine magnetic resonance imaging as an alternative to echocardiography in the detection of viable myocardium after acute infarction.* Am Heart J, 1995. **130**(1): p. 134-40.
200. Gutberlet, M., et al., *Myocardial viability assessment in patients with highly impaired left ventricular function: comparison of delayed enhancement, dobutamine stress MRI, end-diastolic wall thickness, and TI201-SPECT with functional recovery after revascularization.* Eur Radiol, 2005. **15**(5): p. 872-80.
201. Ibanez, B., et al., *Effect of early metoprolol on infarct size in ST-segment-elevation myocardial infarction patients undergoing primary percutaneous coronary intervention: the Effect of Metoprolol in Cardioprotection During an Acute Myocardial Infarction (METOCARD-CNIC) trial.* Circulation, 2013. **128**(14): p. 1495-503.
202. Weaver, W.D., et al., *Comparison of primary coronary angioplasty and intravenous thrombolytic therapy for acute myocardial infarction: a quantitative review.* JAMA, 1997. **278**(23): p. 2093-8.
203. Robbers, L.F., et al., *Myocardial infarct heterogeneity assessment by late gadolinium enhancement cardiovascular magnetic resonance imaging shows predictive value for ventricular arrhythmia development after acute myocardial infarction.* Eur Heart J Cardiovasc Imaging, 2013.
204. Lincoff M, R.M., Aylward P et al. , *Inhibition of delta-Protein Kinase C by Delcasertib as an Adjunct to Primary Percutaneous Coronary Intervention for Acute Anterior ST-Segment Elevation Myocardial Infarction.*

Results of the PROTECTION AMI Randomized Controlled Trial. European Heart Journal - in press, 2014.
205. Alfakih, K., et al., *A comparison of left ventricular mass between two-dimensional echocardiography, using fundamental and tissue harmonic imaging, and cardiac MRI in patients with hypertension.* Eur J Radiol, 2004. **52**(2): p. 103-9.
206. Cerqueira, M.D., et al., *Standardized myocardial segmentation and nomenclature for tomographic imaging of the heart. A statement for healthcare professionals from the Cardiac Imaging Committee of the Council on Clinical Cardiology of the American Heart Association.* Circulation, 2002. **105**(4): p. 539-42.

207. Hombach, V., et al., *Sequelae of acute myocardial infarction regarding cardiac structure and function and their prognostic significance as assessed by magnetic resonance imaging.* Eur Heart J, 2005. **26**(6): p. 549-57.
208. Christenson, R.H., et al., *Relation of temporal creatine kinase-MB release and outcome after thrombolytic therapy for acute myocardial infarction. TAMI Study Group.* Am J Cardiol, 2000. **85**(5): p. 543-7.
209. Elsman, P., et al., *Impact of infarct location on left ventricular ejection fraction after correction for enzymatic infarct size in acute myocardial infarction treated with primary coronary intervention.* Am Heart J, 2006. **151**(6): p. 1239 e9-14.
210. Birnbaum, Y., et al., *Prediction of the extent and severity of left ventricular dysfunction in anterior acute myocardial infarction by the admission electrocardiogram.* Am Heart J, 2001. **141**(6): p. 915-24.
211. Bosimini, E., et al., *Electrocardiographic evolutionary changes and left ventricular remodeling after acute myocardial infarction: results of the GISSI-3 Echo substudy.* J Am Coll Cardiol, 2000. **35**(1): p. 127-35.
212. Gaudron, P., et al., *Progressive left ventricular dysfunction and remodeling after myocardial infarction. Potential mechanisms and early predictors.* Circulation, 1993. **87**(3): p. 755-63.
213. Bolognese, L., et al., *Impact of microvascular dysfunction on left ventricular remodeling and long-term clinical outcome after primary coronary angioplasty for acute myocardial infarction.* Circulation, 2004. **109**(9): p. 1121-6.
214. Brodie, B.R., et al., *Importance of time to reperfusion for 30-day and late survival and recovery of left ventricular function after primary angioplasty for acute myocardial infarction.* J Am Coll Cardiol, 1998. **32**(5): p. 1312-9.
215. Kosuge, M., et al., *Early peak creatine kinase activity is not always a marker of successful reperfusion with myocardial salvage in patients with reperfused anterior acute myocardial infarction.* Am Heart J, 2001. **141**(5): p. 759-64.
216. Grover, S., G. Srinivasan, and J.B. Selvanayagam, *Evaluation of myocardial viability with cardiac magnetic resonance imaging.* Prog Cardiovasc Dis, 2011. **54**(3): p. 204-14.
217. Ezekowitz, J.A., et al., *Predicting chronic left ventricular dysfunction 90 days after ST-segment elevation myocardial infarction: An Assessment of Pexelizumab in Acute Myocardial Infarction (APEX-AMI) Substudy.* Am Heart J, 2010. **160**(2): p. 272-8.
218. Eitel, I., et al., *Comprehensive Prognosis Assessment by CMR Imaging After ST-Segment Elevation Myocardial Infarction.* J Am Coll Cardiol, 2014. **64**(12): p. 1217-26.
219. Larose, E., et al., *Predicting late myocardial recovery and outcomes in the early hours of ST-segment elevation myocardial infarction traditional measures compared with microvascular obstruction,*

salvaged myocardium, and necrosis characteristics by cardiovascular magnetic resonance. J Am Coll Cardiol, 2010. **55**(22): p. 2459-69.
220. Eitel, I., et al., *Prognostic significance and determinants of myocardial salvage assessed by cardiovascular magnetic resonance in acute reperfused myocardial infarction.* J Am Coll Cardiol, 2010. **55**(22): p. 2470-9.
221. Heidary, S., et al., *Quantitative tissue characterization of infarct core and border zone in patients with ischemic cardiomyopathy by magnetic resonance is associated with future cardiovascular events.* J Am Coll Cardiol, 2010. **55**(24): p. 2762-8.
222. Chia, S., et al., *Utility of cardiac biomarkers in predicting infarct size, left ventricular function, and clinical outcome after primary percutaneous coronary intervention for ST-segment elevation myocardial infarction.* JACC Cardiovasc Interv, 2008. **1**(4): p. 415-23.
223. Chin, C.T., et al., *Comparison of the prognostic value of peak creatine kinase-MB and troponin levels among patients with acute myocardial infarction: a report from the Acute Coronary Treatment and Intervention Outcomes Network Registry-get with the guidelines.* Clin Cardiol, 2012. **35**(7): p. 424-9.
224. De Luca, G., et al., *Preprocedural TIMI flow and mortality in patients with acute myocardial infarction treated by primary angioplasty.* J Am Coll Cardiol, 2004. **43**(8): p. 1363-7.
225. Rahimtoola, S.H., *The hibernating myocardium.* Am Heart J, 1989. **117**(1): p. 211-21.
226. Marshall, R.C., et al., *Identification and differentiation of resting myocardial ischemia and infarction in man with positron computed tomography, 18F-labeled fluorodeoxyglucose and N-13 ammonia.* Circulation, 1983. **67**(4): p. 766-78.
227. Tillisch, J., et al., *Reversibility of cardiac wall-motion abnormalities predicted by positron tomography.* N Engl J Med, 1986. **314**(14): p. 884-8.
228. Vanoverschelde, J.L., et al., *Chronic myocardial hibernation in humans. From bedside to bench.* Circulation, 1997. **95**(7): p. 1961-71.
229. Yabe, T., et al., *Quantitative measurements of cardiac phosphorus metabolites in coronary artery disease by 31P magnetic resonance spectroscopy.* Circulation, 1995. **92**(1): p. 15-23.
230. Rimoldi, O.E. and P.G. Camici, *Positron emission tomography for quantitation of myocardial perfusion.* J Nucl Cardiol, 2004. **11**(4): p. 482-90.
231. Karamitsos, T.D., et al., *Patients with syndrome X have normal transmural myocardial perfusion and oxygenation: a 3-T cardiovascular magnetic resonance imaging study.* Circ Cardiovasc Imaging, 2012. **5**(2): p. 194-200.
232. Beache, G.M., et al., *Attenuated myocardial vasodilator response in patients with hypertensive hypertrophy revealed by oxygenation-*

dependent magnetic resonance imaging. Circulation, 2001. **104**(11): p. 1214-7.
233. Karamitsos, T.D., et al., *Blunted myocardial oxygenation response during vasodilator stress in patients with hypertrophic cardiomyopathy*. J Am Coll Cardiol, 2013. **61**(11): p. 1169-76.
234. Sharma, P., et al., *Effect of Gd-DTPA-BMA on blood and myocardial T1 at 1.5T and 3T in humans.* J Magn Reson Imaging, 2006. **23**(3): p. 323-30.
235. Huber, A., et al., *Magnetic resonance perfusion of the myocardium: semiquantitative and quantitative evaluation in comparison with coronary angiography and fractional flow reserve.* Invest Radiol, 2012. **47**(6): p. 332-8.
236. Czernin, J., et al., *Influence of age and hemodynamics on myocardial blood flow and flow reserve.* Circulation, 1993. **88**(1): p. 62-9.
237. Rentrop, K.P., et al., *Changes in collateral channel filling immediately after controlled coronary artery occlusion by an angioplasty balloon in human subjects.* J Am Coll Cardiol, 1985. **5**(3): p. 587-92.
238. Alfakih, K., et al., *Normal human left and right ventricular dimensions for MRI as assessed by turbo gradient echo and steady-state free precession imaging sequences.* J Magn Reson Imaging, 2003. **17**(3): p. 323-9.
239. Watkins, S., et al., *Validation of magnetic resonance myocardial perfusion imaging with fractional flow reserve for the detection of significant coronary heart disease.* Circulation, 2009. **120**(22): p. 2207-13.
240. Braunwald, E. and J.D. Rutherford, *Reversible ischemic left ventricular dysfunction: evidence for the "hibernating myocardium".* J Am Coll Cardiol, 1986. **8**(6): p. 1467-70.
241. Fallavollita, J.A., B.J. Malm, and J.M. Canty, Jr., *Hibernating myocardium retains metabolic and contractile reserve despite regional reductions in flow, function, and oxygen consumption at rest.* Circ Res, 2003. **92**(1): p. 48-55.
242. Shen, Y.T. and S.F. Vatner, *Mechanism of impaired myocardial function during progressive coronary stenosis in conscious pigs. Hibernation versus stunning?* Circ Res, 1995. **76**(3): p. 479-88.
243. Uren, N.G., et al., *Relation between myocardial blood flow and the severity of coronary-artery stenosis.* N Engl J Med, 1994. **330**(25): p. 1782-8.
244. Deanfield, J.E., et al., *Myocardial ischaemia during daily life in patients with stable angina: its relation to symptoms and heart rate changes.* Lancet, 1983. **2**(8353): p. 753-8.
245. Heusch, G., et al., *'Myocardial hibernation'--questions and controversies.* Cardiovasc Res, 1997. **36**(3): p. 301-9.
246. Jahnke, C., et al., *Navigator-gated 3D blood oxygen level-dependent CMR at 3.0-T for detection of stress-induced myocardial ischemic reactions.* JACC Cardiovasc Imaging, 2010. **3**(4): p. 375-84.

247. Zhou, X., et al., *Artifact-reduced two-dimensional cine steady state free precession for myocardial blood- oxygen-level-dependent imaging.* J Magn Reson Imaging, 2010. **31**(4): p. 863-71.
248. Hanrahan, E.O., et al., *Overall survival and cause-specific mortality of patients with stage T1a,bN0M0 breast carcinoma.* J Clin Oncol, 2007. **25**(31): p. 4952-60.
249. Romond, E.H., et al., *Trastuzumab plus adjuvant chemotherapy for operable HER2-positive breast cancer.* N Engl J Med, 2005. **353**(16): p. 1673-84.
250. Tan-Chiu, E., et al., *Assessment of cardiac dysfunction in a randomized trial comparing doxorubicin and cyclophosphamide followed by paclitaxel, with or without trastuzumab as adjuvant therapy in node-positive, human epidermal growth factor receptor 2-overexpressing breast cancer: NSABP B-31.* J Clin Oncol, 2005. **23**(31): p. 7811-9.
251. Guarneri, V., et al., *Long-term cardiac tolerability of trastuzumab in metastatic breast cancer: the M.D. Anderson Cancer Center experience.* J Clin Oncol, 2006. **24**(25): p. 4107-15.
252. Guglin, M., R. Cutro, and J.D. Mishkin, *Trastuzumab-induced cardiomyopathy.* J Card Fail, 2008. **14**(5): p. 437-44.
253. Chen, J., et al., *Incidence of heart failure or cardiomyopathy after adjuvant trastuzumab therapy for breast cancer.* J Am Coll Cardiol, 2012. **60**(24): p. 2504-12.
254. Alfakih, K., et al., *Assessment of ventricular function and mass by cardiac magnetic resonance imaging.* Eur Radiol, 2004. **14**(10): p. 1813-22.
255. Jones, A.L., et al., *Management of cardiac health in trastuzumab-treated patients with breast cancer: updated United Kingdom National Cancer Research Institute recommendations for monitoring.* Br J Cancer, 2009. **100**(5): p. 684-92.
256. Leong, D.P., et al., *Predictors of long-term benefit of cardiac resynchronization therapy in patients with right bundle branch block.* Eur Heart J, 2012. **33**(15): p. 1934-41.
257. Leong, D.P., et al., *Effects of myocardial fibrosis and ventricular dyssynchrony on response to therapy in new-presentation idiopathic dilated cardiomyopathy: insights from cardiovascular magnetic resonance and echocardiography.* Eur Heart J, 2012. **33**(5): p. 640-8.
258. Nousiainen, T., et al., *Comparison of echocardiography and radionuclide ventriculography in the follow-up of left ventricular systolic function in adult lymphoma patients during doxorubicin therapy.* J Intern Med, 2001. **249**(4): p. 297-303.
259. Alexander, J., et al., *Serial assessment of doxorubicin cardiotoxicity with quantitative radionuclide angiocardiography.* N Engl J Med, 1979. **300**(6): p. 278-83.
260. Villani, F., R. Meazza, and C. Materazzo, *Non-invasive monitoring of cardiac hemodynamic parameters in doxorubicin-treated patients:*

comparison with echocardiography. Anticancer Res, 2006. **26**(1B): p. 797-801.
261. Motoki, H., et al., *Torsion analysis in the early detection of anthracycline-mediated cardiomyopathy.* Eur Heart J Cardiovasc Imaging, 2012. **13**(1): p. 95-103.
262. Dodos, F., et al., *Usefulness of myocardial performance index and biochemical markers for early detection of anthracycline-induced cardiotoxicity in adults.* Clin Res Cardiol, 2008. **97**(5): p. 318-26.
263. Mitani, I., et al., *Doxorubicin cardiotoxicity: prevention of congestive heart failure with serial cardiac function monitoring with equilibrium radionuclide angiocardiography in the current era.* J Nucl Cardiol, 2003. **10**(2): p. 132-9.
264. Lightfoot, J.C., et al., *Novel approach to early detection of doxorubicin cardiotoxicity by gadolinium-enhanced cardiovascular magnetic resonance imaging in an experimental model.* Circ Cardiovasc Imaging, 2010. **3**(5): p. 550-8.
265. Fallah-Rad, N., et al., *The utility of cardiac biomarkers, tissue velocity and strain imaging, and cardiac magnetic resonance imaging in predicting early left ventricular dysfunction in patients with human epidermal growth factor receptor II-positive breast cancer treated with adjuvant trastuzumab therapy.* J Am Coll Cardiol, 2011. **57**(22): p. 2263-70.
266. Urbanova, D., et al., *Natriuretic peptides: biochemical markers of anthracycline cardiac toxicity?* Oncol Res, 2008. **17**(2): p. 51-8.
267. Cardinale, D., M. Civelli, and C.M. Cipolla, *Troponins in prediction of cardiotoxic effects.* Ann Oncol, 2006. **17**(1): p. 173; author reply 173-4.
268. Nagarajan, V., A.V. Hernandez, and W.H. Tang, *Prognostic value of cardiac troponin in chronic stable heart failure: a systematic review.* Heart, 2012. **98**(24): p. 1778-86.
269. Barendswaard, E.C., et al., *Right ventricle wall motion abnormalities in patients treated with chemotherapy.* Clin Nucl Med, 1991. **16**(7): p. 513-6.
270. Yeh, E.T., et al., *Cardiovascular complications of cancer therapy: diagnosis, pathogenesis, and management.* Circulation, 2004. **109**(25): p. 3122-31.
271. Chen, M.H., R. Kerkela, and T. Force, *Mechanisms of cardiac dysfunction associated with tyrosine kinase inhibitor cancer therapeutics.* Circulation, 2008. **118**(1): p. 84-95.
272. Cruickshank, K., et al., *Aortic pulse-wave velocity and its relationship to mortality in diabetes and glucose intolerance: an integrated index of vascular function?* Circulation, 2002. **106**(16): p. 2085-90.
273. Sutton-Tyrrell, K., et al., *Elevated aortic pulse wave velocity, a marker of arterial stiffness, predicts cardiovascular events in well-functioning older adults.* Circulation, 2005. **111**(25): p. 3384-90.

274. Boutouyrie, P., et al., *Aortic stiffness is an independent predictor of primary coronary events in hypertensive patients: a longitudinal study.* Hypertension, 2002. **39**(1): p. 10-5.
275. Chaosuwannakit, N., et al., *Aortic stiffness increases upon receipt of anthracycline chemotherapy.* J Clin Oncol, 2010. **28**(1): p. 166-72.
276. Groenink, M., et al., *Changes in aortic distensibility and pulse wave velocity assessed with magnetic resonance imaging following beta-blocker therapy in the Marfan syndrome.* Am J Cardiol, 1998. **82**(2): p. 203-8.
277. Mizia-Stec, K., et al., *Anthracycline chemotherapy impairs the structure and diastolic function of the left ventricle and induces negative arterial remodelling.* Kardiol Pol, 2013. **71**(7): p. 681-90.
278. Keltai, K., et al., *Doxorubicin selectively suppresses mRNA expression and production of endothelin-1 in endothelial cells.* Vascul Pharmacol, 2010. **53**(5-6): p. 209-14.
279. Yavas, G., et al., *Concomitant trastuzumab with thoracic radiotherapy: a morphological and functional study.* Ann Oncol, 2011. **22**(5): p. 1120-6.
280. Liu C, C.D., Teixido-Tura G, Chugh AR, Redheuil A, Gomes AS, Prince MR, Hundley W, Bluemke DA and Lima JA. , *Aortic size, distensibility, and pulse wave velocity changes with aging: longitudinal analysis from Multi-Ethnic Study of Atherosclerosis (MESA).* Journal of Cardiovascular Magnetic resonance, 2012. **14(suppl 1)**: p. 126.